Department of Physics and Astronomy
University of Heidelberg

Master Thesis in Physics
submitted by

Martin Klassen

born in Trier (Germany)

2017

Consistent Models of Dark Matter at the LHC

This Master Thesis has been carried out by Martin Klassen at the
Institute for Theoretical Physics
under the supervision of
Dr. Martin Bauer & Prof. Dr. Tilman Plehn

Abstract

In this thesis we study universal properties of dark matter models with a pseudoscalar mediator at the Large Hadron Collider (LHC). To obtain a renormalizable simplified model a second Higgs doublet is considered. We keep effective couplings to dark matter to maintain our discussion as general as possible, but we mention possible ultraviolet (UV) completions. Simplified models are self-consistent and unitary. Constraints from Higgs signal strength measurements, flavor and electroweak precision observables as well as searches for heavy Higgs bosons are taken into account. The remaining parameter space coincides with a region in which the observed relic density can be reproduced even by considering constraints from direct and indirect detection experiments. We analyze possible missing transverse energy signatures for the preferred parameter space. We show that for a large set of parameters, due to a resonant enhancement, the mono-Z channel provides stronger limits than the mono-jets from initial state radiation. A common feature of these searches is that they lose sensitivity above the top-threshold where the mediator can decay into a pair of top quarks. We emphasize that mono-X searches are complementary to direct and indirect detection experiments. We expect mono-Z searches to almost entirely probe the well-motivated region in the parameter space at the LHC in the near future and thereby constrain a large class of for pseudoscalar mediator models.

Zusammenfassung

In dieser Arbeit analysieren wir das Potenzial von Suchen nach Dunkler Materie am Large Hadron Collider (LHC) mit Hilfe von renormalisierbaren Modellen mit einem pseudoskalaren Mediator, der Bestandteil eines zweiten Higgs Dubletts ist. Dabei wählen wir effektive Kopplungen an Dunkle Materie, um unsere Diskussion allgemein zu halten, aber diskutieren ebenfalls vollständige Modelle. Die effektiven Modelle sind ebenfalls in sich selbst konsistent und unitär. Wir berücksichtigen Einschränkungen an den Parameterraum aus Messungen der Higgs Signalstärken, Flavor Observablen, elektroschwachen Präzisionsmessungen und Suchen nach schweren Partnern des Higgs Bosons. Zusätzlich suchen wir nach Parametern mit denen der Dunkle Materie Kandidat für einen signifikanten Anteil der beobachteten kosmischen Energiedichte Dunkler Materie verantwortlich ist. Dabei beziehen wir die Ausschlussgrenzen von direkten und indirekten Nachweisexperimenten ein. Im restlichen Parameterraum analysieren wir mögliche Signaturen am LHC mit fehlender transversaler Energie (Mono-X). Das Signal eines einzelnen Z-Bosons ist in unserem Fall resonant verstärkt und liefert stärkere Limits als Suchen nach Jets, die vom Anfangszustand abgestrahlt wurden. Eine Gemeinsamkeit aller Suchen ist, dass sie Sensitivität oberhalb der Top-Schwelle verlieren, ab der der pseudoskalare Mediator in zwei Top-Quarks zerfallen kann. Wir möchten betonen, dass diese Mono-X Studien komplementär zu den direkten und indirekten Nachweisexperimenten sind.Wir erwarten, dass Mono-Z Suchen recht bald einen Großteil des motivierten Parameterraums am LHC testen können und dadurch eine große Klasse an Modellen mit pseudoskalaren Mediatoren einschränken.

Contents

1 Introduction

The nature of dark matter remains one of the leading questions in particle physics for almost a century since its first prediction by Zwicky in 1933 [1]. From several indications, such as the observation of galaxy rotation curves, gravitational lensing studies of the Bullet Cluster, simulations of structure formation and measurements of the cosmic microwave background, we know that dark matter is the main contribution to the matter content of our universe [2–5]. In particular, the energy densities for dark energy, dark matter and baryonic matter as measured by the Plank experiment are $\Omega_\Lambda = 0.683$, $\Omega_{\mathrm{DM}} = 0.268$ and $\Omega_b = 0.049$ [5]. As of yet only little is known about the properties of dark matter; a whole range of potential candidates exists. Among the best-motivated ones are the so-called weakly interacting massive particles (WIMPs), axions and heavy sterile neutrinos. They all have distinct masses and couplings to the Standard Model, and hence a broad range of attempts exist to detect dark matter. Interesting examples are missing transverse energy searches at the Large Hadron Collider (LHC).

In this thesis we study the potential of dark matter searches at colliders. Thereby, we analyze extensions of the Standard Model with a single mediator and a Dirac dark matter candidate. The explicit treatment of the mediator becomes important in interactions with large momentum transfers, which is certainly the case for collisions at the LHC, where effective field theory descriptions break down [6]. Hence we introduce so-called simplified models which consider the mediator explicitly. These class of models allow studying universal signatures for a large class of more complete theories describing the dark sector. The corresponding mediators are assumed to be neutral, and the couplings to the Standard Model fermions are constrained by flavor physics [7]. Hence, the spin-0 mediators are supposed to have Yukawa-like couplings, whereas the spin-1 mediators should have universal couplings to all particles carrying the same flavor [8]. Therefore, the spin-1 mediators obey strong restrictions from di-jet and di-lepton searches [9, 10], which provide for a large region in the perturbatively allowed parameter space stronger bounds than the mono-X searches we mainly focus on. On the other hand, for the spin-0 mediators, the couplings between the dark matter and the leptons as well as quarks are suppressed by their masses. Direct detection experiments set stringent limits on mediators with scalar couplings. Hence, we concentrate our collider searches on pseudoscalar mediators as their scattering cross sections between the nuclei and dark matter are velocity suppressed [11]. These searches are complementary to direct and indirect detection experiments and important to probe the nature of dark matter.

As the Standard Model does not provide a pseudoscalar, we are required to extend it for example by a second Higgs doublet to preserve gauge invariance. This results from the fact that the couplings of a gauge singlet pseudoscalar to fermions would lead to unitarity violating amplitudes. The couplings in simplified models are hence expected to emerge from additional states which result in an enriched phenomenology. These extra particles cannot be extremely heavy due to electroweak precision measurements [12, 13]. New signatures, such as a resonantly enhanced mono-Z or mono-Higgs final state, can break the usual hierarchy of mono-X searches, where the mono-jet initial state radiation usually provides the dominant exclusion limits [14]. Depending on the respective UV completion of the simplified models, additional signatures occur or are enhanced. We want to focus on the universal signatures, which are present in a large class of complete models. These signals can be obtained by studying consistent gauge invariant simplified models with a pseudoscalar mediator. Constraints are derived from the phenomenol-

ogy of the two Higgs doublet model, such as measurements of the Higgs signal strengths or searches for heavy partners of the Higgs. We investigate the remaining parameter space for a region in which the dark matter candidate can explain the observed relic density and derive constraints from direct and indirect detection experiments. We finally perform a collider search for the allowed window in the parameter space, calculate the reach of the various dark matter final states at the LHC and provide a projection for a high luminosity data set as we also show in [15].

The remainder of this thesis is structured as follows. In Chapter 2, we review the evidence pointing towards the existence of dark matter and give an overview of the various candidates. Then we concentrate on the WIMP and its thermal freeze-out production. We continue with a study of the different search strategies, where we show that collider searches are complementary to the direct and indirect detection experiments. We end this chapter by deriving simplified models from effective field theories, discuss possible mediators interacting with the dark sector, provide a gauge invariant extension of the Standard Model by a pseudoscalar and mention corresponding UV completions.
In Chapter 3, we begin with a review of two Higgs doublet models focusing on type I and II implementations of the Yukawa couplings. We continue with a study of the extension by a Dirac dark matter particle presenting the simplified model on which this analysis is based before we describe the branching ratios of the additional Higgs particles.
In Chapter 4 and Chapter 5 we present the constraints on the parameter space of the simplified model from measurements of the Higgs coupling strengths, flavor physics, electroweak precision observables, stability requirements of the scalar potential, the observed relic density and direct as well as indirect detection experiments.
In Chapter 6, we study the reach of dark matter searches at the LHC and their future potential at high luminosity and conclude in Chapter 7 with a summary.

2 Dark Matter and Where to Find It

We begin this chapter with a review of the first hints pointing towards the existence of dark matter and provide a summary of the best motivated dark matter candidates [16]. We will continue with a discussion of the various search strategies aiming for a direct proof of the presence of dark matter particles. Finally, we will present different mediators between the Standard Model and the dark sector and will connect them to the distinct searches.

2.1 Evidence for Dark Matter

Today, even without a direct observation, we expect dark matter to make up about 26.8 % of the total energy in the universe. Hence, it is about five times more abundant than ordinary baryonic matter which accounts for 4.9 %, whereas the main contribution is assumed to be dark energy with 68.3 %. These numerical values are obtained from the Planck Cosmic Microwave Background (CMB) power spectrum fitted to the Standard Model of cosmology, also known as the ΛCDM model [5].
The history of dark matter research can be traced back to the 1930s, when the astronomer Fritz Zwicky mentioned for the first time the presence of additional non-baryonic matter in the Coma Cluster. He followed the nomenclature of Kapteyn, Oort and Jeans, who studied the kinematics of stars in the Milky Way [17–19], and consolidated the name "dark matter". In the 1970s cosmological observations of galaxy rotation curves provided stronger claims for the necessity of additional matter in the outer regions of a variety of galaxies. From there on more and more hints pointing towards the existence of dark matter were discovered. In the scope of this thesis, we will mention the ones that are most relevant to our research.

Galactic Clusters

In the early 1930s, Zwicky investigated the dynamics of galactic clusters by studying their redshifts [1]. Thereby he found ambiguities in the rotation velocities of some galaxies in the Coma Cluster. To gain a better understanding of this problem he applied the Virial theorem to this cluster to estimate its mass. He first derived the velocity dispersion by assuming values for the numbers of galaxies, the average mass of a single galaxy and the size of the cluster to calculate the potential energy. He then concluded that the ratio to the observed averaged velocity distribution is off by a factor of approximately 12. This discrepancy he explained by the hypothesis, that there exists dark matter in the Coma Cluster whose amount is larger than the luminous matter.
In 1937 he extended his study of the Coma Cluster by using the observed velocity dispersion of 700km/s to get an estimate on the average mass of a galaxy [3]. Assuming 1000 galaxies in the cluster which itself spread out over 2×10^6 light-years he found the average mass of a galaxy to be $4.5 \times 10^{10} \mathrm{M}_\odot$. Comparing this to the average luminosity of a galaxy of 8.5×10^7 times that of the sun, he obtained a mass to light ratio of roughly 500. Even as it turns out today that this factor was overestimated by about one order of magnitude due to a wrong estimate of the Hubble constant, this high discrepancy in the measured to visible mass is a strong indicator for the existence of dark matter.

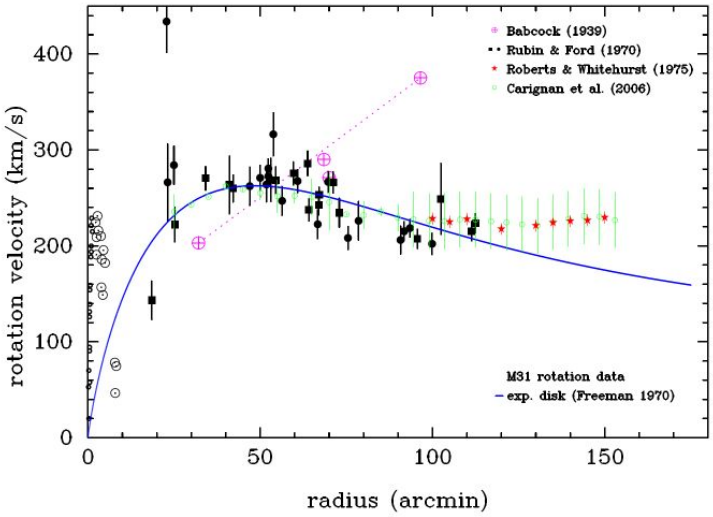

Figure 2.1: Measured rotation curves of the galaxy M31. The purple points are emission lines from the outer region measured by Babcock, the black points were obtained by Rubin and Ford in 1970, whereas the red and green points are the 21-cm HI line data from Roberts and Whitehurst as well as Carignan et al. The solid blue line represents the rotation curve of an exponential disc simulated by Freeman [2]. The data from the 21-cm measurements indicates the mass discrepancy in the outer region. Figure taken from [20].

Galaxy Rotation Curves

Vera Rubin and Kent Ford, through their study of galaxy rotation curves in the 1970s, opened a new chapter of evidence for the presence of additional dark matter especially in the outer regions of spiral galaxies. They investigated the behavior of stars with regards to their motion around the center of the galaxies. As most of the visible matter sits in the center of a galaxy one would naively expect, due to Kepler's third law, that the velocities of the stars would drop as they are located further outside the center. But what they found was that the rotation curves remained flat to the furthest distances they could observe.

A couple of years later, with the radio measurement of the spectral 21-cm line of hydrogen becoming available, one was now able to explore further distances. Also in these outer regions of the galaxies, the rotation curves remained flat, compare the work of Freeman [2]. He concluded that the mass distribution of the dark matter has to be different than the exponential one of ordinary matter.

Many more rotation curves of galaxies were studied by various groups/scholars, all leading to the same conclusion that a halo of dark matter particles is spread out to the furthest distances of the spiral galaxies. An example for such a rotation curve is given for the M31 galaxy in Figure 2.1, where a variety of measurements were considered.

The Cosmic Microwave Background

Another indicator for the existence of dark matter is the investigation of the Cosmic Microwave Background (CMB), which was predicted by Gamow as early as the 1940s [21]. The CMB describes the relic radiation produced shortly after the big bang and is observed today as a homogeneous blackbody spectrum with a temperature of 2.726K with only very tiny angular temperature fluctuations, so-called anisotropies [22]. In the early universe about 380,000 years after the Big Bang, the photons decoupled from the baryons which were still in a thermal bath and the universe became transparent. The observation of this radiation by Penzias and Wilson [23] confirmed the theory of the Big Bang. The variations of the temperature fluctuations follow a Gaussian distribution if expanded in spherical harmonics and

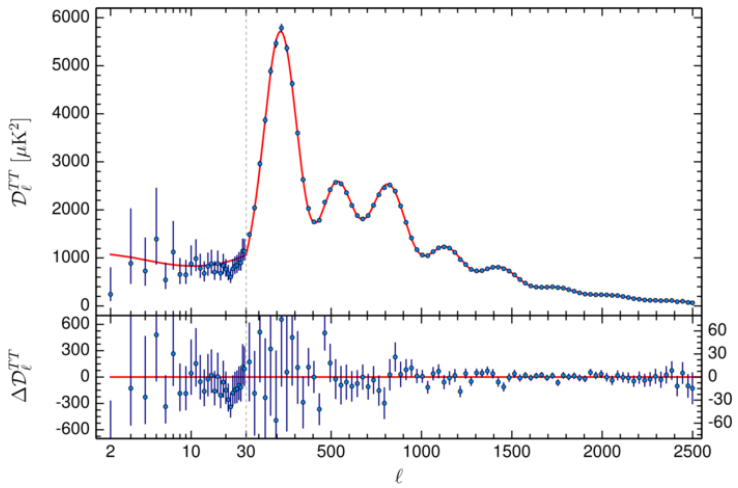

Figure 2.2: Power spectrum of Cosmic Microwave Background measured by the Planck satellite in 2015. The red line represents a fit to the data by using the ΛCDM model. Figure taken from the Plack collaboration [24].

hence can be mapped to a power spectrum. This spectrum was measured by the WMAP and PLANCK satellites and can be seen in Figure 2.2. The various peaks and in particular their positions as well as their heights reveal cosmological information. In particular, it turns out that the spectrum can only be well described if one allows for a cosmological constant Λ and cold dark matter in a six parameter fit. The assumed model is called the Λ-CDM model, which is often referred to as the Standard Model of cosmology as it provides a parametrization of the Big Bang cosmology. From the first peak of the spectrum the total mass density is found to be $\Omega_m = 0,317$ and with the ratio of the amplitudes of the first and second peak the baryonic density is extracted to be $\Omega_b = 0,049$. Hence the dark matter content to the total energy of the universe follows to be $\Omega_{DM} = 0,268$.

Gravitational Lensing and Colliding Clusters

Massive objects bend the path of light through spacetime as predicted by general relativity. Hence lensing can be used to obtain the masses of galaxies and clusters as was predicted by Zwicky in 1937. A bright distant source as a quasar has to lie beyond the object of study to make use of the gravitational lensing effect for such measurements. The distortion of the light due to the lens can then be projected onto the mass of the galaxy. The obtained light to mass ratios yield comparable results to the evidence from the dynamics of clusters and galaxies. Weak gravitational lensing observations relying on the statistical treatment of background sources around the lens also allow a measurement of the light to mass ratio and point towards the existence of dark matter.
Studies of gravitational lensing of two colliding clusters provide substantial evidence for dark matter. The most famous example is the so-called Bullet Cluster, which can be found in Figure 2.3. In this collision one can rather well separate the non-interacting stars from the electromagnetically interacting gas. The stars are only slown down due to their gravitational interaction, whereas the gas heats up in the collision and radiates X-rays. Its velocity is much more reduced than that of the stars. As in the two clusters, the main contribution of the matter content is expected to be contained in the gas; the gravitational lens of background objects should be following the gas. However, what was observed is that the gravitational lensing peaked at the two visible galaxies containing the non-interacting stars. This leads to the conclusion that the baryonic matter in the galactic clusters is surrounded by a non-interacting dark matter halo which sets limits to self-interacting dark matter. Furthermore, it provides

Figure 2.3: Two colliding galaxy clusters forming the so-called Bullet Cluster. In red the measured X-ray spectrum of the interaction gas is displayed, which is expected to be the leading mass contribution for the baryonic matter. In blue the weak gravitational lensing measured mass distribution is shown. The evidence for the existence of dark matter can be extracted from the separation of the two regions, and the larger than predicted mass distribution in the outer region. Figure taken from the Chander X-Ray Observatory [25].

strong restrictions on models where the cosmological observations requesting the existence of dark matter are explained by modified Newtonian dynamics.

Structure Formation

As the last indication, we want to discuss the role of dark matter in the structure formation of the early universe. At this moment we refer to the process where stars, galaxies and clusters formed for the first time in the early universe out of density perturbation in the matter distribution. It is assumed that the universe started out as a homogeneous distribution of matter which then collapsed into structures due to gravitational potentials which grow in time. As baryonic matter interacts with radiation, which was the dominant constituent in the early universe, the density fluctuations which were required to build these gravitational potentials were washed out. Hence there was not enough time for structures to form without the presence of dark matter. As dark matter does not interact strongly with radiation, potentials of dark matter could first develop. In these gravitational potentials, the baryonic matter could then shape structures. Simulations of the evolution of the universe, such as the Millennium's simulation [4], are very successful if they consider non-relativistic dark matter as well as dark energy in their set-ups. The process of structure formation, therefore, requires the dark matter to be cold as otherwise the density perturbations are washed out by the kinetic energy of the dark matter. This provides limits on the fraction of hot dark matter.

2.2 An Overview of Dark Matter Candidates

At the present date, only a few properties of dark matter are known which results in a vast parameter space in its coupling strength as well as in its mass range. This leads to widely different candidates. Before presenting a preliminary selection of these proposed particles, we summarize some of the features of dark matter. As initially introduced to explain the missing matter in the observed rotation curves of galaxies, dark matter is assumed to have a gravitational interaction. Moreover, due to its nomenclature to be dark and its non-observation by a variety of experiments one assumes no electromagnetic charge. Neither is dark matter able to carry a color charge as otherwise it should have been discovered already due to the constraints from structure formation. One allows for additional very weak couplings to the

Standard Model via the weak force. This is the interaction which might allow for a direct measurement of dark matter as the gravitational interaction is orders of magnitudes too small for a direct discovery. The dark matter particle should be stable on the timescale of the universe as otherwise, one would not be able to reproduce the measured relic density of today. From simulations of structure formation, we deduce that dark matter must be mainly cold as otherwise the small density perturbations are washed out. This requirement translates into non-relativistic dark matter velocities and provides one of the reasons why the neutrinos, which are the only particles in the Standard Model which in principle could be dark matter, can only make up a fraction of the observed dark matter. It should be mentioned that one can always create a model breaking one or several of these assumptions but most of the theories include these basic properties.

As we have seen in the prior section, a variety of arguments for the existence of dark matter are present, but its nature remains unknown even as its abundance is well measured. Several attempts are trying to explain dark matter as a new particle connected to the Standard Model. Two fundamentally different approaches can explain the non-observation of dark matter in direct detection. On the one hand the couplings between the visible and the dark sector could be based on very small couplings; on the other hand the new particles could be rather heavy and therefore hard to detect due to a low number density. For these two scenarios, there exist distinct search strategies. In the former, experiments aim at high intensity and precision to detect very weakly coupled particles, whereas for very heavy particles high energy experiments are advantageous. We are now presenting some dark matter candidates where the range of couplings and masses can partially be found in Figure 2.4.

WIMPs

Weakly Interacting Massive Particles (WIMPs) are among the most promising candidates from a theoretical perspective although they have escaped any direct detection attempt so far. As our proposed dark matter particle will belong to this class of particles we will spend an entire Section 2.3 to discuss their properties, their production mechanism as well as to provide an introduction to the so-called WIMP miracle.

Sterile Neutrinos

Measurements of the beta spectrum of tritium lead to the conclusion that Standard Model neutrino masses must be below 2.1 eV [26] if results from flavor oscillations are considered. Hence, neutrinos are too light to account for dark matter as they are not able to form structures. The underlying reason for this is their high velocity leading to the fact that they are hot dark matter, whose abundance is restricted by structure formation. In fact, they move too fast to collapse into larger structures formed by their own gravitational potential, as is shown in [27]. They are a sub-dominant constituent of the entire dark matter present in the universe.

The branching ratios of the Z boson to invisibles and the corresponding total width exclude a fourth light neutrino which in principle could have been a dark matter candidate. Nevertheless, a potential massive sterile neutrino is a likely candidate. This neutrino is required to be a singlet under all Standard Model symmetries. A frequently discussed example is that these neutrinos are the right-handed partners of the active neutrinos and might obtain their masses via the so-called see-saw mechanism. In general, they can have Majorana masses, and as they are expected to be heavy, they would have non-relativistic velocities. In particular, they would be neutral as well as weakly interacting and hence would be a natural dark matter candidate. Current and proposed experiments searching for neutrino dark matter are wide-spread and use different techniques. The detectors at PIENU at TRIUMF or PEN at PSI aim at a measurement

of flavor universality; GERDA as well as SuperNEMO, among others, search for neutrinoless double beta decays; meson decays are studied at BABAR, Belle II and LHCb; whereas fixed targets experiments are performed for example by the SHiP collaboration at CERN [28] and references therein.

Axions

Axions are pseudo-Nambu-Goldstone bosons emerging from the spontaneous breaking of the Peccei-Quinn symmetry and can be candidates for cold dark matter. They were first introduced in 1977 to solve the strong CP problem in quantum chromodynamics [29]. Originating from a spontaneously broken global, chiral symmetry the axion should be massless. However, it obtains a small mass due to non-trivial QCD vacuum effects as the symmetry breaking arises from a chiral anomaly. If one assumes that the axion is produced by the so-called misalignment mechanism its mass turns out to be far smaller than that which is obtained from the thermally produced WIMPs. The axion mass is favored by current cosmological models to be in the range of 10^{-5} to 10^{-3} eV, which indeed is a likely mass for a dark matter candidate non-thermally produced. The bounds are derived from limits on stellar cooling as well as from the relic density [30]. The axion is expected to be electrically neutral leading to a very weak coupling to ordinary matter. Since the axion is motivated by particle physics and occurs naturally in many extensions of the Standard Model like in string theory, it is an appealing candidate for dark matter. Axions can be directly detected due to their coupling to two photons. This effect is used in light shining through the wall experiments and in axion-haloscopes such as CAST or ADMX [31] and references therein. There exists a whole variety of proposed axion-like particles as well as hidden photons which could be detected with similar experiments. So far, no experimental hints to the existence of the axion have been found indicating that the coupling to ordinary matter must be extremely weak. As they only have an indirect impact on collider searches, we shall leave the discussion here, with mentioning that in a complete theory an axion-like particle could provide the pseudoscalar mediator required in a consistent simplified theory as it is shown in [14].

Primordial Black Holes

The recent detection of gravitational waves by the LIGO collaboration has strengthened the hypothesis that black holes formed in the early universe can be a valid dark matter candidate. Kamionkowski et al. showed that the primordial black hole merging rate is comparable with the one estimated by LIGO assuming that they contribute to the dark matter [32]. A mechanism is required to stop the decay of the primordial black holes due to Hawking radiation shortly after the Big Bang. They could, for example, be stabilized by quantum gravity effects if their masses reach the Planck scale and then could be considered as a valid dark matter candidate. Primordial black holes are nearly collision-less, non-relativistic and are expected to have formed in the early history of the universe so that they could have supported structure formation. On the other hand, they are strongly constrained by astrophysical and cosmological observations. There are prospects that with further observations of gravitational waves more information, and limits set on this dark matter candidate, can be extracted.

In this section we only discussed a fraction of dark matter candidates, but we have already seen that there exists a broad range of different proposed and justified dark matter candidates. They all occupy their distinct parameter spaces and hence all require specialized search strategies. We now turn to the investigation of the WIMPs to gain a deeper understanding of this broadly studied candidate.

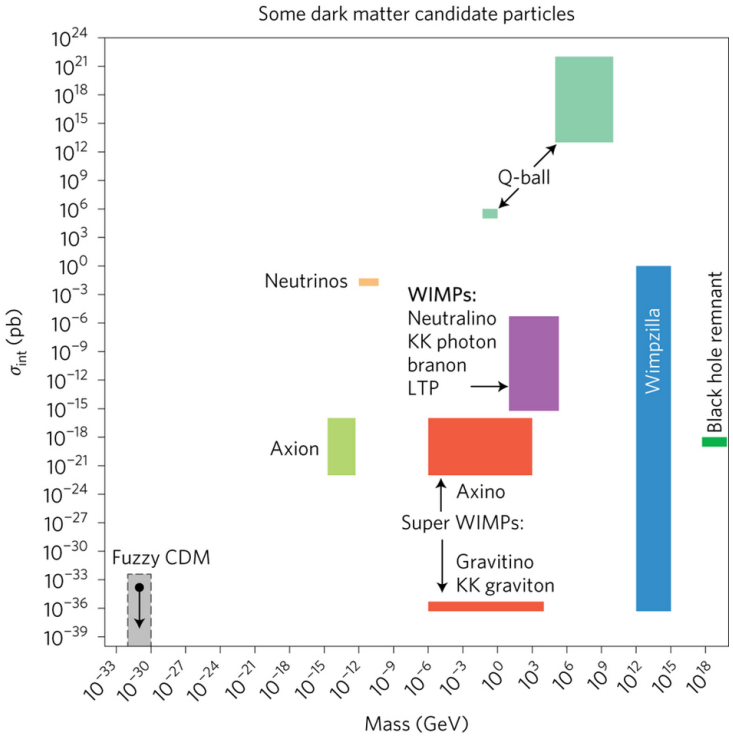

Figure 2.4: Incomplete landscape of dark matter candidates in the cross section to mass parameter space. WIMPs (purple) are among the most frequently discussed candidates, SuperWIMPs (red) are their supersymmetric partners, whereas WIMPzillas (blue) represent the high mass limit. Further candidates are axions (light green), neutrinos(orange), primordial black holes (dark green), Q-balls(green) and light fuzzy cold dark matter (gray). Figure taken from [30].

2.3 The WIMP and Its Miracle

Weakly interacting massive particles are among the best-motivated candidates for dark matter. They are predicted in many extensions of the Standard Model where an additional conserved quantum number is introduced, such as parity. Such a new particle needs to be electric- and color-neutral in order be in agreement with structure formation. Then it can be recognized as a valid dark matter candidate. A famous example is the lightest neutralino χ_0, which is a mixture of the superpartners of the Standard Model bosons in supersymmetric theories. In such a case the conserved quantum number is the so-called R-parity, a $\mathbb{Z}_2$ symmetry, which is defined as $P_R = (-1)^{3(B-L)+2s}$. Here B represents the number of baryons, L the lepton number and s corresponds to spin quantum number. Standard Model particles carry a charge of +1 under R-parity, whereas supersymmetric particles have a charge of -1 [33]. Further candidates emerge from theoretical predictions, such as the lightest Kaluza-Klein excitations in extra dimensions with a KK-parity or - in Little Higgs models - the lightest T-odd particles [30] and references therein. Many more WIMP models have been suggested and the definition of a WIMP has broadened since.

The WIMP interacts with the Standard Model particles through gravity and the weak force only. Sometimes a new interaction with cross sections below the weak scale is suggested. WIMPs are assumed to have been produced in a thermal bath in the early universe, where they were in thermal equilibrium with the Standard Model particles. Their masses are constrained to be of the order of the weak scale. Hence, due to their large masses they have non-relativistic velocities and therefore are a well-grounded candidate for cold dark matter.

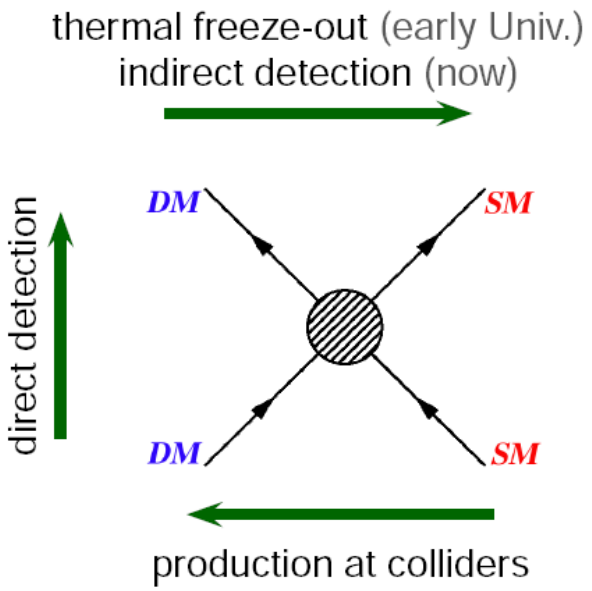

Figure 2.5: Overview of dark matter interactions with the Standard Model. Left to Right: Dark matter annihilation to Standard Model particles (indirect detection), Right to Left: Dark matter production at colliders, Up to Top: Dark matter scattering on Standard Model particles (direct detection). Figure taken from [34].

A lot of effort has already gone into the attempt to detected WIMPs, but so far, a clear hint to their existence remains missing. We will mention the different WIMP search strategies in Section 2.4, and continue with providing an overview of the thermal history of WIMPs in the universe before performing a detailed calculation deriving their current relic abundance.

Thermal Freeze-out

WIMPs are expected to have a thermal production mechanism and, similar to the photons and neutrinos, to have been decoupled from the thermal equilibrium in the early universe. It is assumed that in the period before decoupling the dark matter was in thermal equilibrium with the Standard Model particles. More precisely the WIMPs were able to annihilate into Standard Model particles, especially fermions, and were again created by them via pair production in an interaction of the following type

$$\chi\bar{\chi} \leftrightarrow f\bar{f} \ , \tag{2.1}$$

where χ represents the dark matter or its antiparticle, whereas f stands for the Standard Model fermions. The two relevant processes are displayed in Figure 2.5. If we read this plot from left to right, the shown interaction represents dark matter annihilation into Standard Model particles, whereas looking at the process from right to left the figure can be interpreted as dark matter being pair-produced. As the universe starts expanding and therefore at the same time begins cooling down, the kinetic energy of these light particles decreases. Consequently, the annihilation of baryonic matter into dark matter becomes inefficient. This process is increased as the fundamental particles start to hadronize at low enough temperatures. On the other hand, the annihilation of the dark matter into baryons remains present leading to an exponential drop of the dark matter number density. Because of the decreasing number density, enforced by the annihilation of dark matter as well as the expansion of the universe, this interaction becomes as well very inefficient. Then the amount of dark matter in the entire universe would stay roughly constant, whereas the number density decreases cubic as the volume of the universe

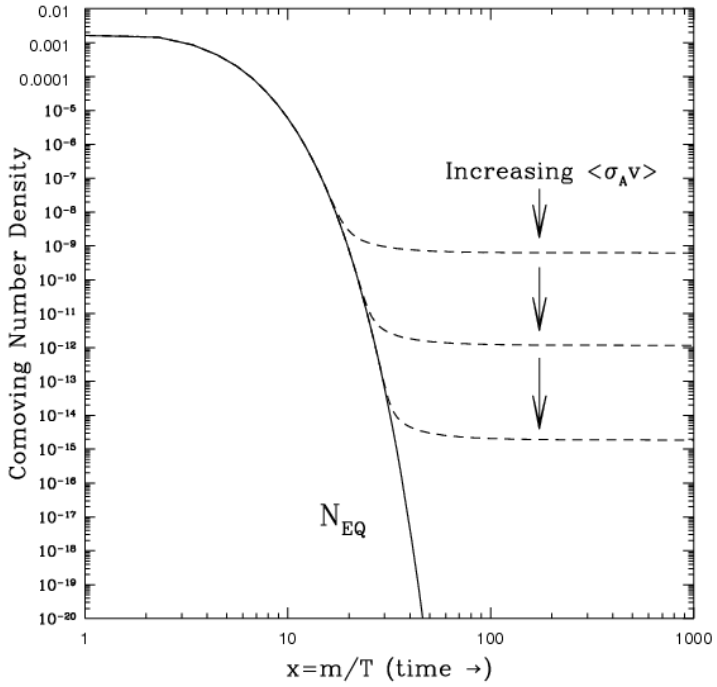

Figure 2.6: The thermal freeze-out of a WIMP is schematically presented. As the universe cools the dark matter pair production stops at roughly $x = m_\chi/T = 2$ and an exponential decrease of the comoving dark matter number density occurs. At a certain value of x depending on the thermal averaged cross section the number density Y does no longer follow the Y^{EQ} line but freezes out to the actual density represented by the dashed curves. Thereby an increasing annihilation rate $\langle \sigma_{\chi\bar{\chi}\to f\bar{f}}\, v \rangle$ leads to a smaller relic density as the curves leave the equilibrium density at later times corresponding to smaller temperatures. Typical values for x_{fo} of WIMPs are about 20-30. Figure taken from [35].

still expands. This process is often referred to as thermal freeze-out. Thereby the present relic density of today depends strongly on the cross section of the annihilation. If we assume the velocity averaged cross section to be larger the dark matter would annihilate more efficient and therefore the relic abundance would decrease. This behavior is schematically shown in Figure 2.6, where the comoving dark matter number density is plotted against the time. The current relic density tends to cross sections of the weak scale if we assume a WIMP with a corresponding mass in the GeV range. This we will substantiate now by performing a proper calculation of the relic density by making use of the Boltzmann equation.

The WIMP Miracle

As the WIMPs are assumed to have undergone the process of thermal-freezeout we are going to study this formalism in more depth to derive the so-called WIMP miracle. We start by using the Boltzmann transport equations to calculate the relic density by following closely the work of [22, 27, 30, 36, 37]. We will need to make some justified approximations to derive an analytic solution, as generally this problem can only be solved numerically.

The Boltzmann equation in its most general form is a non-linear differential equation describing the variation of the number density $n(t)$ as a function of the time. As space-time in our universe is expanding, a scale factor $a(t)$ in the line-element, defined by the Friedman-Robertson-Walker metric, is introduced. The Hubble constant providing a measure for the expansion of the universe is defined as

$H(t) = \frac{\dot{a}(t)}{a(t)}$. Due to the expansion of the universe the number density is not constant which is also considered in the Boltzmann equation in equilibrium

$$\frac{d}{dt}\left[n(t)a(t)^3\right] = 0 \quad \rightarrow \quad \frac{dn(t)}{dt} + 3H(t)n(t) = 0 \ . \tag{2.2}$$

In thermal equilibrium the dark matter particles χ can either be pair-produced or annihilate in processes with Standard Model fermions f as $\chi\bar{\chi} \rightarrow f\bar{f}$. These fermions are expected to have no chemical potential and moreover should be in thermal equilibrium with the photons as well as other light particles. A requirement on the dark matter being in thermal equilibrium with the cosmic plasma is that the temperature of the early universe must be larger than the mass of the WIMPs. Staying in thermal equilibrium necessitates that the particles interact frequently. The interaction rate per particle is defined as $\Gamma = \sigma v n_\chi$ where σ is the cross section of the scattering of two particles and v their relative velocity. The thermal equilibrium is maintained as long as the expansion rate $H(t)$ is much smaller than the scattering rate. Phrased differently, as the expansion can be parametrized by the time and the time can be expressed in terms of the temperature when the universe starts to expand and cools, WIMPs no longer stay in thermal equilibrium for temperatures where the expansion rate is larger than the annihilation rate. Then the WIMPs can no longer efficiently annihilate as their abundance becomes too small that two dark matter particles collide at sufficient rates. This temperature at which the expansion and the annihilation become equal is called the freeze-out temperature. For these temperatures, the dark matter density stops decreasing exponentially, as in the cooling phase, but drops with the inverse of the increasing volume due to the expansion of the universe. We calculate the dark matter abundance after the thermal freeze-out by using the number density obtained from the out of equilibrium Boltzmann equation. We assume that in the phase where $n_\chi(t) > n_\chi^{EQ}(t)$ the WIMPs annihilate faster than they can be produced. This leads to a depletion rate $\sigma_{\chi\bar{\chi}\rightarrow f\bar{f}} v n_\chi^2$ where the square of the number density traces back to the presence of two dark matter particles in the interaction. As the WIMPs are considered to be cold dark matter, they should have non-relativistic velocities. Therefore, we need to average over the thermal velocities and write the averaged product of cross section and velocity as $\left\langle \sigma_{\chi\bar{\chi}\rightarrow f\bar{f}}\ v \right\rangle$. For the Boltzmann equation out of equilibrium we then find

$$\frac{dn_\chi(t)}{dt} + 3H(t)n_\chi(t) = -\left\langle \sigma_{\chi\bar{\chi}\rightarrow f\bar{f}}\ v \right\rangle \left(n_\chi(t)^2 - n_\chi^{EQ}(t)^2\right) \ . \tag{2.3}$$

In thermal equilibrium the relation $n_\chi(t)^2 = n_\chi^{EQ}(t)^2$ holds and the equation (2.2) is restored in which case the variation of the number density emerges only from the expansion of the universe. From thermodynamics of the early universe we make use of the result that $a(T)T \propto \frac{1}{g_{\text{eff}}(T)}$ is constant. Hence the available degrees of freedom g_{eff} as well must be constant at the time of decoupling. We then can rewrite the number density by $Y(t) = \frac{n_\chi(t)}{T^3}$ to obtain

$$\frac{dY(t)}{dt} = -\left\langle \sigma_{\chi\bar{\chi}\rightarrow f\bar{f}}\ v \right\rangle T(t)^3 \left(Y(t)^2 - Y^{EQ}(t)^2\right) \ . \tag{2.4}$$

Changing the variables once more by defining $x = m_\chi/T$ and assuming that the decoupling occurred during radiation domination the time can be expressed through x via the Hubble constant as $x = \sqrt{2tH(x=1)}$. With these assumptions the Boltzmann equation can now be written as

$$\frac{dY(x)}{dx} = -\frac{\lambda(x)}{x^2}\left(Y(x)^2 - Y^{EQ}(x)^2\right) \ , \tag{2.5}$$

with $\lambda(x)$ being defined as

$$\lambda(x) := \frac{\sqrt{90} M_{Pl} m_\chi}{\pi \sqrt{g_{\text{eff}}}} \left\langle \sigma_{\chi\bar{\chi}\to f\bar{f}}\ v \right\rangle (x) \ . \tag{2.6}$$

Here we used $H(t)^2 = \frac{\rho_r(t)}{3M_{Pl}^2} = \left(\frac{\pi\sqrt{g_{\text{eff}}}}{\sqrt{90}\frac{T}{2M_{Pl}}} \right)^2$ which was obtained from the Friedman equation by inserting the relativistic energy density for bosons and fermions, respectively. The Planck mass is given by $M_{Pl} \approx 1.221 \times 10^{19}$ GeV.

In general, the above equation (2.6) needs to be solved numerically to obtain the freeze-out temperature T_f from which the abundance can be calculated. With a few approximations we are able to derive an analytic solution. We start by expanding the velocity-averaged cross section, where we only consider the leading s-wave contribution which is independent of the velocity. If we then consider the time of decoupling, the annihilation cross section can be estimated by a non-relativistic weak interaction which can be expressed in terms of

$$\sigma_{\chi\bar{\chi}\to f\bar{f}} \approx \frac{\pi\alpha^2 m_\chi^2}{sin_w^4 m_W^4} \ . \tag{2.7}$$

Setting the velocity to $v = \sqrt{\frac{2T}{m_\chi}}$ we arrive at

$$\left\langle \sigma_{\chi\bar{\chi}\to f\bar{f}}\ v \right\rangle_0 (x_{\text{dec}}) \approx \sqrt{\frac{2}{x_{\text{dec}}}} \frac{\pi\alpha^2 m_\chi^2}{\sin^4\Theta_W m_W^4} \ , \tag{2.8}$$

where Θ_w is the Weinberg angle and m_W the mass of the W gauge boson. Furthermore, it can be shown that $Y^{EQ}(x)$ decreases exponentially with $e^{-x_{\text{dec}}} \approx 10^{-12}$. We can rewrite equation (2.5) as

$$\frac{dY(x)}{dx} = -\frac{\lambda(x)}{x^2} Y(x)^2 \ . \tag{2.9}$$

The function $\lambda(x)$ has no strong dependence on the variation of the temperature so that it can be taken as roughly constant. The simplified Boltzmann equation (2.9) can now be solved by the ansatz $Y(x) = 1/\bar{Y}(x)$ which then leads to

$$\frac{1}{Y(x)} = -\frac{\lambda}{x} + \frac{1}{Y(x\to\infty)} \ . \tag{2.10}$$

In the limit of decreasing temperature $x \to \infty$ one obtains $Y_\infty = \frac{x_\infty}{\lambda(x_\infty)}$, where x_∞ should be sufficiently large to be able to decouple, but on the other hand should be sufficiently small to keep g_{eff} only slightly varying. For $g_{\text{eff}}(x_{\text{dec}})$ a value of 86.25 can be found for energies in the range of 5-80 GeV. As we now have specified the WIMP energy density at late times we can relate the energy density $m_\chi n(T_\infty)$ to the today's density $\rho_\chi(T_0)$. When the WIMPs decouple the number density decreases with $a^{-3}(T)$ and we get

$$\rho_\chi(T_0) = m_\chi \left(\frac{a_\infty T_\infty}{a(T_0) T_0} \right)^3 \frac{T_0^3}{T_\infty^3} n(T_\infty) = m_\chi \frac{1}{28} T_0^3 \frac{x_\infty}{\lambda(x_\infty)} \ , \tag{2.11}$$

where we have used $\frac{g_{\text{eff}}(T_0)}{g_{\text{eff}}(T_{\text{dec}})} = \frac{1}{28}$. For the relic density we can derive

$$\Omega_\chi h^2 = \frac{x_\infty}{28\lambda(x_\infty)} \frac{m_\chi T_0^3}{3M_{Pl}^2 H_0^2} \approx 0.12 \frac{x_{\text{dec}}}{28} \frac{\sqrt{g_{\text{eff}}}}{10} \left(\frac{50\ \text{GeV}}{m_\chi} \right)^2 \ , \tag{2.12}$$

where we have inserted $\lambda(x_{\mathrm{dec}})$ as given in equation (2.6) as well as the velocity-averaged cross section (2.8) and set $x_\infty \approx x_{\mathrm{dec}}$. If we assume an electroweak interaction with a weak coupling, then the dark matter particle receives a mass of the electroweak scale. This is often referred to as the WIMP miracle.

Instead of the dark matter mass, we can estimate the required cross section by directly inserting the function $\lambda(x_{\mathrm{dec}})$ and obtain

$$\Omega_\chi h^2 \approx 0.12 \frac{x_{\mathrm{dec}}}{28} \frac{\sqrt{g_{\mathrm{eff}}}}{10} \frac{2 \times 10^{-26}\ \mathrm{cm}^3 s}{\langle \sigma_{\chi\bar{\chi}\to f\bar{f}}\ v \rangle} \ . \tag{2.13}$$

This corresponds again to a weakly interacting particle with a mass in the GeV range. For a WIMP with a mass of for example 50 GeV we obtain a cross section of about 10 pb which is roughly the size of a cross section of a non-relativistic electroweak interaction. The fact that the scale of the dark matter mass is comparable to the scale of electroweak symmetry breaking is remarkable and makes the WIMP the most widely discussed cold dark matter candidate motivated by theory.
As a side remark two further classes of WIMPs exist which we are going to mention them shortly. On the one hand WIMPzillas show that the mass of a WIMP can be much larger than the weak scale and on the other hand SuperWIMPS as KK gravitons $G^1_{\mu\nu}$, gravitinos $\tilde{G}$ or axinos $\tilde{a}$ which can have much smaller cross sections than the ordinary WIMP [30].

A whole variety of experiments with different methods aim for an explicit discovery of a cold dark matter WIMP particle. We continue with providing an overview of these distinct search strategies.

2.4 Different Approaches to Search for Dark Matter

In this section, we want to focus on the different search strategies which were developed to discover particle dark matter. Thereby we concentrate mainly on the discovery potential for WIMPs. We start with a collection of indirect detection observatories before we move on to a short review of direct experiments and their underlying working principles [38]. Finally, we will expand our discussion to the prospects of dark matter searches at colliders and in particular at the LHC [6].

2.4.1 Indirect Detection

Indirect detection experiments search for remnants which were produced by the annihilation of two dark matter particles. The annihilation process is shown in Figure 2.5 by reading the diagram from left to right. The remnants are Standard Model particles and hence possible signals can be transmitted by a huge variety of particles like gamma rays, neutrinos, electrons, protons, positrons, antiprotons, deuterons as well as antideuterons [39]. One can use these particles to extract or constrain properties of the dark matter.
As WIMPs are assumed to be thermally produced and their abundance can be described by the decoupling from the thermal bath, they should still be able to annihilate at this present day into a pair of Standard Model particles. The discovery reach of a search for WIMPs mainly relies on their annihilation cross section and their local relic density. It is therefore advantageous to explore regions in the universe with a high dark matter abundance. Objects which are surrounded by large dark matter halos are for example the galactic center, the center of the Milky Way or dwarf spheroidal satellite galaxies. The problem is that these targets contain a large amount of ordinary matter which generate a huge spectrum of background radiation. This makes indirect detection extremely challenging and the astrophysical back-

grounds must be very well understood to become sensitive to the dark matter annihilation cross sections of the weak scale. We now want to give a small overview of some of the experiments which search for inconsistencies in the distributions of the Standard Model particles which might be emerging from dark matter annihilation.
A variety of different gamma ray experiments exists which require the knowledge of the dark matter distribution which often is among the leading uncertainties in the measurements. The Fermi-Large-Area-Telescope as well as the imaging atmospheric Cherenkov telescopes as HESS, MAGIC and VERITAS search for high energetic gamma rays. They can be produced by annihilation of the dark matter to quarks and gauge bosons with subsequent hadronization finally giving a continuous spectrum via pion decays or by direct annihilation into gamma rays providing a smoking gun signal. A new telescope CTA is set up which is expected to increase sensitivity by an order of magnitude compared to the prior generation.
A further search channel is provided by neutrinos. In this case the sun, as well as the earth, can be suitable objects to observe. As the dark matter particles might have scattered elastically with a nucleus of such a galactic object, it can have transferred enough momentum to be trapped in the corresponding gravitational potential. This could lead to a sufficient dark matter density to provide a WIMP source. Examples of neutrino telescopes searching for such signatures are Ice Cube, AMANDA or ANTARES.
Experiments like AMS or PAMELA search for charged cosmic-rays and antimatter such as electrons, protons or positrons. They might have been produced through cascade decays into secondary particles after the dark matter has annihilated into Standard Model particles.
If dark matter consists of primordial black holes, gravitational wave experiments as LIGO can be considered as indirect dark matter experiments.
References to the above experiments can be found in [38–40]. Furthermore, we can use the rather precisely measured CMB. Here the annihilation of two dark matter particles into highly energetic baryons at the time of the last scattering influences the temperature and polarization of the CMB which can be studied [41, 42]. In Section 5.3 we will show that the limits derived from the CMB indeed yield the strongest bounds coming from indirect dark matter searches.
We will only consider constraints extracted from the CMB spectrum and from the forecast of the performance of the CAT telescope [43] on the WIMP annihilation cross section as these are the only experiments which are in actual reach for our obtained interaction strength.

2.4.2 Direct Detection

Direct detection experiments search for interactions between dark matter and ordinary matter in an almost background free environment. They aim to observe elastic scattering of the dark matter particles with nuclei of the experiment. The interaction is schematically drawn in Figure 2.5 by reading it from the bottom to the top. In the corresponding detectors nuclear recoils are measured with different techniques which mainly rely on the measurement of ionization, phonons or scintillation. This is possible as the dark matter transfers energy to the nuclei in the elastic scattering which is then emitted as radiation. Typical recoil energies are about 1-100 keV for WIMPs. These energies are relatively small and if one considers the tiny scattering cross sections of the WIMPs, it occurs to be extremely challenging to discriminate possible signal events from backgrounds emerging from electric recoil interactions or neutrons faking nuclear recoils. Due to this reason direct detection experiments are stored in deep underground laboratories using the concrete as shielding against cosmic rays that could produce such energetic neutrons. The detectors need to be shielded from decay products of radioactive elements in the surroundings as well as from radiation emerging from the components of the experiment itself. In such reactions neutrons can be

produced which can fake a WIMP nuclear recoil. Most of the time neutrons perform multiple scattering with the active detector material and hence can be discriminated as background. Many experiments only perform their analysis with the inner part of their detector material, the so-called fiducial volume, which is shielded from backgrounds emerging from impurities in the detector. A huge variety of methods have been developed for the discrimination of signal and background events. Sometimes the signal is split into two components acting differently to nuclear and electron recoils which are often the dominant background.

One methodology to detect nuclear recoils is the use of cryogenic detectors which are operating at low temperatures. They measure the heat, or the phonons released by the dark matter interacting with an atom of the crystal. Examples of cryogenic detectors are CRESST, EDELWEISS or EURECA. Another class of experiments are detectors with noble liquids as xenon or argon looking for scintillation produced by a nuclear recoil. The strongest limits currently are given by the XENON1T experiment where a dual phase time projection chamber detects scintillation as well as ionization produced by particles passing through the detector. Further experiments of this kind are PandaX and LUX. Another approach to search for dark matter is to aim at a detection of modular variations of measured events over a background. As the earth orbits the sun the detector has a relative velocity to the dark matter halo. DAMA is an experiment which falls in this category and claims an observation of a measured annual modulation, but this has never been confirmed by any other experiment. Experiments as DRIFT make use of the motion of the solar system around the galactic center and are sensitive to directional measurements. Also bubble chambers as PICASSO are especially sensitive to spin-dependent interactions between WIMPs and fluorine atoms measuring phase transitions in the detector.

All the presented experiments, [38, 44] and references therein, rely on the elastic scattering of a WIMP with a target nucleus. The nuclear recoil rate can then be translated into a scattering cross section between the WIMP and the nucleus. This rate depends on the local dark matter abundance. If the profile of the dark matter halo is such that the density at the earth is small then the direct experiments lose sensitivity, whereas collider searches are independent of the dark matter halo. The detectors are sensitive to spin-dependent as well as spin-independent interactions. For spin-independent interactions the rate increases with the square of the atomic mass as a similar coupling to protons and neutrons is assumed. Whereas for spin-dependent interactions no enhancement with the atomic number is provided. This results in the fact that spin-independent interactions are better constrained.

All experiments which are not relying on the annular modulation basically follow a certain behavior. They have a maximal sensitivity in a WIMP mass range of 10-100 GeV, compare Figure 2.7 for a spin-independent interaction. Towards smaller WIMP masses these experiments lose sensitivity as the energy transfer of the dark matter particles becomes too small to detect a nuclear recoil as the kinetic energies are rather low as we consider cold dark matter. On the other hand, for larger WIMP masses the sensitivity decreases as well due to a decreasing number density which reduces the interaction rate.

Currently the experiments have the advantageous situation that an ideal detector is basically free from any backgrounds. However, for the future experiments with higher sensitivities a new challenge can arise in form of a neutrino background, the so-called neutrino floor, which is also displayed in Figure 2.7. This background is irreducible and caused by solar, atmospheric and supernova neutrinos, respectively. At low recoil energies the dominant background is due to solar neutrinos coherently scattering in the detector which can then be misidentified as WIMPs with masses of 5-10 GeV. For higher WIMP masses atmospheric neutrinos as well as the ones emerging from supernovae become the leading distortion, but they have cross sections orders of magnitude lower than the one for solar neutrinos which is about 5×10^{-45} cm^2. Hitting this neutrino background is not the end of direct detection experiments but it makes

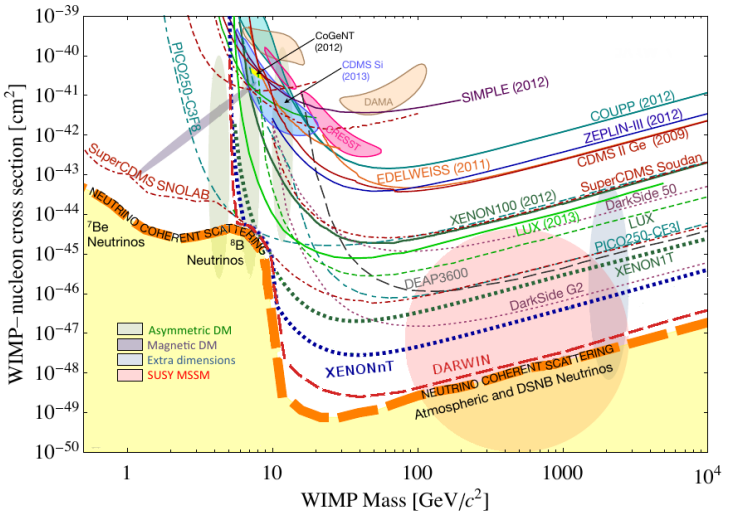

Figure 2.7: A selection of spin-independent WIMP-nucleon cross section limits (solid lines) and projections (dotted lines) for direct detection experiments. The shaded, enclosed regions show hints for a possible signal, whereas the purely shaded regions indicate preferred parameter spaces for a variety of models. The orange band represents the background from solar, atmospheric, and diffuse supernovae neutrinos. Figure taken from [44]

them way more challenging. Methods to circumvent this problem are either background subtraction, directional or annual modulation measurements.

2.4.3 Collider Searches

A priori dark matter searches at colliders seem slightly counter-intuitive as it is questionable if the dark matter has sufficiently strong interactions with ordinary matter to be produced in Standard Model particle collisions, as shown in Figure 2.5 if read from right to left. Moreover, it is unknown whether the center of mass energy required to produce the mass of a dark matter pair is kinematically available at hadron colliders like the LHC. As the dark matter is assumed to be long lived and coupled only very weakly to the Standard Model it should not interact with the detector. The only remaining signature is a Standard Model particle recoiling against missing transverse energy which could then be seen by the detector. This imbalance of transverse energy occurs because the dark matter pair is required to recoil against an object to be detectable as it itself passes the detector without any interaction, whereas the transverse energy needs to be conserved. Of course, the dark matter can be produced without any radiation, but then this event would just not be recorded. Nevertheless, due to several reasons these searches experience an increasing interest. The Standard Model backgrounds are rather well understood which allows for studies of the missing transverse energy spectra. Due to the assumption of dark matter production via thermal freeze-out in the early universe the velocity averaged annihilation cross section has been estimated to be approximately $\langle \sigma_{\chi\bar{\chi}\to f\bar{f}}\, v \rangle \approx 3 \times 10^{-26}\ \mathrm{cm^3 s^{-1}}$. Considering that the production cross section is of a comparable order, this should allow for sizable rates for collisions producing dark matter at colliders. Despite the opportunity to search for dark matter particles emerging from decay chains of long-lived particles as they might occur in supersymmetry we mainly focus our discussion on two scenarios which are the leading channels for WIMPs. The first is pair-produced dark matter with initial, intermediate or final state radiation. Here additional radiated particles are detected by the experiments and carry large transverse momenta which are not balanced by a signal in the opposite direction. These signals are called mono-X signatures where X can refer to jets, photons, Z /$W^{\pm}$ bosons or a Higgs. Typical backgrounds are Standard Model s-channel processes with a Z boson as mediator

producing a neutrino pair where additional particles are radiated off from the initial state. The second possibility is an extended sector allowing for a new heavy scalar particle to be produced which allows a resonant decay into the mediator of the dark sector and some Standard Model particles. An example for such a process could be the production of a heavy Higgs decaying into a Z boson and a pseudoscalar which further decays to dark matter. The advantage is that in this case the heavy Higgs as soon it is produced must decay as it is unstable leading to a resonant production of a heavy on-shell Higgs particle. In all these searches no excess has been found so far at the LHC and other colliders. At this point we want to stress that a discovery of a mono-X signal will not allow us to draw direct conclusions of all the properties of the dark matter particle. Hence further input from direct and indirect experiments as well as cosmological observations would be necessary. Another point which is worth mentioning is that even if collider searches seem to be promising for WIMP-like dark matter the cross sections for axions or sterile neutrinos are too small to be observable at the LHC. However, with the results obtained from mono-X searches we are still able to make a statement about the thermal production mechanism of dark matter.

During this thesis we want to work out for which type of mediators in a simplifies model collider searches yield the most constraining results and more precisely which mono-X channel is providing the strongest limits on our WIMP dark matter model. Therefore, we are going to discuss the potential of the different mediators in Section 2.6. Beforehand we work out the differences between effective field theories and simplified models.

2.5 From Effective Field Theories to Simplified Models

In the previous section, we have shown that there is a considerable variety of potential mono-X signatures of dark matter at the LHC. We continue by discussing the minimal constituents needed to build models which yield such signals. In doing so we need to find a balance between generality, meaning we try to keep the number of assumptions we put into our model as low as possible, and plausibility referring to consideration of consistency such as CP and flavor conservation or the existence of a perturbative, ultraviolet completion in accord with the Standard Model gauge group before the electroweak symmetry breaking. We begin with a theory that has the smallest amount of necessary new parameters and from there develop a more complete and in this sense a more consistent theory. This process is often referred to as the bottom-up approach starting with so-called effective field theories. This section we mainly build with the review found in [6].

2.5.1 Effective Field Theories

In an effective field theory only the dark matter particle is introduced as an additional degree of freedom as extension to the Standard Model Lagrangian. This represents the minimal approach to couple dark matter to the Standard Model particles. The mediator in this case is assumed to be too heavy and hence kinetically not accessible at a collider to become a propagating state. A famous example of an effective field theory is the Fermi interaction of four fermions in a beta decay of a neutron to a proton, an electron and an anti-electron neutrino. It turns out that the cross section in this interaction scales with the center of mass energy squared. Already at energies of 100 GeV the coupling is no longer unitary and must be replaced by a UV complete theory with the exchange of a W or Z boson.
The operators occurring in effective field theories can have mass dimensions larger than the renormalizable mass dimension four. In case of an effective field theory including dark matter, they contain only two additional parameters, the dark matter mass m_χ and a new energy scale Λ. There is a huge class of

effective operators describing couplings between dark matter and quarks or gluons. An example of a dimension 6 operator is given by the axial vector operator

$$\mathcal{O} = \frac{1}{\Lambda^2} \left(\bar{q}\gamma^\mu\gamma^5 q\right) \left(\bar{\chi}\gamma_\mu\gamma^5\chi\right) \ , \tag{2.14}$$

with χ being the fermionic dark matter particle. The study of different dark matter effective field theories leads to experimental limits on Λ depending on m_χ where the strongest limits are derived from operators including couplings of the dark matter to quarks and gluons. Another interesting option is the coupling between dark matter and gauge bosons as well as the Higgs. Then these particles produced at a collider can decay to dark matter pairs and one can obtain mono-V or mono-Higgs signatures. Moreover, dark matter can couple to the Standard Model via the so-called Higgs-portal which has been studied intensely for scalar dark matter [45]. This model is strongly constrained and only survives at the Higgs-pole where the dark matter mass is half the Higgs mass and the Higgs decays resonantly. Despite its widely constrained parameter space, this class of theories remains an attractive candidate because it is one of the simplest ways to connect dark matter to baryonic matter and furthermore, the interaction is renormalizable. In the fermionic case the portal can be expressed in terms of the following Lagrangian

$$\mathcal{O} = \frac{1}{\Lambda} H^\dagger H \bar{\chi}\chi \ . \tag{2.15}$$

Here the operator has mass dimension 5 and is hence no longer renormalizable. In the region where the dark matter mass is lighter than half the Higgs mass the branching ratio of Higgs decaying into invisibles is providing the strongest bounds, whereas in the other case the production is suppressed.
The strength of an effective theory is that bounds on all kinds of models classified by their effective operators can be set without requiring the knowledge of the UV complete theory. Nevertheless, the validity of this simplification needs to be checked. It turns out that effective field theories struggle with mainly two distinct difficulties. They partially fail to reproduce kinematic distributions from complete models and sometimes predict distributions which cannot be described by any meaningful fundamental theory. For a better understanding of these odds we investigate how effective operators emerge from a more complete theory. A fundamental theory to the axial vector operator in (2.14) could for example be obtained with a spin-1 particle V^μ which couples axially to dark matter and quarks

$$\mathcal{L}_{\mathcal{DM}} = \frac{m_V^2}{2} V^\mu V_\mu + g_q V^\mu \bar{q}\gamma_\mu\gamma^5 q + g_\chi V^\mu \bar{\chi}\gamma_\mu\gamma^5\chi \ . \tag{2.16}$$

Assuming an s-channel interaction of the two particles with a center of mass energy of $\sqrt{s}$ the matrix element of the propagator is given by

$$\mathcal{M} \propto \frac{g_q g_\chi}{m_V^2 - s} \ . \tag{2.17}$$

We can restore the effective coupling if the mass of the mediator m_V is much larger than the center of mass energy $\sqrt{s}$ as we can define

$$\frac{1}{\Lambda^2} = \frac{g_q g_\chi}{m_V^2} \ . \tag{2.18}$$

We can conclude that for mediators with masses around a few TeV an interaction between quarks and dark matter at the LHC is not accurately described by the contact interaction. This behavior is portrayed in Figure 2.8 where the kinematic distribution of the missing transverse energy $\not{E}_T$ is shown for various

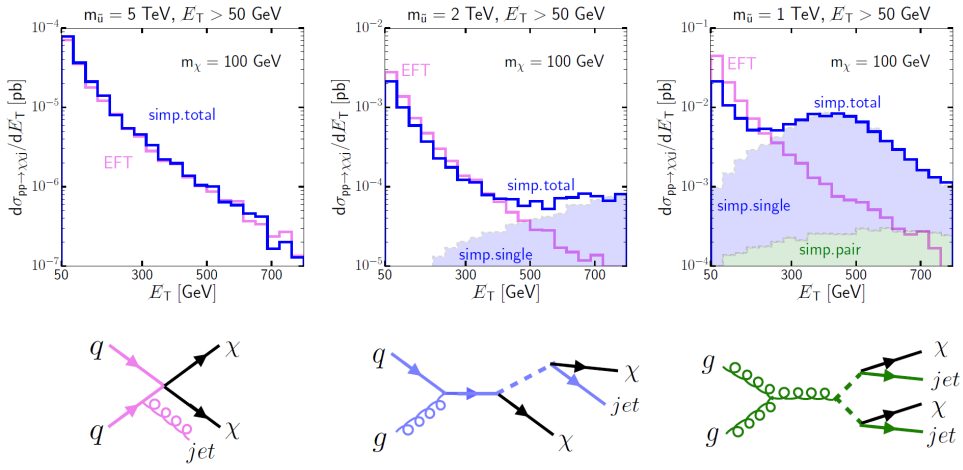

Figure 2.8: $\not{E}_T$ distributions for a simplified t-channel model in comparison to an effective field theory for a color charged, scalar mediator with different masses $m_{\tilde{u}} \in \{1, 2, 5\}$ TeV as well as the corresponding contributing Feynman diagrams for the t-channel contribution (pink), resonant mediator production (blue) and pair production of the mediator (green). Figure taken from [46].

mediator masses in terms of a t-channel simplified model. We want to present a toy model of a simplified model which we will derive in complete detail in the next section. Such a theory containing explicitly a t-channel mediator can be motivated for example by supersymmetry where a fermionic dark matter particle interacts via a $\tilde{u}$ mediator to up-type quarks [46]. Hence the mediator needs to carry a color charge. The effective interaction can be parametrized by the Lagrangian

$$\mathcal{L}_{\mathcal{DM}} = y_{\tilde{u}}(\bar{u}_R\chi)\tilde{u} + h.c. \; . \tag{2.19}$$

The generic t-channel contribution leading to a mono-jet signature is given by the process

$$u\bar{u} \to \chi\bar{\chi}g \qquad \text{while} \qquad ug \to \chi\tilde{u} \to \chi(\bar{\chi}u) \tag{2.20}$$

leads to a resonant production of an on-shell mediator, shown as the blue Feynman diagram where $\tilde{u}$ is represented by the dotted line. The prior interaction is shown in the pink diagram where the mediator $\tilde{u}$ has been integrated out as the state is too heavy to be produced on-shell at the LHC. The green Feynman diagram represents the pair production of the mediator decaying into dark matter and two jets which can be read as

$$gg/q\bar{q} \to g \to \tilde{u}\tilde{u}^\dagger \to (\bar{\chi}u)(\chi\bar{u}) \; . \tag{2.21}$$

For heavy mediators the effective Lagrangian of the mono-jet production can be written as a dimension six operator containing a four-fermion interaction as

$$\mathcal{L}_{\mathcal{DM},\text{eff}} = \frac{c_{u\chi}}{\Lambda^2}(\bar{u}_R\chi)(\bar{\chi}u_R) \; , \tag{2.22}$$

where we set the energy scale to match the effective theory with the complete supersymmetric theory to the mediator mass $\Lambda = m_{\tilde{u}}$. Hence, the coupling constant $y_{\tilde{u}}$ is expressed by the Wilson coefficient $c_{u\chi}$. This operator describes the t-channel and the single resonant production.
We finally want to mention that the $\not{E}_T$ distribution obtained by an effective field theory approach agrees

with the slightly more fundamental simplified t-channel model which takes the added mediator into consideration for large mediator masses, compare the left panel of Figure 2.8. This can be understood as the heavy mediators, here 5 TeV, cannot be on-shell as the center of mass energy of 13 TeV at the LHC is distributed among the partons in the proton. Therefore, the EFT yields a valid description of the differential cross section depending on the missing transverse energy which basically goes hand in hand with the distribution obtained from the simplified model. As the mediator tends to have a mass in the reach of the LHC, in this case 2 TeV, one can observe an enhancement due to a resonant on-shell production of the mediator in the spectrum towards larger $\not{E}_T$. On the other hand, for small $\not{E}_T$ the EFT provides still a rather good approximation. Decreasing the mediator mass once more to 1 TeV aside the increasing single resonant production a contribution from pair production of the mediator occurs, as can be seen in the right panel. In this case the assumption of small momentum transfer in the studied interaction is entirely broken and the EFT does no longer describe the correct spectrum of the kinematic distributions as seen at the collider. Hence it becomes necessary to consider more fundamental theories which take the mediator as an available degree of freedom into account.

We want to stress that even if the validity of the EFT breaks down at a certain mediator mass the sensitivity of the searches for dark matter only depends on the suppression scale Λ. The LHC loses sensitivity at Λ larger than a few TeV for effective dark matter operators due to the reason that the cross sections become too small if the couplings remain perturbative. This results in the requirement of more fundamental theories for processes with large momentum transfers compared to the corresponding mediator masses. Hence, EFTs are only valid in processes with small momentum transfers. Discarding events containing to high momentum transfers from the analysis is called EFT truncation. If the dark matter is mediated by the weak force, as assumed in the case of WIMPs, the kinematic distributions are not at all well modelled by the EFT and a new framework is required which are simplified models.
Even if for WIMP collider searches the EFT is not the proper toolkit it can still give relevant bounds for low energy processes as for the dark matter annihilation in the early universe or for direct detection experiments.

2.5.2 Simplified Models

In simplified models we interpret the mediator as an additional light propagating state accessible to the LHC besides the dark matter particle. More specifically all interactions including the mediator should be renormalizable, i.e. their mass dimensions have to be smaller than or equal to four. New parameters which occur due to the presence of the additional particle, influence the kinematic observables and therefore make searches for dark matter at colliders more challenging. Nonetheless, it is important to work these models out as there is no method for mapping bounds obtained from EFTs onto more complete models containing a light mediator. Moreover, EFTs rarely predict hard missing transverse energy spectra well, which in turn can be reproduced better by simplified models. Another motivation is given by the dark matter abundance where heavy mediators struggle to yield the measured relic density, whereas this is no difficulty for the light mediators.
An overview of various simplified models which are the basis of dark matter searches at ATLAS and CMS can be found in [47]. As an example, we want to have a closer look at s-channel mediators with couplings to quarks and dark matter. In the discussion of the origin of the effective theory we had already introduced the simplified model of an axial-vector mediator

$$\mathcal{L}^{V_5}_{\mathcal{DM}} = V^\mu \sum_q g_q \bar{q}\gamma_\mu\gamma^5 q + g_\chi V^\mu \bar{\chi}\gamma_\mu\gamma^5\chi \ , \tag{2.23}$$

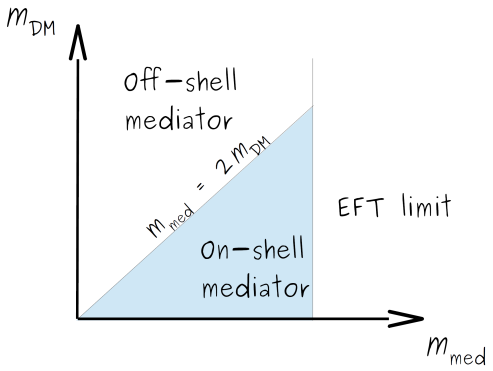

Figure 2.9: Sketch of the parameter space depending on the mediator as well as the dark matter mass in simplified dark matter models. Figure taken from [6].

where the vector mediator can be written as

$$\mathcal{L}^{V}_{\mathcal{DM}} = V^{\mu} \sum_{q} g_q \bar{q} \gamma_{\mu} q + g_{\chi} V^{\mu} \bar{\chi} \gamma_{\mu} \chi \ . \tag{2.24}$$

These spin-1 mediators are then required to couple with the same strength to all quark flavors to be consistent with minimal flavor conservation. The Lagrangian of a spin-0 scalar mediator ϕ can be written as

$$\mathcal{L}^{\phi}_{\mathcal{DM}} = \frac{1}{\sqrt{2}} \phi \sum_{q} g_q y_q \bar{q} q + g_{\chi} \phi \bar{\chi} \chi \ , \tag{2.25}$$

and in the case of a pseudoscalar A

$$\mathcal{L}^{A}_{\mathcal{DM}} = \frac{1}{\sqrt{2}} A \sum_{q} g_q y_q \bar{q} \gamma^5 q + g_{\chi} A \bar{\chi} \gamma^5 \chi \ . \tag{2.26}$$

The Yukawa-like coupling originates from the assumption of minimal flavor violation. Hence, in the case of spin-0 mediators in the s-channel the couplings of dark matter to the Standard Model are strongest to top quarks.

All of the above described simplified models are in principle entirely described by five parameters. These are the masses of the mediator M_{med} and the dark matter m_{χ}, the two couplings g_q and g_{χ} as well as the width of the mediator Γ_{med}. Expressing the width in terms of the other parameters, by applying the narrow width approximation, the simplified models can be characterized by the remaining four parameters only. The narrow width assumption is roughly valid for $\Gamma_{\text{med}}/M_{\text{med}} \lesssim 0.3$. As kinematic distributions often depend on the couplings in a rather simple way they are usually fixed to certain values and experimental bounds are hence displayed in the parameter space of the two masses as shown in Figure 2.9.

In this sketch three distinct regions can be specified. If the mediator mass is assumed to be very heavy the mediator cannot be produced on-shell at the collider and one obtains the effective field theory limit. Dark matter collider searches are not very promising in this regime as the production cross section is rather low for couplings respecting the perturbativity bound. The production of dark matter at colliders is suppressed in regions where $M_{\text{med}} < 2m_{\chi}$. In this case the mediator needs to go off-shell to produce dark matter. Thus it is more promising to directly search for the mediator itself than for a mono-X signal. There is a huge variety of such mediator searches decaying into Standard Model particles. An Example is a dark photon Z' search at LHCb in muon final states or in charm meson decays [48].

The most interesting region is where we achieve a resonant enhancement of the dark matter production at a collider as the mediator can be produced on-shell and then decays into a pair of dark matter particles. In this case the mass of the mediator must be larger than twice the dark matter mass, $M_{\text{med}} > 2m_\chi$. The LHC mono-X searches focus on this region which is marked blue in the sketch.
The disadvantage of this simplification is that a rescaling of the experimental results to models with different couplings is now no longer trivial. However, this problem can be approached by applying the narrow-width approximation to split the cross section of any mono-X signal into the production cross section of the mediator, the additional particle X and to the branching ratio of the mediator into the dark matter pair. This factorization can be performed in the on-shell region. Then bounds for models with an s-channel mediator can simply be obtained by rescaling the branching ratio for the studied model and the one used in the experimental analysis.
T-channel simplified models can be constructed where either a scalar mediator couples to color and then decays into a dark matter fermion and a quark, as it is assumed in the underlying model of Figure 2.8, or the dark matter carries a flavor charge known under the name of flavored dark matter. Compared to the s-channel there are additional mono-jet signals as the mediator can radiate gluons or decay into dark matter and a jet. A pair-produced mediator can then yield a signature of two jets and two dark matter particles. Further examples of simplified models are theories containing scalar dark matter particles or fermionic mediators [49, 50].
Like the effective field theories also the simplified models require a valid mapping of the complete theory to the more general model to provide relevant constraints. Even if the simplified models contain more information than the EFTs they can still miss some of the phenomenology of the fundamental dark matter theories as additional states or couplings are not considered. To avoid these problems, we try to aim for the construction of consistent simplified models which obey gauge invariance and perturbative unitarity in the allowed parameter space.
Although simplified models were originally introduced to solve the unitarity violation of effective field theories they can lose validity at high energies in some cases. This for example can be observed in s-channel mono-W searches with spin-1 mediators as well as in the t-channel along with colored scalar mediators. They require the existence of additional interactions to preserve unitarity. Moreover, axial vector mediators do not decouple from their longitudinal mode providing limits on the dark matter mass. Even if the couplings are perturbative due to a proper choice of the dark matter mass the cross section scales with the center of mass energy leading to a similar issue as the known unitarity problem within the Standard Model without a Higgs. This can be resolved by introducing a mechanism generating the mediator mass.
A last point we want to mention in this context is the requirement that the UV complete theory should be anomaly free in the Standard Model gauge group. For spin-1 mediators this leads to couplings of the mediator to leptons providing strong bounds from the searches of di-lepton resonances. Mediators which are constructed such that they only involve couplings to quarks therefore predict new states cancelling these anomalies. However, these additional particles often do not change the phenomenology of the model notably. Nevertheless, simplified models can restore unitarity in mono-jet searches up to very large energy scales.
Conserving gauge invariance after the breaking can be troublesome. An example would be a scalar or pseudoscalar s-channel mediator being a Standard Model singlet coupling to a pair of quarks as $\bar{q}q = \bar{q}_L q_R + \bar{q}_R q_L$ and $\bar{q}\gamma^5 q = \bar{q}_L q_R - \bar{q}_R q_L$, respectively. These interactions would violate the gauge symmetry before electroweak symmetry breaking, but they can be obtained from mixing of the mediator with the Standard Model Higgs. As the couplings to fermions are then inherited from the Higgs, minimal flavor violation is automatically implemented. Following this thought we can conclude that the production cross section obtains its leading contribution from gluon fusion via a top loop which results

in potentially strong mono-jet signals. Furthermore, couplings to gauge bosons should be present leading to mono-V signatures. While this sounds rather promising in the first place there is the drawback that all these potential mono-X signals need to be small due to the measured Higgs branching ratios. For dark matter particles with masses below half the Higgs mass the branching ratio of Higgs into invisibles $\mathrm{Br}(h \to \text{invisible} < 0.23)$ [51,52], provides strong restrictions as we will show later. Even for masses above this threshold, limits from the Higgs signal strengths which we will discuss in Section 4.1 lead to small mixing angles. To put all this information together, in a simplified model with Higgs mixing obeying gauge invariance, the strongest bounds are given by Higgs physics instead of mono-X searches.
Extending the Standard Model by a second Higgs doublet allows the mediator to obtain its couplings to the Standard Model particles from the second Higgs doublet which softens the restrictions. This possible extension is attractive as the second Higgs doublet contains a heavy, neutral scalar and a pseudoscalar degree of freedom, besides two charged states, and naturally ensures CP-conserving interactions between the pseudoscalar mediator and the Standard Model fermions. One argument for the increasing interest in two Higgs doublet simplified models arises from the existence of additional signatures. The heavy scalar Higgs can for example decay into the pseudoscalar mediator decaying further into a dark matter pair as well as a Z boson or a Standard Model Higgs leading to enhanced mono-Z and mono-Higgs signals, respectively.
We started with an almost model independent effective field theory approach to provide a description of the interaction between dark and baryonic matter and from there derived the framework of simplified models reflecting the underlying phenomenology before we gave an overview of different extensions motivated by theoretical principles. These extended models on the other hand could have been also derived from a so-called top-down approach where one starts with an UV complete theory and then maps it onto a simplified model. An example is the next-to-minimal super-symmetric Standard Model Higgs sector which can be mapped to a simplified model consisting of two Higgs doublets and a spin-0 mediator being a singlet under the Standard Model gauge group [33].

After we have given arguments why the treatment of dark matter searches at colliders should be following the approach of simplified models we continue with a discussion of the various possible classes of mediators which are the link between the dark sector and the Standard Model. As we have already started to present options how one can implement such mediators in simplified models in a gauge invariant way, we want to give a slightly more detailed overview of UV completions in the end of this chapter in Section 2.7.

2.6 Possible Mediators

In a simplified model, the particle transmitting the interaction is considered explicitly. A whole variety of possible mediators between the Standard Model and the dark sector exists. They all have distinct properties and therefore they all behave differently under the various searches. In this section we want to elaborate for which type of mediator a collider search is most promising.
These mediators most likely must be extensions to the Standard Model as links to the dark sector via the Higgs portal or weak bosons are strongly constrained. The Higgs portal for example only survives direct detection bounds in a region where the dark matter mass is exactly half the Higgs mass. Hence, we need a new particle present in interactions connecting dark matter and the Standard Model. As we require the mediator to be able to decay into a pair of two dark matter fermions, the mediator itself can be either a spin-1 or a spin-0 particle. Moreover, spin-1 mediators can transform as vectors or axial-vectors under parity, whereas spin-0 mediators can be scalars or pseudoscalars. Due to the strong constraints to flavor

changing neutral currents spin-1 mediators are expected to have universal couplings to the Standard Model quarks and leptons with identical electric charges. These couplings lead to substantial limits from di-jet measurements as well as di-lepton resonance searches. The same does not hold true for spin-0 mediators as their couplings are suppressed by their masses due to the Yukawa couplings. We start our review with the vector mediator shown in the left plot of Figure 2.10.

Vector Mediator

For dark matter masses above 10 GeV the most robust limits stem from direct detection experiments. The shape of these restrictions is influenced by the decreasing number density as well as the cut-off from the momentum transfer in the scattering process. They can exclude cross sections as small as 10^{-46} cm^2 at their highest sensitivity. Due to the limited sensitivity of the detectors to the nuclear recoil energies of the dark matter scattering, the strongest bounds for light dark matter (below 10 GeV) come from di-jet searches. This fact can be understood because the mediator in an s-channel process can always decay back into the quarks and gluons from which it was produced in the first place. This interaction has no dependence on the dark matter mass itself. Di-jet searches are however limited for low mass resonances due to high QCD backgrounds. Furthermore, the strong limits from di-jets show that a sizable mono-X signal can only be expected if the coupling to the dark matter of the mediator is way stronger than the one to quarks. This would lead to the situation that the mediator would mostly decay invisible if it is on-shell mediators and the mass of the dark matter pair is smaller than the mediator mass. In this case mono-X signatures could dominate di-jet measurements, whereas for off-shell mediators only visible decays are possible, which leads to the fact that the most stringent bounds emerge from the di-jets.
The collider searches for missing transverse energy are almost within reach of the results from the di-jet measurements in case of the CMS mono-jet search. For high dark matter masses these mono-X searches at the LHC lose sensitivity compared to direct detection experiments as the LHC does not provide the energy required for the pair production of a WIMP. On the other hand, direct detection experiments struggle with low masses as the momentum transfer is too small to be registered. The mono-X searches at the LHC provide only the limits shown in Figure 2.10 if the dark matter couples to gluons and quarks via the vector mediator and the dark matter abundance is as expected. If the dominant coupling is to color neutral states such as leptons, they are suppressed by the lepton masses. Limits from direct detection experiments such as CRESST-II and CDMSlite do not play an important role in constraining dark matter models with vector mediators. A common feature we can see for both spin-1 mediators is that the different mono-X searches follow the same hierarchy where mono-jets provide the strongest bounds followed by mono-photon and mono-Z signatures which we are going to discuss more in Chapter 6.

Axial-Vector Mediator

Comparing the axial-vector to the vector mediator, one directly observes that the direct detection experiments no longer yield any relevant restrictions. The underlying reason is that the matrix element of the scattering between a WIMP and a nucleus of the experiment scales with the velocity of the dark matter. As the WIMPs are assumed to have non-relativistic velocities of the order of $v = 10^{-3}$c, the amplitude is about six orders of magnitude smaller than for the case of a vector mediator. Moreover, the axial coupling is spin-dependent which leads to a reduction of the atomic number of the nucleus used in the detectors. Therefore, the best limits over the entire WIMP mass range are given by di-jet searches followed by a variety of mono-X searches performed by CMS. For masses above 10 GeV several indirect

searches provide exclusion bounds, but they are again negligible compared to the ones coming from the di-jets. These searches are performed in the experiments PICASSO, PICO-60, Super-K and IceCube.

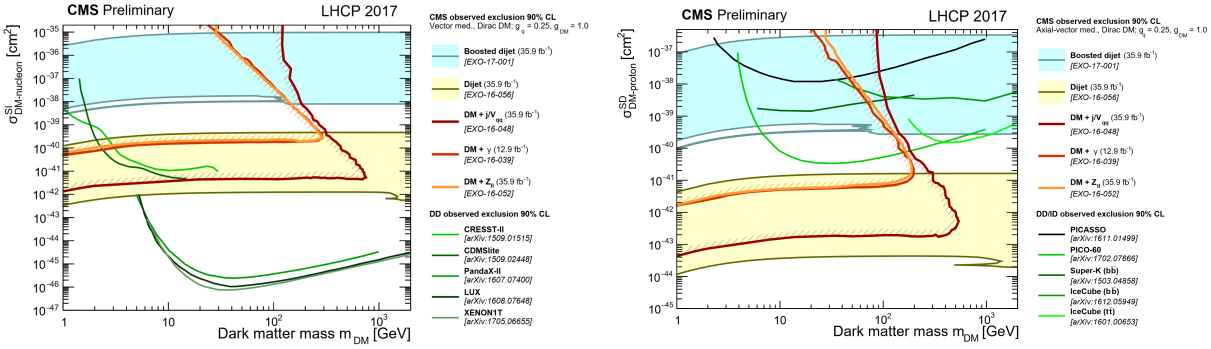

Figure 2.10: Left: Comparison of CMS results at 90 % C.L. for a vector mediator to exclusion limits from direct detection experiments XENON1T 2017, LUX 2016, PandaX-II 2016, CDMSLite 2015 and CRESST-II 2015 in the $m_{\mathrm{DM}} - \sigma_{\mathrm{SI}}$ plane. Right: Comparison of CMS results at 90 % C.L. for an axial-vector mediator to exclusion limits from indirect detection experiments PICASSO, PICO, IceCube with $t\bar{t}$, $b\bar{b}$ annihilation channels and Super-Kamiokande ($b\bar{b}$) in the $m_{\mathrm{DM}} - \sigma_{\mathrm{SD}}$ plane.
The CMS contours are obtained for Dirac dark matter with couplings $g_q = 0.25$ and $g_{\mathrm{DM}} = 1.0$ without including constraints from the relic density. The absolute exclusion potential as well as the relative strength of the various CMS searches depend strongly on the chosen coupling and model scenario. Figures taken from [53].

Scalar Mediator

Like for the vector mediators, the strongest bounds for dark matter masses above 10 GeV for scalar mediators are obtained by direct detection experiments, compare left the plot of Figure 2.11. On the contrary, for lighter dark matter the searches for missing transverse energy provide better limits than a variety of direct detection experiments such as CRESST-II and CDMSLite. Di-jet and di-lepton searches are suppressed by the mass of the leptons or the light quarks due to their Yukawa-like couplings and hence do not provide any relevant constraints. It is worth mentioning that it is rather challenging to create a complete self-consistent model with such light dark matter with pure scalar couplings. As we will show in Section 4.1 scalar couplings in a two Higgs doublet model are further constrained by a fit to the Higgs signal strength measurements. Nevertheless, for light dark matter (below 10 GeV) collider searches are an important tool to constrain the relevant parameter space for models with scalar mediators.

Pseudoscalar Mediator

In the case of a pseudoscalar mediator neither direct detection experiments nor di-jet searches can provide any considerable bounds. The underlying reasons are that the cross sections are velocity suppressed as well as they do not receive an enhancement from the atomic number of the nucleon, as it was the case for the axial-vector mediators. Moreover, the spin-0 particles have no vector-like couplings to the fermions so that they are suppressed by their light masses. Hence the only constraints come from indirect detection experiments such as Fermi-LAT. Such constraints are orders of magnitudes smaller than those from collider searches for dark matter with WIMP masses, compare the right plot of Figure 2.11. This makes this class of mediators particularly interesting for mono-X studies at the LHC and from now on we will focus our study on simplified models containing pseudoscalar mediators.

Having identified the mediator for dark matter collider searches, we now need to think about ways to

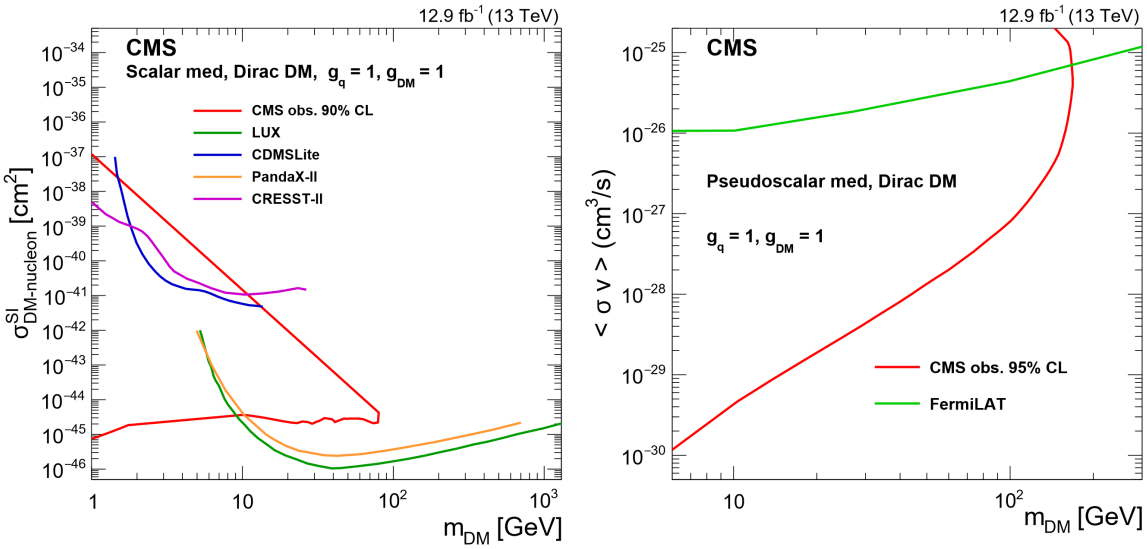

Figure 2.11: Left: Comparison of the CMS result at 90 % C.L. for a scalar mediator to exclusion limits from direct detection experiments LUX, PandaaX-II, CDMSLite and CRESST-II in the $m_{\mathrm{DM}} - \sigma_{\mathrm{SI}}$ plane. Right: Comparison of the CMS result at 95 % C.L. for a pseudoscalar mediator to the exclusion limit from the velocity-averaged dark matter annihilation cross section upper limit from the indirect detection experiment Fermi-LAT. Comparable limits from direct detection experiments are absent as the scattering cross section is suppressed at non-relativistic velocities for a pseudoscalar mediator.
The red solid line shows the CMS exclusion contour for the mono-jet search at 12.9 fb^{-1} of 13 TeV data in case of Dirac dark matter with couplings $g_q = 1.0$ and $g_{\mathrm{DM}} = 1.0$ without including constraints from the relic density. The absolute exclusion potential of the two CMS searches depends strongly on the chosen coupling and model scenario. Figures taken from [54].

add a pseudoscalar to the Standard Model in a gauge invariant way. We already started this discussion during the review of the properties of simplified models and we will continue it in the next section.

2.7 Extending the Standard Model by a Pseudoscalar

As we have just worked out, collider searches reach their full potential by setting constraints on simplified models with pseudoscalar mediators. The Standard Model does not contain such a degree of freedom which means that we must extend it by this new particle. Beyond Standard Model theories like supersymmetry naturally contain such a pseudoscalar. In the phenomenological study of extensive theories containing many additional parameters, the use of simplified models becomes very handy as they only take those particles into consideration that are relevant for the connection to the dark matter. In the review of simplified models, we have pointed out the importance of a consistent implementation of the pseudoscalar by respecting the invariance of all the Standard Model gauge symmetries.
We have already seen that seemingly renormalizable simplified models with a gauge singlet pseudoscalar mediator can be troublesome regarding unitarity violating amplitudes, which emerge from breaking the electroweak symmetry. This can be explained by the fact that in a simplified model, additional states which not directly contribute to the gate to the dark sector are neglected. The couplings in these models should therefore be interpreted as derived from a gauge invariant scalar sector inherited from the additional particles. Due to electroweak precision bounds obtained from complete theories the masses of these particles are restricted as we will show in Chapter 4. The existence of these particles can lead to new specific signatures as well as to an enhancement of some of the mono-X signals, which are often dependent on the way the gauge invariance of the pseudoscalar coupling is regained. We want to discuss

the signatures occurring in simplified models with a pseudoscalar mediator which are universal for a wide class of UV complete theories. Two different approaches of a gauge invariant implementation of a pseudoscalar will therefore be presented.

We start by extending the Standard Model by one pseudoscalar mediator A which is supposed to be a singlet under all Standard Model gauge symmetries. For the dark matter candidate, we simply take a Dirac fermion χ. The corresponding Lagrangian describing the interaction of the mediator with quarks $Q_i = (u_i, d_i)$, $q_i \in \{u_i, d_i\}$ and leptons $L_i = (\nu_i, l_i)$, l_i (where i represents the flavor index) and the dark matter can then be written as

$$\mathcal{L} = \sum_{i,j=1}^{3} y_{ij}^{q} \frac{A}{\Lambda} \bar{Q}_i \gamma_5 q_j H + \sum_{i,j=1}^{3} y_{ij}^{l} \frac{A}{\Lambda} \bar{L}_i \gamma_5 l_j H + c_s A \bar{\chi} \gamma_5 \chi + h.c. \,. \tag{2.27}$$

We assume Yukawa-like couplings to the Standard Model and furthermore require the presence of the $SU(2)_L$ Higgs boson H to ensure gauge invariance of the interactions with the baryonic fermions. It is worth mentioning that the couplings of the mediator to the dark matter are renormalizable, but the coupling to quark and leptons are suppressed by an energy scale of new physics Λ because these interactions are of mass dimension five. The scale Λ is normally linked to the mass of the additional heavy states which are integrated out. Examples of such states are color-charged fermions as well as inert scalar doublets which - due to their non-observations at colliders - set the new energy scale to rather high values. From this fact a suppression of the production of the pseudoscalar mediator can be concluded. This can be better understood as follows: If the Higgs takes on its vacuum expectation value v, the coupling to the quarks read as $y_{ij}^{q} \frac{v}{\Lambda}$. If the Yukawa couplings y_{ij}^{q} are comparable to the Standard Model ones, then the cross section of the A production is a factor of $\frac{v}{\Lambda}$ smaller than the Higgs production. Due to the Yukawa-like coupling the interaction with top-quarks should provide the leading contribution to the production cross section via gluon fusion at the LHC. The branching ratio of the mediator into dark matter should yield the primary decay channel because the coupling is not suppressed by Λ and c_s is considered to be $\mathcal{O}(1)$. The sub-leading branching fraction should be the decay into a pair of tops if the mediator mass is sufficiently large, but this process is suppressed by the ratio $\frac{v}{\Lambda}$ like in the case of the production. As this extension is rather minimal in the sense of added particles it is no surprise that this simplified theory does not yield any new dark matter signatures besides the already discussed initial and final state radiation.

This is different in the second example which we want to introduce, where we extend the Standard Model by an additional $SU(2)_L$ Higgs doublet containing a pseudoscalar particle. This can be expressed by the following Lagrangian where we assumed a coupling of type II to Standard Model fermions which is an arbitrary choice and we will generalize to type I in a later discussion

$$\mathcal{L}_{\text{simp}} = \sum_{i,j=1}^{3} y_{ij}^{u} \bar{Q}_i H_1 u_j + \sum_{i,j=1}^{3} y_{ij}^{d} \bar{Q}_i H_2 d_j + \sum_{i,j=1}^{3} y_{ij}^{l} \bar{L}_i H_2 l_j + c_\chi \frac{H_1^\dagger H_2}{\Lambda} \bar{\chi}\chi + c_5 \frac{H_1^\dagger H_2}{\Lambda} \bar{\chi}\gamma_5\chi + m_\chi \bar{\chi}\chi + h.c. \,, \tag{2.28}$$

where we added an additional mass term which we will discuss when we study the mechanism generating the mass of the dark matter particle in Chapter 3. In comparison to the gauge singlet extension, the couplings to the dark matter particles are now suppressed, whereas the couplings to the Standard Model fermions become renormalizable. Furthermore, the restrictions on Λ due to the existence of new states are weakened as they neither need to be charged under $SU(2)_L$ nor under color. This leads to a larger production cross section which can become even larger than the Higgs production rate for certain sets of

parameters. The branching ratio of the pseudoscalar into dark matter $BR(A \to \bar{\chi}\chi)$ on the other hand can, in particular for light mediators below the top threshold, remain the dominant one. This results from the Yukawa-like couplings of the Standard Model fermions to the mediator which are inherited directly from the Higgs. Therefore, these branching ratios scale with the small masses of the light fermions as m_f/v. The additional Higgs doublet provides four new degrees of freedom, which next to the pseudoscalar are a heavy, scalar Higgs and two charged Higgs particles. These allow for a rich phenomenology and hence many interesting dark matter signatures which can be searched for at colliders. The above Lagrangian contains a scalar c_χ as well as a pseudoscalar c_5 coupling to dark matter, which are both complex as long as we do not explicitly require CP-conservation. Further operators constructed out of two times the same Higgs doublet $H_i^\dagger H_i \bar{\chi}\chi$ do not provide pseudoscalar couplings. They mainly influence the results of direct detection exclusion limits and are discussed in this scope but neglected otherwise. They can be argued to be non-existent by implying a new softly broken symmetry under which the Standard Model singlets $H_u^\dagger H_d$, $\bar{\chi}\chi$, $\bar{\chi}\gamma_5\chi$ carry some charge. This symmetry needs to be softly broken as we will derive later: An additional mass term of the form $m_\chi \bar{\chi}\chi$ is required to assure one recovers the right relic abundance and this term carries a charge. Flavor physics provides the underlying idea of the symmetry used in this simplified model as the motivation is given by the Froggatt-Nielsen mechanism [55] which in general aims to describe the mass hierarchy among the generations of fermions. In such a model, the quarks and fermions would carry charges scaling with their masses and the lighter fermions would require higher order insertions of the $H_u^\dagger H_d$ operator, compare [56] and Chapter 3. Combining the fermion mass hierarchy and the dark matter production in a simplified model with a pseudoscalar framework remains an interesting task for the future. We next want to draw our attention to possible UV completions of the above two Higgs doublet simplified model.

2.7.1 UV Completions of the Two Higgs Doublet Simplified Model

For the above simplified model, we have seen that the interaction between the pseudoscalar mediator and the dark matter is suppressed by the energy scale where the new physics occurs in the extension by a second Higgs doublet. We want to present two possible UV completions which can lead to these effective couplings. The additional particles must be heavy compared to the Standard Model particles, the scalar and pseudoscalar components of the two Higgs doublets as well as the dark matter particle. In the first example we introduce a Standard Model singlet pseudoscalar a which has a mixing with the $H_u^\dagger H_d$ combination and deal as the mediator to dark matter

$$\mathcal{L} = \sum_{i,j=1}^{3} y_{ij}^u \bar{Q}_i H_u u_j + \sum_{i,j=1}^{3} y_{ij}^d \bar{Q}_i H_d d_j + \sum_{i,j=1}^{3} y_{ij}^l \bar{L}_i H_d l_j + \kappa a H_u^\dagger H_d + c_a a \bar{\chi}\gamma_5\chi + h.c. \,. \tag{2.29}$$

This model has an exciting phenomenology due to the presence of two pseudoscalars which allow for a wide range of specific signatures such as mono-Z and mono-h signals which are in detail discussed in [14]. A slightly more complicated dark sector is presented in the second example, where an additional electroweak fermion doublet $\psi = (\chi^+ \chi^0)$ assures the UV completion

$$\mathcal{L} = \sum_{i,j=1}^{3} y_{ij}^u \bar{Q}_i H_u u_j + \sum_{i,j=1}^{3} y_{ij}^d \bar{Q}_i H_d d_j + \sum_{i,j=1}^{3} y_{ij}^l \bar{L}_i H_d l_j + c_1 \bar{\psi} H_u^\dagger \chi + c_2 \bar{\psi} \tilde{H}_d \chi + h.c. \,. \tag{2.30}$$

This often occurs in doublet-singlet dark matter models, see e.g. [57]. Each of these UV completions predicts their own model-specific signatures which allow us to distinguish them. Nevertheless, in the scope of our study we want to focus on universal signatures which arise in all pseudoscalar mediator

models which can be mapped to the simplified model (2.28).

We have motivated the importance of studying the phenomenology of a pseudoscalar simplified model, where we extend the Standard Model by a second Higgs doublet, from the theoretical as well as from the experimental perspective. Hence, we will continue with a review of Two Higgs Doublet Models (2HDM) after shortly presenting the motivation of our simplified model in terms of the flavon theory [56].

3 Construction of a Consistent Simplified Dark Matter Model

All theories including a description of the behavior of dark matter require an extension of the Standard Model Lagrangian. In particular, a coupling between the dark sector and the baryonic particles needs to be introduced. As the model we study in this thesis was originally motivated by flavor physics the corresponding interaction falls in the class of so-called Higgs portals where a spin-0 particle acts as the mediator. The Froggatt-Nielsen mechanism [55] is an attempt to describe the mass hierarchy in the fermion sector by adding an additional flavor symmetry to the Standard Model. Only the top quark Yukawa coupling is considered as a renormalizable operator and all the other couplings emerge from an effective field theory with higher order operators of the type [56]

$$\mathcal{O}_{FN} = y \left(\frac{S}{\Lambda}\right)^n \bar{Q}_L H q_R \quad . \tag{3.1}$$

One can achieve natural values for the coupling strengths y by choosing the ratio between the vacuum expectation value of the Froggatt-Nielsen scalar $\langle S \rangle = f$ and the energy scale Λ of new physics as well as the number of insertions n of the flavon S accordingly. As soon as the flavon obtains its vev at a certain energy scale f the flavor symmetry breaks. In this mechanism neither the breaking scale f nor the new physics scale Λ are fixed by the theory. The flavor breaking scale can be related to the electroweak scale if one assumes $S/\Lambda = H^\dagger H/\Lambda^2$ [56]. In this case the combination $H^\dagger H$ is a singlet under all Standard Model symmetries. Hence, the number of insertions of the flavon n is not fixed by the flavor symmetry but set arbitrarily. One can overcome this problem by considering a model with two Higgs doublets. In this class of models, one can construct the flavon out of the two doublets coupling to the up- and down-type quarks, respectively, and obtains the operator $H_u H_d/\Lambda^2$. This operator has the advantage that it can carry an additional symmetry even though it is a singlet under the known Standard Model symmetries. Moreover, the flavor breaking scale is now set to the electroweak scale and Λ is expected to be in the TeV range.

We choose this operator as the portal to the dark sector and introduce a dark symmetry which only affects the dark matter and the above operator. This forbids the combinations of same flavor Higgs doublets $H_i H_i/\Lambda^2$ with $i \in u, d$. As we will show later this is interesting in the context of dark matter as these terms only contribute to scalar couplings which are extremely restricted by direct detection experiments as well as a global fit to the Higgs signal strength measurements. More importantly this symmetry ensures that the dark matter only couples to the extended Higgs sector. This for example avoids exclusive interactions with the Standard Model Higgs which are again strongly constrained by Higgs portal studies.

Besides the portal to the dark sector we also need a dark matter candidate. We choose the dark matter χ to be fermionic as it is suggested by the underlying mechanism. Thereby the choice of a Dirac or Majorana particle does not play a major role as this choice only varies some results by a factor of two

if the dark matter candidate is its own anti-particle. When we started to construct the simplified dark matter model we only considered the following interaction

$$\mathcal{L}_{DM} = c_\chi \frac{H_u H_d}{\Lambda} \bar{\chi}\chi \ . \tag{3.2}$$

We assume that the leading production mode of dark matter results from a trilinear coupling where one of the Higgs particles acquires its vacuum expectation value and the second one decays into a pair of dark matter fermions. The quartic couplings are suppressed by an additional phase space factor. With the above Lagrangian only scalar interactions are obtained if one considers the Hermitian conjugated terms as well. During this thesis we show that it is impossible to reproduce the relic density with exclusive scalar interactions if one respects the bounds from direct detection experiments as well as the limits from the Higgs signal strengths fit. One ad hoc solution to this problem is to introduce an imaginary coupling constant. This so obtained pure pseudoscalar interactions would allow to obey most of the discussed constraints. As such interactions would violate CP, but as we require CP-conservation in the scalar potential, we do not consider this as an attractive solution. It should be mentioned that CP-violating couplings can open an entirely new class of models with exciting phenomenology. For example, aiming at an explanation of baryogenesis.
As we are interested in receiving CP-conserving pseudoscalar couplings we add the following term to the Lagrangian

$$\mathcal{L}_{DM,\gamma_5} = c_5 \frac{H_u H_d}{\Lambda} \bar{\chi}\gamma_5\chi \ , \tag{3.3}$$

where $\gamma_5 = i\gamma^0\gamma^1\gamma^2\gamma^3$ is a combination of the four Dirac-matrices. This link between the Standard Model and the dark sector naturally provides CP-conserving pseudoscalar couplings. Furthermore, no arguments are prohibiting the existence of this operator if one considers the dark matter to be a fermion. As discussed above this coupling could be as well imaginary resulting in CP-violating scalar interactions which are again restricted by direct detection. Hence, we reach a starting point to study the obtained simplified model with an additional Higgs doublet containing a pseudoscalar mediator. A widespread and straightforward framework to extend the Standard Model to our needs are the so-called two Higgs doublet models which are well motivated by supersymmetry. The most important and relevant properties of two Higgs doublet models will be discussed in the following sections.

3.1 Review of the Two Higgs Doublet Model

The Standard Model of particle physics contains one complex Higgs doublet which reproduces the experimental data rather well. Nevertheless, there is still some space for extensions of the Higgs sector by adding an additional singlet field or a second $SU(2)_L$ doublet. Extending the Standard Model by a second Higgs doublet leads to a rich phenomenology, but one must be careful not to violate constraints from both experiments and theory. Two important constraints, which will set bounds on the allowed parameter space of our model, are derived from the so-called ρ parameter and the absence of Flavor Changing Neutral Currents (FCNCs). The prior gives a measure for the ratio of the $W^\pm$ & Z boson masses and is defined as

$$\rho = \frac{M_W^2}{M_Z^2 cos^2\Theta_W} \ . \tag{3.4}$$

The ρ parameter in the Standard Model is given by the Higgs structure and at tree-level predicted to be one. This coincides well with the experimentally measured data where ρ is indeed very close to one. In extended theories the ρ parameter depends at tree-level as follows on the number n of scalar multiplets ϕ_i with weak isospins I_i, weak hypercharges Y_i and the vacuum expectation values of the neutral components v_i as in [58],

$$\rho = \frac{\sum_{i=1}^{n} \left[I_i(I_i+1) - \frac{1}{4} Y_i^2 \right] v_i}{\sum_{i=1}^{n} \frac{1}{2} Y_i^2 v_i} \ . \tag{3.5}$$

Hence, $SU(2)$ singlets with $Y = 0$ and $SU(2)$ doublets with $Y = \pm 1$ are valid extensions by conserving $\rho = 1$ as they both fulfill $I(I+1) = \frac{3}{4} Y^2$. There exist further models with larger representations satisfying $\rho = 1$, but these representations lead to more complicated Higgs sectors.

The second constraint which needs to be respected is the existence of FCNCs. In the Standard Model these interactions are automatically vanishing at tree-level as the couplings between the fermions and the Higgs can be diagonalized as they are rotated in the mass eigenbasis. This does not necessarily hold true for extended Higgs sectors, but we will show in the proceeding of this work that under the assumptions of specific symmetries they can be canceled at tree-level. But before we address this problem, we first need to set the basis by studying the Higgs potential and the corresponding particle content of the two complex Higgs doublets.

Nevertheless, we shortly want to mention the main motivation for the study of the two Higgs doublet model besides the attractive feature of conserving the ρ parameter. They are well motivated by supersymmetric theories where they occur naturally to cancel anomalies and provide mass to quarks of one of the two flavor families. Moreover, two Higgs doublet models can partially fill the gap of the missing explanation of baryogenesis. Here, the generation of a sufficient amount of baryon asymmetry is possible due to the extended mass spectrum allowing more sources of CP-violation. The LHC should be within reach of a large set of the parameter space of two Higgs doublet models.

The Scalar Potential of the Two Higgs Doublet Model

The most general scalar potential of the two Higgs doublet model has a rich vacuum structure and contains CP-conserving, CP-violating as well as charge-violating minima. There exists a total of 14 renormalizable operators with mass dimension ≤ 4 which can be constructed from the two Higgs doublets H_1 and H_2 respecting the $SU(2)_L \times U(1)_Y$ gauge symmetry. The potential can then be written as

$$\begin{aligned} V_{\text{2HDM}} = {} & \mu_1 H_1^\dagger H_1 + \mu_2 H_2^\dagger H_2 - \left(\mu_3 H_1^\dagger H_2 + h.c. \right) + \lambda_1 \left(H_1^\dagger H_1 \right)^2 + \lambda_2 \left(H_2^\dagger H_2 \right)^2 \\ & + \lambda_3 \left(H_1^\dagger H_1 \right) \left(H_2^\dagger H_2 \right) + \lambda_4 \left(H_1^\dagger H_2 \right) \left(H_2^\dagger H_1 \right) + \left[\lambda_5 \left(H_1^\dagger H_2 \right)^2 + h.c. \right] \\ & + \left[\lambda_6 \left(H_1^\dagger H_1 \right) \left(H_1^\dagger H_2 \right) + h.c. \right] + \left[\lambda_7 \left(H_2^\dagger H_2 \right) \left(H_1^\dagger H_2 \right) + h.c. \right] \ , \end{aligned} \tag{3.6}$$

where μ_3 and $\lambda_{5,6,7}$ can be in general complex leading to the 14 parameters in the potential which can be reduced to 11 due to redefinition of the corresponding basis [58].

In our study we consider a CP-conserving two Higgs doublet model with an additional softly broken $\mathbb{Z}_2$ symmetry under which $H_1^\dagger H_2$ carries a global charge [1]. As soon as we require CP-conservation in the Higgs sector and neglect the term which softly breaks this symmetry we can distinguish between scalars

[1] Considering these symmetries no FCNCs mediated by the Higgs at tree-level are present. They lead to $\lambda_5 = \lambda_6 = \lambda_7 = 0$ but as long as $\mu_3 \neq 0$ this leads to finite FCNCs at one loop

and pseudoscalars which were mixed states before and now transform as CP eigenstates. The scalar potential with the two doublets H_1 and H_2 is then given as

$$\begin{aligned}\tilde{V}_{\text{2HDM}} = &\mu_1 H_1^\dagger H_1 + \mu_2 H_2^\dagger H_2 - \mu_3 \left(H_1^\dagger H_2 + H_2^\dagger H_1\right) + \frac{\lambda_1}{2}\left(H_1^\dagger H_1\right)^2 + \frac{\lambda_2}{2}\left(H_2^\dagger H_2\right)^2 \\ &+ \lambda_3 \left(H_1^\dagger H_1\right)\left(H_2^\dagger H_2\right) + \lambda_4 \left(H_1^\dagger H_2\right)\left(H_2^\dagger H_1\right) \ ,\end{aligned} \tag{3.7}$$

where we assume without loss of generality that $\mu_3 \in \mathbb{R}$. The presence of the term $\mu_3 H_1^\dagger H_2 + h.c.$ allows us to provide a mass to the pseudoscalar which is in the massless case can be axions. We are left with 7 parameters in the scalar potential of which three are of mass dimension two and four are dimensionless $\mu_1, \mu_2, \mu_3, \lambda_1, \lambda_2, \lambda_3, \lambda_4$.

The parameters characterizing the potential can be expressed in terms of physical parameters. These are the four scalar masses $m_h = 125$ GeV, $M_H, M_H^\pm$, and M_A, the vacuum expectation values of the two Higgs doublets $\langle H_a \rangle = (0, v_a/\sqrt{2})^T$ with $a \in \{1, 2\}$ which are obtained from the global minimum of the potential and can be written in terms of $v = \sqrt{v_1^2 + v_2^2} = 246$ GeV as well as the ratio between the two vevs $\tan\beta = t_\beta = v_1/v_2$, and the mixing angle α of the two neutral scalars parametrized by $\cos(\beta - \alpha) = c_{\beta-\alpha}$. This translation is given by the following relations

$$\mu_1 = -\frac{1}{2c_\beta}\left(m_H^2 c_\alpha c_{\beta-\alpha} - m_h^2 s_\alpha s_{\beta-\alpha}\right) + m_A^2 s_\beta^2 \ , \tag{3.8}$$

$$\mu_2 = -\frac{1}{2s_\beta}\left(m_h^2 c_\alpha s_{\beta-\alpha} + m_H^2 s_\alpha c_{\beta-\alpha}\right) + m_A^2 c_\beta^2 \ , \tag{3.9}$$

$$\mu_3 = M_A^2 s_\beta c_\beta \ , \tag{3.10}$$

$$\lambda_1 = \frac{m_H^2 c_\alpha^2 + m_h^2 s_\alpha^2 - M_A^2 s_\beta^2}{v^2 c_\beta^2} \ , \tag{3.11}$$

$$\lambda_2 = \frac{m_H^2 s_\alpha^2 + m_h^2 c_\alpha^2 - M_A^2 c_\beta^2}{v^2 s_\beta^2} \ , \tag{3.12}$$

$$\lambda_3 = \frac{(M_H^2 - M_h^2) s_\alpha c_\alpha + (2M_{H^\pm}^2 - M_A^2) s_\beta c_\beta}{v^2 s_\beta c_\beta} \ , \tag{3.13}$$

$$\lambda_4 = \frac{2(M_A^2 - M_{H^\pm}^2)}{v^2} \ , \tag{3.14}$$

which are derived in [59]. On the other hand, the physical masses can be expressed in terms of the parameters describing the potential as

$$M_h^2 = \frac{\mu_3 c_{\beta-\alpha}^2}{s_\beta c_\beta} + v^2\left[\lambda_1 c_\beta^2 s_\alpha^2 + \lambda_2 s_\beta^2 c_\alpha^2 - 2(\lambda_3 + \lambda_4) c_\alpha c_\beta s_\alpha s_\beta\right] \ , \tag{3.15}$$

$$M_H^2 = \frac{\mu_3 s_{\beta-\alpha}^2}{s_\beta c_\beta} + v^2\left[\lambda_1 c_\beta^2 c_\alpha^2 + \lambda_2 s_\beta^2 s_\alpha^2 + 2(\lambda_3 + \lambda_4) c_\alpha c_\beta s_\alpha s_\beta\right] \ , \tag{3.16}$$

$$M_A^2 = \frac{\mu_3}{s_\beta c_\beta} \ , \tag{3.17}$$

$$M_{H^\pm}^2 = \frac{\mu_3}{s_\beta c_\beta} - \frac{v^2}{2}\lambda_4 \ . \tag{3.18}$$

Field Content of a Two Higgs Doublet Model

The two complex $SU(2)_L$ Higgs doublets in the above potential (3.15) contain 8 real fields

$$H_a = \begin{pmatrix} \phi_a^+ \\ \frac{v_a+\rho_a+i\eta_a}{\sqrt{2}} \end{pmatrix} \qquad \text{with } a \in 1,2 \ . \tag{3.19}$$

Three of these fields provide the longitudinal degrees of freedom for the $W^\pm$ and Z bosons which acquire masses after the electroweak symmetry breaking. We are therefore left with five physical Higgs fields. These are two charged Higgs bosons $H^\pm$, two neutral scalars h, H where the lighter one is associated with the Standard Model Higgs and one neutral pseudoscalar A if we assume CP to be conserved. A variety of distinct bases for the two Higgs doublets exist as they all have different advantages. The one given in (3.19) is the interaction basis. Another frequently used one is the so-called Higgs basis in which only one Higgs acquires a vev. In the phenomenology study of the two Higgs doublet model being the portal to dark matter we want to work with the Higgs mass basis. We can transform the fields in the following way, compare [58, 59] for more detailed discussions.
The neutral CP-even mass eigenstates h and H are orthogonal combinations of ρ_1 and ρ_2 given by

$$H = \rho_1 \cos\alpha + \rho_2 \sin\alpha \ , \tag{3.20}$$

$$h = -\rho_1 \sin\alpha + \rho_2 \cos\alpha \ . \tag{3.21}$$

Note that the lighter CP-even state is the one called h and the Standard Model Higgs boson would be defined as

$$\begin{aligned} H^{\mathrm{SM}} &= \rho_1 \cos\beta + \rho_2 \sin\beta \\ &= H\cos(\alpha-\beta) - h\sin(\alpha-\beta) \ . \end{aligned} \tag{3.22}$$

We can achieve that the light Higgs h becomes the Standard Model Higgs boson by setting $\cos(\beta-\alpha) = 0$. This is the so-called alignment limit. The neutral Goldstone boson can be written in terms of $G^0 = \eta_1 \cos\beta + \eta_2 \sin\beta$ and the physical pseudoscalar as

$$A = \eta_1 \sin\beta - \eta_2 \cos\beta \ . \tag{3.23}$$

For the two charged scalar components we find

$$G^\pm = \phi_1^\pm \cos\beta + \phi_2^\pm \sin\beta \ , \tag{3.24}$$

$$H^\pm = -\phi_1^\pm \sin\beta + \phi_2^\pm \cos\beta \ . \tag{3.25}$$

Combining all these expressions we can express the two Higgs doublets H_a in the mass eigenbasis as follows

$$H_1 = \begin{pmatrix} c_\beta G^+ - s_\beta H^+ \\ \frac{c_\beta v + c_\alpha H - s_\alpha h + i(c_\beta G^0 - s_\beta A)}{\sqrt{2}} \end{pmatrix} \ , \tag{3.26}$$

$$H_2 = \begin{pmatrix} s_\beta G^- + c_\beta H^- \\ \frac{s_\beta v + s_\alpha H - c_\alpha h + i(s_\beta G^0 + c_\beta A)}{\sqrt{2}} \end{pmatrix} \ . \tag{3.27}$$

We use this parametrization in the remainder of this thesis as it represents the physical states we want to work with and moreover directly contains the CP-odd pseudoscalar A.

Yukawa Sector of the Two Higgs Doublet Model

The couplings between the fermions and the additional scalars provide restrictions to the two Higgs doublet framework as in the most general case such interactions can have flavor changing neutral currents at tree-level which are strongly constrained by experimental data. Nevertheless, already the requirement that only one of the two Higgs doublets couples to all fermions of a specific charge is sufficient to avoid FCNCs. This is often referred to as natural flavor conservation which is already at hand if a $\mathbb{Z}_2$ symmetry acts on one of the two doublets and if the right-handed fermion singlets transform appropriately. The Yukawa couplings can then be written as

$$\mathcal{L}_{\text{Yuk}} = -\sum_{a=1,2} \left(y_u^a \bar{Q} \tilde{H}_a u_R + y_d^a \bar{Q} H_a d_R + y_l^a \bar{L} H_a l_R + h.c. \right) \ , \tag{3.28}$$

where y_f^a are the Yukawa coupling matrices of the three fermion generations [60]. We suppressed the flavor indices. Then Q and L represent the left-handed quark and lepton doublets, respectively, whereas u_R, d_R and l_R are the right-handed up/down-type quarks as well as the charged lepton singlets. $\tilde{H}_a = \epsilon H_a^*$ is the conjugated Higgs boson as $\epsilon = i\sigma_2$ is a two-dimensional antisymmetric tensor and σ_2 is the second Pauli matrix. Flavor can be naturally conserved in four different ways if the two doublets couple to the fermions of a given charge as follows

Model	u_R^i	d_R^i	l_R^i
Type I	H_2	H_2	H_2
Type II	H_2	H_1	H_1
Lepton-specific	H_2	H_2	H_1
Flipped	H_2	H_1	H_2

Table 3.1: Two Higgs doublet models naturally conserving flavor. The two Higgs doublets are assigned to the up/down-type quarks and charged leptons where by convention the up-type quarks always couple to H_2. [61]

In the remainder of this work we only consider the two models of type I and II and omit further discussions of the flipped lepton models where the leptons couple to the two doublets as the down- instead of the up-type quarks. As we investigate the Lagrangian and especially the Yukawa couplings after electroweak symmetry breaking, we want to focus on the different behavior of the two models in the perspective of the coupling to the dark sector. We can write the Yukawa terms of the Lagrangian as

$$\begin{aligned} \mathcal{L}_{\text{Yuk}}^{\text{2HDM}} = &\sum_{j=1}^{3} \sum_{f=u,d,l} \left(g_{hf} \bar{f}_j f_j h + g_{Hf} \bar{f}_j f_j H - i g_{Af} \bar{f}_j \gamma_5 f_j A \right) \\ &- \frac{\sqrt{2}}{v} H^+ \sum_{i,j=1}^{3} \left(\bar{u}_i \left(\kappa_{H^+d} V_{ij} m_{d_j} P_R - \kappa_{H^+u} m_{u_i} V_{ij} P_L \right) d_j + \kappa_{H^+l} \bar{\nu} m_l P_R l \right) + h.c. \ , \end{aligned} \tag{3.29}$$

where i, j denote flavor indices and f is summed over all fermions carrying the same electric charge meaning that u, d and l are representing their type of fermions [61].
The couplings between the Standard Model fermions and the neutral scalars $\varphi = h, H, A$ can be written in terms of rescaled Standard Model Higgs Yukawa couplings. They can be expressed as $g_{\varphi f} = \kappa_{\varphi f} m_f / v$ with $\kappa_{\varphi f}$ given in Table 3.2. The couplings of the charged Higgs to fermions are in principle the same as the pseudoscalar ones ($\kappa_{H^+ f} = \kappa_{Af}$) besides the fact that they are multiplied by the corresponding entry

of the CKM matrix V_{ij}. It is important to point out that the couplings of the two distinct two Higgs doublet models of type I and II have different dependencies on $\tan\beta$ as well as on $\cos(\beta-\alpha)$. In the alignment limit, where $\sin(\beta-\alpha)=0$, the scaling restricts itself to depend only on $\tan\beta$. This leads to different branching ratios of the new scalars decaying into fermions and influences their production cross section. We are going to discuss this in more depth in Section 3.3.

Type I	Type II	
$\kappa_{hu}=\kappa_{hd}=\kappa_{h\ell}=s_{\beta-\alpha}+\frac{c_{\beta-\alpha}}{t_\beta}$	$\kappa_{hu}=s_{\beta-\alpha}+\frac{c_{\beta-\alpha}}{t_\beta}\,,$	$\kappa_{hd}=\kappa_{h\ell}=-s_{\beta-\alpha}-c_{\beta-\alpha}t_\beta$
$\kappa_{Hu}=\kappa_{Hd}=\kappa_{H\ell}=c_{\beta-\alpha}-\frac{s_{\beta-\alpha}}{t_\beta}$	$\kappa_{Hu}=c_{\beta-\alpha}-\frac{s_{\beta-\alpha}}{t_\beta}\,,$	$\kappa_{Hd}=\kappa_{H\ell}=c_{\beta-\alpha}+s_{\beta-\alpha}t_\beta$
$\kappa_{Au}=\kappa_{Ad}=\kappa_{A\ell}=-\frac{1}{t_\beta}$	$\kappa_{Au}=-\frac{1}{t_\beta}\,,$	$\kappa_{Ad}=\kappa_{A\ell}=t_\beta$

Table 3.2: Scaling factors of the Yukawa couplings between the scalars $h, A, H, H^\pm$ and fermions in a two Higgs doublet model of type I and type II, respectively.

Before we combine the two Higgs doublet model with the dark sector we want to mention that we checked the implemented Yukawa couplings which are in agreement with [61]. The three- and four-Higgs vertices, which represent the corresponding Higgs self-couplings, agree with [59]. The self-interactions become essential for specific decay patterns which we will discuss during the collider searches where especially the interaction vertex $H\to AZ$ turns out to be the driving part for the mono-Z searches. The leading contributions emerge from the trilinear terms where one of the Higgs bosons has acquired a vacuum expectation value.

3.2 A Two Higgs Doublet Model & Its Extension to the Dark Sector

We studied the two Higgs doublet model in a large extend in the previous section. One further step is now required in which we add the dark matter to the extended model. We chose a Dirac fermion χ which is assumed to be the dark matter particle. As we have seen in Section 2.7 one consistent way of implementing a pseudoscalar dark matter interaction was given by (2.28). Here we also took the original motivation of a two Higgs doublet model acting as a flavon into consideration. By identifying the subscripts u and d as 1 and 2 and comparing these to Table 3.2 the model mentioned above can be seen as an extended version of a two Higgs doublet model of type II which was in detail discussed in the previous section. The Yukawa couplings corresponding to the assignment of type II can be transformed into the assignments of type I by replacing $H_d\to\tilde{H}_1$. The general Lagrangian of the simplified dark matter model we work with during this study was already given in (2.28). Like in the previous section we are interested in the couplings after electroweak symmetry breaking. The Yukawa part of the Lagrangian of the dark matter sector is then given as

$$\mathcal{L}^{\text{DM}}_{\text{Yuk}}=\sum_{\varphi=h,H,A} g_{\varphi\chi}\bar{\chi}\chi\varphi - ig_{\varphi 5}\bar{\chi}\gamma_5\chi\varphi\ , \tag{3.30}$$

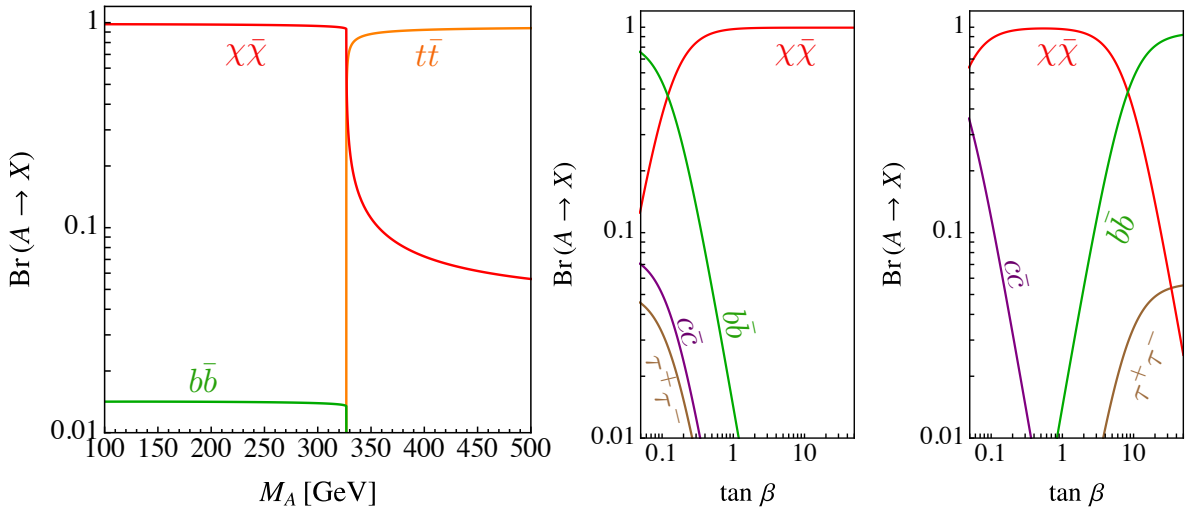

Figure 3.1: The dominant branching ratios of the pseudoscalar A for fixed $M_H = M_H^\pm = 500$ GeV, $c_5 = 1$, $c_\chi = 0$, $m_\chi = 1$ GeV and $\cos(\beta - \alpha) = 0$. Left: In dependence of the pseudoscalar mass M_A and $\tan\beta = 1$. Center (and right): In dependence of $\tan\beta$ for $M_A = 200$ GeV with Yukawa couplings as in a 2HDM of type I (II). Figure taken from [15].

where the scalar couplings to the dark matter can be parametrized as

$$g_{h\chi} = \left(\frac{2\,(c_{\beta-\alpha} + t_\beta s_{\beta-\alpha})}{1+t_\beta^2} - c_{\beta-\alpha}\right) \mathrm{Re}[C_\chi]\ , \tag{3.31}$$

$$g_{h5i} = \left(\frac{2\,(c_{\beta-\alpha} + t_\beta s_{\beta-\alpha})}{1+t_\beta^2} - c_{\beta-\alpha}\right) \mathrm{Im}[C_5]\ , \tag{3.32}$$

$$g_{H\chi} = \left(\frac{2\,(t_\beta c_{\beta-\alpha} - s_{\beta-\alpha})}{1+t_\beta^2} + s_{\beta-\alpha}\right) \mathrm{Re}[C_\chi]\ , \tag{3.33}$$

$$g_{H5} = \left(\frac{2\,(t_\beta c_{\beta-\alpha} - s_{\beta-\alpha})}{1+t_\beta^2} + s_{\beta-\alpha}\right) \mathrm{Im}[C_5]\ , \tag{3.34}$$

$$g_{A\chi} = \mathrm{Im}[C_\chi]\ , \tag{3.35}$$

$$g_{A5} = \mathrm{Re}[C_5]\ , \tag{3.36}$$

where we defined $C_\chi = c_\chi v/\Lambda$ and $C_5 = c_5 v/\Lambda$. Note that there is no tree-level interaction between the charged Higgs and the dark matter as the dark matter does not carry an electric charge.

The Mass of the Dark Matter Particle

The dark matter particle χ automatically obtains a mass from the extended Higgs mechanism via the terms in (2.28) containing the operator $H_1^\dagger H_2 \bar\chi\chi$ and $H_1^\dagger H_2 \bar\chi\gamma_5\chi$ if both Higgs doublets acquire their vevs. The mass term obtained from the breaking of the electroweak symmetry can be written as

$$m_\chi^{\mathrm{EW}} = 2\frac{v_1 v_2}{\Lambda}\left(\mathrm{Re}[c_\chi]\bar\chi\chi + i\mathrm{Im}[c_5]\bar\chi\gamma_5\chi\right) = 2\frac{v^2}{\Lambda}\sin\beta\cos\beta\left(\mathrm{Re}[c_\chi]\bar\chi\chi + i\mathrm{Im}[c_5]\bar\chi\gamma_5\chi\right)\ . \tag{3.37}$$

This equation only depends on $\tan\beta$. For renormalizable couplings c_χ and c_5 as well as a sizable energy scale Λ the dark matter particle can only achieve a sufficiently large mass to agree with the dark matter relic abundance for values of $\tan\beta \gg 10$. This is a non-preferred region in the parameter space for

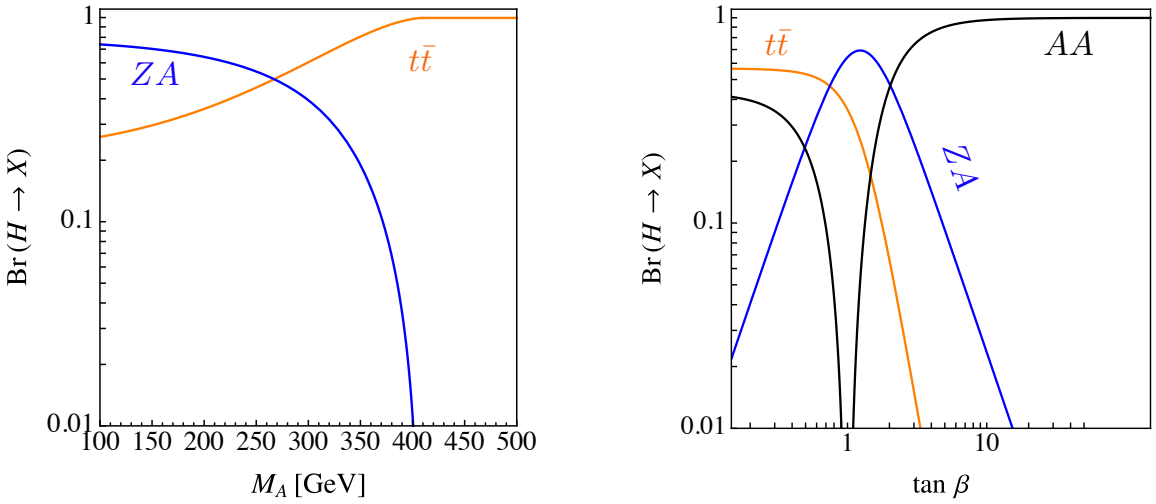

Figure 3.2: The dominant branching ratios of the heavy neutral scalar H for fixed $M_H = M_H^{\pm} = 500$ GeV and $\cos(\beta - \alpha) = 0$. Left: In dependence of the pseudoscalar mass M_A and $\tan\beta = 1$. Right: In dependence of $\tan\beta$ for a pseudoscalar mass $M_A = 200$ GeV. Figure taken from [15].

various constraints we derive. Bounds from the relic density as well as direct detection experiments will set stringent restrictions and force $\mathrm{Re}[c_\chi]$ to be very small. On the other hand, the imaginary part of c_5 needs to be zero if we require our potential to be CP-conserving. Hence, we need to introduce an additional mass term which has the same origin as the μ_3 coupling in the scalar potential as they both are obtained from the U(1) breaking. Then the total mass for the dark matter particle is defined as

$$m_\chi^{\mathrm{tot}} = 2\frac{v^2}{\Lambda}\sin\beta\cos\beta\,(\mathrm{Re}[c_\chi]\bar{\chi}\chi + i\mathrm{Im}[c_5]\bar{\chi}\gamma_5\chi) - m_\chi\bar{\chi}\chi\ , \tag{3.38}$$

where for the preferred region of $\tan\beta$ the contribution from the Higgs mechanism only contributes up to 2 GeV to the total mass. The introduced additional mass term $m_\chi\bar{\chi}\chi$ adds a new parameter to the simplified model, the mass of the dark matter candidate m_χ. This mass term softly breaks the introduced symmetry under which the dark matter and the operator $H_1^\dagger H_2$ are charged. Since we can always reparametrize the free input mass m_χ we will neglect from now on the contribution of the electroweak symmetry breaking and will refer to m_χ^{tot} as m_χ for simplicity.
One word of caution becomes necessary if we allow for a mass contribution coming from the imaginary part of the coupling constant c_5. By allowing such a CP-violating term the mass of the dark matter particle would get a complex contribution. This problem can be solved if we perform a rotation by a chiral transformation and a redefinition of the dark matter field. This was done analogously to [62] and can be found more explicitly in [63]. Nevertheless, as it does not play a major role in the proceeding of the phenomenology study of the simplified model we omit a further investigation.

Influence of Additional Symmetric Higgs Doublet Operators

So far we have neglected the operators where two identical Higgs doublets couple to the dark matter. This could be justified by applying the discussed symmetry of the dark sector which only gives a charge

to the combination $H_1^\dagger H_2$. Nevertheless, we shortly want to show their influence on the simplified model. Their Lagrangian can be given in the most general way

$$\mathcal{L}_{\text{sHDO}} = \left(c_{\chi,11} \frac{H_1^\dagger H_1}{\Lambda} + c_{\chi,22} \frac{H_2^\dagger H_2}{\Lambda} \right) \bar{\chi}\chi + \left(c_{5,11} \frac{H_1^\dagger H_1}{\Lambda} + c_{5,22} \frac{H_2^\dagger H_2}{\Lambda} \right) \bar{\chi}\gamma_5\chi + h.c. \,, \tag{3.39}$$

where all the coupling constants $c_{\chi,ii}$ and $c_{5,ii}$ with $i \in \{1,2\}$ are real to preserve unitary. These operators mainly lead to couplings of χ to either the light or heavy Higgs (h, H) and do not provide an interaction between the dark matter and the pseudoscalar A as the Hermitian part contributes to an exact cancellation. Even if these interaction terms have a different dependence on $\tan\beta$ as the scalar couplings given in (3.31) we are only interested in the operators contributing to pseudoscalar couplings. Hence, we omit these operators in the proceeding of our work. In the absence of a symmetry this can be further justified by considering that the above operators need to be small as they can be extracted from limits we derive from direct detection experiments as well as the Higgs signal strength measurement.

Influence of Higher Order Insertions of the Higgs Doublet Operators

As we have pointed out in the beginning of this chapter, the underlying idea of the simplified model emerges from a model which aims for an explanation of the fermion mass hierarchy where the operator $H_1^\dagger H_2$ acts as a flavon. In this case the number of insertions of the operator can differ from one as extracted from (3.1) and can take any arbitrary natural number. Therefore, we shortly want to investigate the case where instead of one we insert the above operator n times:

$$\mathcal{L}_{\text{nHDO}} \;=\; c_\chi \, \frac{\left(H_1^\dagger H_2\right)^n}{\Lambda^{2n-1}} \, \bar{\chi}\chi \;+\; c_5 \, \frac{\left(H_1^\dagger H_2\right)^n}{\Lambda^{2n-1}} \, \bar{\chi}\gamma^5\chi + \, h.c. \,. \tag{3.40}$$

The charge carried by the operator $H_1^\dagger H_2$ is now $1/n$ times the charge of the dark matter operator $\chi\bar{\chi}$ requesting a more complex symmetry group than a $\mathbb{Z}_2$. During the study of the relic density we will shortly work out the influence of the case where we set $n = 2$, which is the next to minimal one. As the number n grows Λ has to become smaller to still obtain sizable dark matter cross sections by remaining the coupling strengths at order one. This restricts higher order insertions [15].

3.3 Branching Ratios of the Higgs Scalars

As we have analyzed the Yukawa couplings in a general two Higgs doublet model and explored the interactions of an extension by a dark sector we now want to examine the branching ratios of the additional Higgs scalars as they will become important during the proceedings of this study. We will restrict ourselves to the so-called alignment limit, sometimes also referred to as decoupling limit if one has a sizable mass hierarchy of the scalars leading to $\cos(\beta - \alpha) = 0$. In this situation the field h has Standard Model-like couplings to the electroweak gauge bosons and hence can be identified with the 125 GeV Higgs discovered at the LHC. The partial widths of the neutral scalar h will therefore not change compared to the ones of the Standard Model Higgs, whereas the branching ratios will only be slightly modified due to the presence of an additional partial width of the decay to dark matter. We hence neglect a lengthy review of the Standard Model Higgs branching ratios. Nevertheless, we will make use of the available data of the Higgs signal strengths to conclude that the alignment limit is preferred by a global fit to these signal strengths. This is reinforced by the study of electroweak precision bounds in the next chapter. We only consider tree-level interactions occurring in the alignment limit and avoid off-shell contributions to the partial

decay widths which sometimes can be sizable and will be mentioned as soon as they become relevant.
For the pseudoscalar A only couplings to fermions lead to sizable branching ratios. The dominant ones are displayed in the left panel of Figure 3.1 in dependence of the pseudoscalar mass M_A for fixed $M_H = M_H^{\pm} = 500$ GeV, $c_5 = 1$, $c_\chi = 0$, $m_\chi = 1$ GeV and $t_\beta = 1$. In this plot as well as the following ones only branching ratios above 1 % are shown. As long as the pseudoscalar mass is below the top mass threshold, $M_A < 2m_t$, the decay into a dark matter pair χ dominates if the decay is kinematically accessible, meaning $M_A > 2m_\chi$. We can understand this by investigating the coupling strength to bottom quarks b or dark matter which scales like $g_{Ab}/g_{A\chi} \sim m_b\Lambda/v^2$. Above the top threshold, due to their heavier mass and therefore larger Yukawa couplings than the bottom quarks, the decay into a pair of top quarks becomes the leading channel. The center (and right) panel of Figure 3.1 show the scaling of the branching ratios with $\tan\beta$ where $M_A = 200$ GeV in a two Higgs doublet model of type I (II). In the case of type I the couplings to all Standard Model fermions and especially the one to the down-type quarks have a $1/\tan\beta$ dependence. Then the decay into a bottom pair dominates for small values of $\tan\beta$ over the charm quarks and tau leptons as a decay to tops is kinematically not allowed. The branching fraction of A into dark matter becomes the dominant one for values of $\tan\beta < 0.2$ as the coupling does not scale with $\tan\beta$. On the other hand, in a type II two Higgs doublet model the decay into $c\bar{c}$ is the largest for extremely tiny $\tan\beta$ and for values of $\tan\beta > 8$ the decay into $b\bar{b}$ takes the lead. In the intermediate parameter range, which for our simplified model is the preferred one, the branching ratio of the dark matter χ exceeds the others and is close to order $\mathcal{O}(1)$.
We continue by studying the branching ratios of the neutral heavy scalar H which are plotted in Figure 3.2 for the parameters $M_H = M_{H^\pm} = 500$ GeV, $c_5 = 1$, $c_\chi = 0$, $m_\chi = 1$ GeV. In the left panel we again fix $\tan\beta = 1$ and scan over the pseudoscalar mass M_A. The dominant branching ratios are $\mathrm{Br}(H \to AA)$, $\mathrm{Br}(H \to ZA)$ as well as the decay into a pair of top quarks $t\bar{t}$, where the coupling of the top does not explicitly depend on the chosen type of two Higgs doublet model. Therefore, no separate treatment of the two implemented types of models is necessary when we study the dependence of the branching ratios on $\tan\beta$. The right panel hence shows the dependence on $\tan\beta$ for both two Higgs doublet models where we fix $M_A = 200$ GeV. For the mass hierarchy $M_H > M_A + M_Z$ in the parameter region of $\tan\beta \in \{0, 7-2\}$, the dominant branching ratio is $H \to ZA$, leading to a mono-Z final signature if we consider the main decay channel of A which is $A \to \chi\bar{\chi}$. If $M_H \leq 2M_A$ the decay $H \to AA$ is kinematically not allowed, but if $M_H > M_A + M_Z$ then the branching ratio $\mathrm{BR}(H \to ZA)$ can still be dominant even for larger values of $\tan\beta$. For larger masses of the pseudoscalar A and $\tan\beta = 1$ a search for a di-top final state becomes more promising, especially if the decay into the ZA final state becomes kinematically forbidden for $M_A > 410$ GeV. On the other hand, if we stick to the light pseudoscalar mass as in the right-hand panel of Figure 3.2 and increase the value of $\tan\beta$ the decay $H \to AA$ becomes the dominant one, whereas for small $\tan\beta$ again di-top yields the leading branching ratio. It is worth mentioning that the decay into two pseudoscalars, which can be present as long as $M_A < M_H/2$, has a pole at $\tan\beta = 1$. As this seems to be a convenient feature for the performed mono-Z search we can raise the question what decay signatures can become relevant if we leave the preferred parameter space of $\tan\beta < 3$. A possible signature can be a search for a mono-hZ final state if we leave the alignment limit. Here, one pseudoscalar decays into dark matter and the second one into a Standard Model Higgs and a Z boson. Nevertheless, we want to stress once more the point that the parameter space giving rise to a mono-Z signal is in perfect agreement with the bounds we will derive in the next two chapters.
The dependence of the branching ratio on the pseudoscalar mass M_A for the heavy charged scalar $H^\pm$ is shown on the left panel of Figure 3.3 where we set $M_H = M_{H^\pm} = 500$ GeV and $\tan\beta = 1$. The parameters of the dark sector stay the same as before, but they do not play a role as no couplings between the charged Higgs and the dark matter exist at tree-level. For the charged Higgs we need to distinguish again the

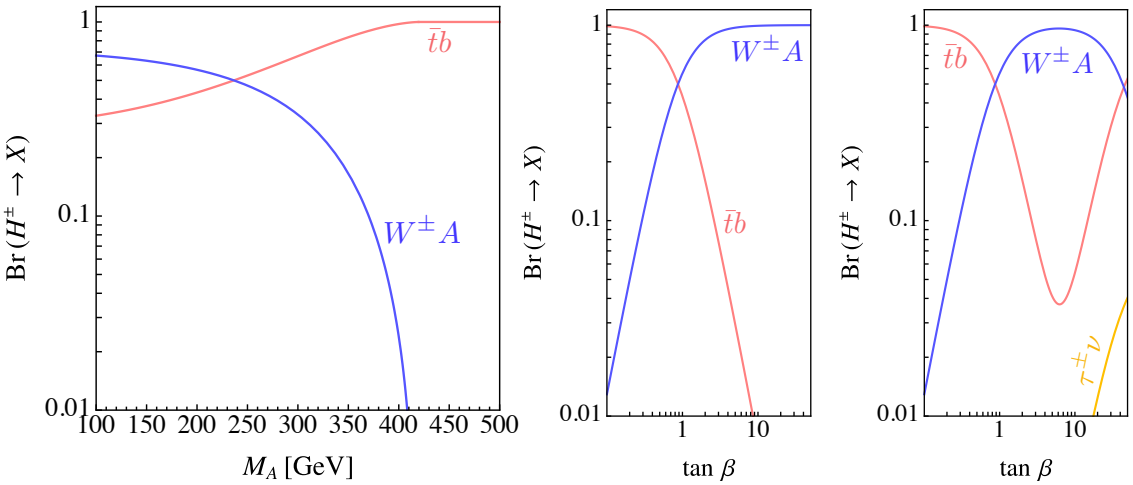

Figure 3.3: The dominant branching ratios of the charged scalar $H^\pm$ for fixed $M_H = M_H^\pm = 500\,\text{GeV}$ and $\cos(\beta - \alpha) = 0$. Left: In dependence of the pseudoscalar mass M_A and $\tan\beta = 1$. Center (and right): In dependence of $\tan\beta$ for $M_A = 200\,\text{GeV}$ with Yukawa couplings as in a 2HDM of type I (II). Figure taken from [15].

different scaling of the branching ratios for both types of Yukawa couplings. Hence, we present on the center (and right) panel of Figure 3.3 the dependence of the branching fractions of the charged scalar on $\tan\beta$ with fixed $M_A = 200\,\text{GeV}$ for the models of type I (II). Like the case of the neutral heavy scalar H where a mono-Z signature was obtained, a mono-W signature can occur if the pseudoscalar again decays dominantly into dark matter. This is the case for $\tan\beta \gtrsim 1$ and $M_{H^\pm} > M_A + M_{W^\pm}$ where the branching ratio $H^\pm \to W^\pm A$ provides the largest contribution. Above these values of $\tan\beta$ the increased coupling of the bottom quark to the charged scalar results in a leading branching fraction of $H^\pm \to \bar{t}b$ for models of type II. For large masses of the pseudoscalar the decay $H^\pm \to \bar{t}b$ takes over and $H^\pm \to W^\pm A$ vanishes for $M_A > 410\,\text{GeV}$.

The partial widths of the pseudoscalar A, heavy scalar H and charged scalar $H^\pm$ leading to the above discussed branching ratios are collected as analytic expressions in Appendix B. We also present the partial width of the light neutral scalar h, which in the alignment limit is associated with the Standard Model Higgs, decaying to the dark matter χ.

4 Constraints Motivated by Phenomenology of Two Higgs Doublet Models

In the previous chapter we have studied the phenomenology of a two Higgs doublet model and some of the implications of the extension by Dirac dark matter fermions. It was found that in the consistent simplified model (2.28) a huge set of input parameters is present. These are the physical masses of the Higgs scalars $M_h, M_H, M_A, M_{H^\pm}$, the vacuum expectation value (vev) v, the ratio of the vevs of the two Higgs doublets $\tan\beta = v_1/v_2$, the scalar mixing angle α, emerging from the two Higgs doublet model as well as the mass of the dark matter candidate m_χ and its couplings C_χ, C_5 which in the most general case can be complex numbers. The scale of new physics Λ can be included in the couplings to the dark sector. We want to address the problem that we need to treat these input parameters to perform a fit of the allowed parameter space. As it is for obvious reasons hard to perform a 10-parameter fit, we need to search for constraints for some of these parameters of the simplified model. In this section we want to study the constraints which can be derived in most general ways from the collider phenomenology of a two Higgs doublet model and which do not necessarily depend on the presence of the dark matter. These are constraints derived from Higgs signal strength measurements, flavor physics, electroweak precision observables, stability requirements as well as collider searches for heavy scalars [15].

4.1 Higgs Couplings

The extension of the Standard Model by a second Higgs doublet has an influence on the branching ratios as well as the total width of the light neutral Higgs which is associated with the Standard Model Higgs, in particular if we take the additional invisible decay channel of the Higgs into dark matter into consideration. Respecting the Glashow-Weinberg [64, 65] condition to avoid tree-level FCNCs leads to the type I and type II two Higgs doublet models, respectively. This can be seen if we remind ourselves of the Yukawa terms in the Lagrangian (2.28) and the corresponding coupling modifiers κ_{hf} as given in Table 3.2. The couplings to fermions in this simplified model depend now on the ratio of the two vevs $\tan\beta$ as well as on the mixing angle α of the two neutral, CP-even scalars h and H which is parametrized by $\cos(\beta-\alpha)$. Not only the couplings of the two neutral, CP-even Higgs bosons to fermions but also the couplings of h to vector bosons change relative to the Standard Model values as we require gauge invariance and so they can be expressed as [66]

$$\begin{aligned}\kappa_{hV} &= g^{\text{2HDM}}_{hVV}/g^{\text{SM}}_{hVV} = \sin(\beta-\alpha)\\ \kappa_{HV} &= g^{\text{2HDM}}_{HVV}/g^{\text{SM}}_{HVV} = \cos(\beta-\alpha)\ ,\end{aligned} \tag{4.1}$$

where $V = W^\pm, Z$. The branching fractions as well as the total width are measured for example by ATLAS and CMS and the obtained values should agree with the experimental data. Hence, measuring theses Higgs coupling strengths in several channels can be translated into strong constraints on any

possible mixing of the light Higgs h with the heavy scalars[1].
We assume that the Higgs boson production and the decay kinematics do not change drastically as the couplings are modified so that the expected rate for an arbitrary process can be derived by simply rescaling the Standard Model couplings. The measured observable at the experiments is the signal strength μ which is the product of the production cross section σ_j of the production mode j and the branching ratio BR_k of a visible decay channel k. For the Standard Model Higgs h the signal strengths can then be written as

$$\mu_{j,k} = \frac{\sigma_j}{\sigma_j^{\mathrm{SM}}} \frac{\mathrm{BR}_k}{\mathrm{BR}_k^{\mathrm{SM}}} = \frac{\sigma_j}{\sigma_j^{\mathrm{SM}}} \frac{\Gamma(h \to k)}{\Gamma(h \to k)^{\mathrm{SM}}} \frac{\Gamma_h^{\mathrm{SM}}}{\Gamma_h} , \tag{4.2}$$

where Γ_h denotes the total width of the Higgs boson h, $\Gamma(h \to k)$ the partial decay width of the Higgs into the final state k and the subscript 'SM' refers to the values in the Standard Model [66]. For the case where $\mu = 1$ the signal strengths are in full agreement with the ones predicted by the Standard Model Higgs. The combined signal strengths from ATLAS and CMS are presented in [67]. The considered contributions to the performed global fit of the Standard Model Higgs signal strengths are for the production channels vector boson fusion, vector boson associated production, gluon fusion via a top quark loop as well as $t\bar{t}$ associated production and allowed final states are bb, ZZ^*, WW, $\gamma\gamma$, $\tau\tau$ and $\mu\mu$. The coupling modifiers κ_{hi}, as summarized for fermions in Table 3.2, and for the vector bosons given in (4.1) are then defined such that

$$\kappa_{hi}^2 = \frac{\sigma_i}{\sigma_i^{\mathrm{SM}}} \quad \text{or} \quad \kappa_{hi}^2 = \frac{\Gamma(h \to i)}{\Gamma(h \to i)^{\mathrm{SM}}} . \tag{4.3}$$

A further constraint can arise from the bound on invisible Higgs decays of $\mathrm{BR}(h \to \text{invisible}) < 0.232$ [68, 69] which becomes relevant for dark matter masses $m_\chi < m_h/2$. In this case an additional decay channel becomes available for h. We write the corresponding partial width as $\Gamma(h \to \chi\bar{\chi})$ and an analytic expression can be found in (B.12). Then the modified total width of the Higgs becomes the sum of all Standard Model partial widths and the decay of h to dark matter,

$$\tilde{\Gamma}_h^{\mathrm{tot}} = \Gamma(h \to \chi) + \sum_j \Gamma(h \to j) . \tag{4.4}$$

Hence for the invisible decay mode we find

$$\mu_{j,k} = \frac{\sigma_j}{\sigma_j^{\mathrm{SM}}} \times \mathrm{BR}_{\mathrm{inv}} = \kappa_{hj}^2 \kappa_{\mathrm{tot}}^2 \frac{\Gamma_h^{\mathrm{SM}}}{\tilde{\Gamma}_h^{\mathrm{tot}}} \qquad \text{with } \kappa_{\mathrm{tot}}^2 = \sum_j \frac{\Gamma(h \to j)}{\Gamma_h^{\mathrm{SM}}} . \tag{4.5}$$

The global fit to the Higgs signal strength measurements based on the combined data of ATLAS and CMS [67] is shown in Figure 4.1. The allowed parameter space for the generic scenario where we prohibit couplings to dark matter by requiring $C_\chi = 0$ is shaded gray for a two Higgs doublet model of type I (left panel) and type II (right panel). We further present the global fit for three couplings to dark matter with values of $C_\chi = 2 \times 10^{-4},\ 1 \times 10^{-3},\ 6 \times 10^{-3}$ where the parameter space available after applying all constraints is shaded yellow, orange and red, respectively. The new energy scale Λ is set to 1 TeV to obtain natural coupling strengths. We set the dark matter mass to $m_\chi = 0$ as the fit is rather independent of the dark matter mass as long as we stay below half of the Higgs mass. Higgs couplings to dark matter can also emerge from the parameter $\mathrm{Im}[C_5]$, but those lead to the same results. The sensitivity on the

[1] For simplified models in which the Higgs mixes with a scalar mediator that couples to dark matter, measurements of Higgs couplings provide a stronger bound on the mixing angle than any mono-X search [15].

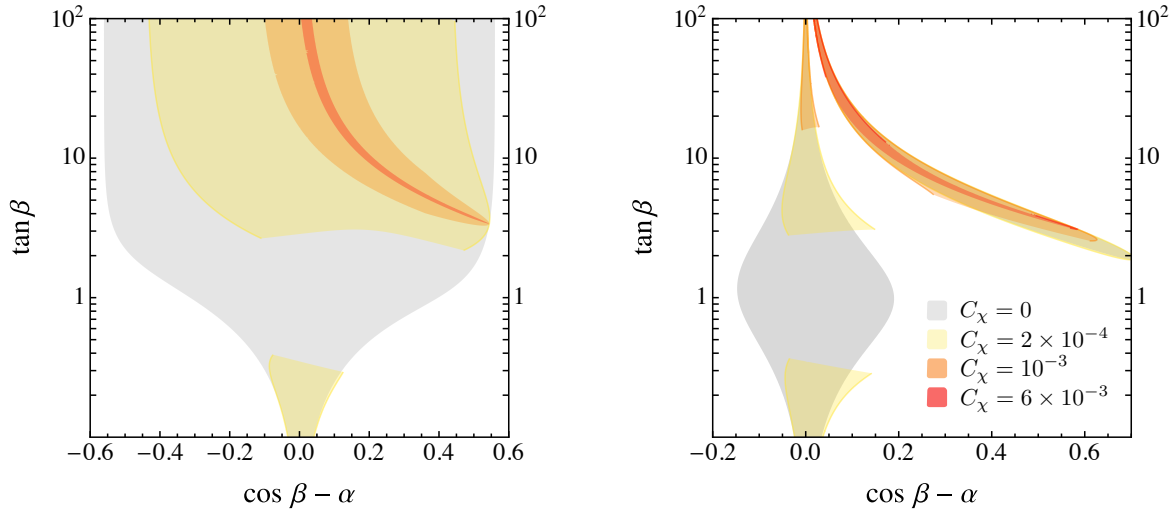

Figure 4.1: Allowed parameter space in the $\cos(\beta-\alpha)-\tan\beta$ plane of a two Higgs doublet model of type I (left) and type II (right) by a global fit to Higgs signal strength measurements for $C_\chi = 0$ (gray), $C_\chi = 2\times10^{-4}$ (yellow), $C_\chi = 1\times10^{-3}$ (orange) and $C_\chi = 6\times10^{-3}$ (red). Figure taken from [15].

dark matter mass in the case of the pseudoscalar coupling is slightly weaker. The remaining allowed parameter space for large values of $\mathrm{Re}[C_\chi]$ or $\mathrm{Im}[C_5]$ coincides with the region in which $g_{h\chi} = g_{h5} = 0$. This region is not stable under additional contributions from loop-induced Higgs couplings or additional operators, such as $H_i H_i^\dagger \bar{\chi}\chi$, $i = 1, 2$. Hence, we can conclude that either the two Wilson coefficients $\mathrm{Re}[C_\chi]$ and $\mathrm{Im}[C_5]$ are largely suppressed or the decay of the Higgs boson to dark matter is kinematically not allowed. Different settings are excluded even in the alignment limit due to measurements of the Higgs coupling strengths.

We shortly want to draw the attention to the small red bands which occur in the upper right corners in Figure 4.1. This especially allows a second separated region in the parameter space for the type II model. This region becomes available as the sign of the couplings of the Higgs to down-type quarks is not fixed and a flipped coupling ($\kappa_{hd} = -1$) allows for a parameter space outside the alignment limit. Here also higher values for the scalar coupling to dark matter become accessible as further decay channels open up and the couplings to down-type quarks are enhanced for larger values of $\tan\beta$, whereas the dark matter coupling does not scale. Nevertheless, we want to point out that this region requires a fair amount of fine-tuning of the couplings so that we stick to the alignment limit where $\cos(\beta-\alpha) = 0$.

4.2 Flavor Physics

As we assume the two Higgs doublet model to fulfill the Glashow-Weinberg condition the absence of tree-level flavor changing interactions of the neutral spin-0 particles h, H and A is naturally ensured. The strongest bounds can hence be derived from one loop interactions where a charged Higgs is exchanged which then can lead to flavor changing neutral currents. The data from the Bell experiment of the measurement $b \to s\gamma$ provides the most restricting limits. In particular, this requires at 95 % C.L. $M_{H^\pm} > 569 - 795$ GeV for two Higgs doublet models of type II and $M_{H^\pm} > 268 - 504$ GeV for type I, where in both cases $\tan\beta = 1$ is assumed [70–72]. These mass ranges depend on the applied method deriving the bound. The corresponding Feynman diagram can be found in Figure 4.2. For the type II

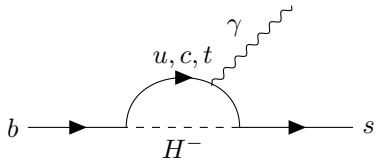

Figure 4.2: Feynman diagram contributing to the rare decay $b \to s\gamma$ which is enhanced in a two Higgs doublet model due to the charged, scalar Higgs $H^{\pm}$. Diagram generated with [73].

models this constraint is rather independent of $\tan\beta$, whereas for type I it scales with $1/\tan^2\beta$ and for $\tan\beta > 2$ becomes less relevant than collider searches for the existence of the charged Higgs. As the unitarity and perturbativity bounds will show, large values of $\tan\beta$ are highly disfavored even for the type I models. Hence, we will use the constraint $M_{H^{\pm}} > 500$ GeV for the remainder of this thesis. Further indirect constraints on $M_{H^{\pm}}$ arise from $Z \to b\bar{b}$ [74–76] and $B_q - B_{\bar{q}}$ mixing [77–80]. We want to mention that these indirect limits on the mass of the charged Higgs can significantly change if more complete models are considered as the observables can be influenced by additional particles like heavy charged fermions running in the loop.

4.3 Electroweak Precision Observables

The presence of the additional neutral and charged scalars as well as the pseudoscalar influence electroweak precision parameters at the one-loop level, especially the tree-level relation between the Z and $W^{\pm}$ boson masses which is usually fixed by the electroweak symmetry breaking. This ratio is parametrized by the so-called ρ parameter defined in equation (3.4). As this parameter in the Standard Model is predicted to be one and the measurements confirm this prediction to a high precision, the mass ratio of the two bosons needs to remain constant. The additional spin-0 particles can give corrections to the tree-level masses at the one-loop level. In the case of the $W^{\pm}$ the heavy charged scalar $H^{\pm}$ and either the heavy neutral scalar or the pseudoscalar can contribute to the loop function, compare to the left Feynman diagram of Figure 4.3. On the other hand, for the Z boson either a pair of oppositely charged scalars runs in the loop or a pseudoscalar and a neutral scalar as shown in the right diagram in Figure 4.3. As a consequence, either the heavy neutral scalar or the pseudoscalar must have a mass of the same size as the charged scalar to ensure that the loop corrections are similar for the $W^{\pm}$ and the Z boson masses to secure the ρ parameter.

As shown in Table A.1 the couplings of the scalars and pseudoscalars to gauge bosons only depend on $\cos(\beta-\alpha)$ so that the obtained constraints hold for both type I and type II two Higgs doublet models as they are independent of $\tan\beta$. These constraints set limits on the mass splitting between the heavy spin-0 mass eigenstates M_H, M_A and $M_{H^{\pm}}$ as well as the mixing angle $\cos(\beta-\alpha)$. As both the global fit to the Higgs signal strength measurements as well as the flavor constraints clearly indicate a preference towards the alignment limit we present the allowed parameter space after a 95 % C.L. fit to the oblique parameters S, T and U in the $M_A - M_H$ plane on the left panel of Figure 4.4. We set $M_{H^{\pm}} = 500$ GeV and $\cos(\beta-\alpha) = 0$ and shaded the remaining parameter space in orange which shows a clear preference for almost degenerated masses $M_H \approx M_{H^{\pm}}$ or $M_H \approx M_A$. This can be explained as the global custodial symmetry present in the Standard Model potential is restored in the complete two Higgs doublet scalar potential (3.7) in the case of the scalar mass degeneracy [81, 82]. For scanning the mass range of the pseudoscalar mediators we choose $M_H = M_{H^{\pm}} = 500$ GeV and show the allowed parameter space in the $\cos(\beta-\alpha) - M_A$ plane on the right panel of Figure 4.4. The electroweak precision bounds prefer the parameter space around the region where the mass spectrum is degenerated ($M_A \approx M_H \approx M_{H^{\pm}}$)

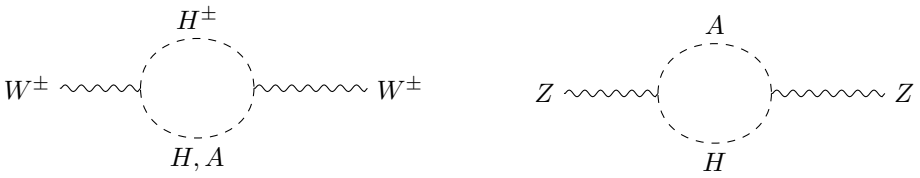

Figure 4.3: Feynman diagrams contributing to one-loop mass corrections of the $W^\pm$ (left) and Z (right) masses. Diagrams generated with [73].

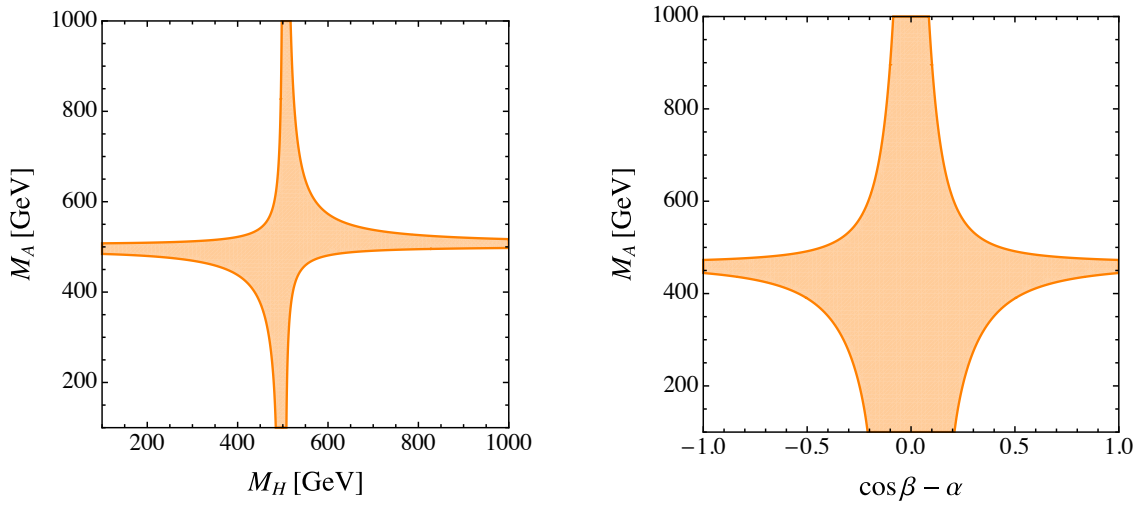

Figure 4.4: Left: Allowed parameter space by a combined fit to the oblique parameters at the 95 % C.L. in the $M_H - M_A$ plane for fixed $M_{H^+} = 500$ GeV and $\cos(\beta - \alpha) = 0$. Right: Allowed parameter space by a combined fit to the oblique parameters at the 95 % C.L. in the $\cos(\beta - \alpha) - M_A$ plane for fixed masses of $M_H = M_{H^\pm} = 500$ GeV. Figure taken from [15].

where the alignment limit is restored. For the type I two Higgs doublet models and for $\tan\beta \gtrsim 1$ these bounds lead to stronger restrictions on $\cos(\beta - \alpha)$ than the global fit to the Higgs coupling strength measurements. Following the same argumentation as in the case of the flavor observables we want to mention that these obtained constraints from electroweak precision measurements are indirect and can be sensitive to the presence of additional particles carrying a $SU(2)_L \times U(1)_Y$ charge. In a complete theory they can lead to cancellations and might soften the constraints. Therefore, the bounds obtained for M_A and $\cos(\beta - \alpha)$ in this section should only be understood as a guide.

4.4 Unitarity, Perturbativity and Stability Requirements

Any physical theory requires the existence of a stable minimum around which perturbative calculations can be performed. A physically valid Higgs scalar potential therefore needs to be bounded from below. Hence, from the scalar potential of our simplified model as given in (3.7), where we have set $\lambda_5 = \lambda_6 = \lambda_7 = 0$, we can derive some restrictions on the relevant λ_is to achieve such a physically stable minimum. These conditions can be translated into the requirement that the potential is not allowed to tend to minus infinity for any given Higgs field value. In the case of the Standard Model this is simply assured by the trivial condition $\lambda > 0$. In the case of the two Higgs doublet model this is way more complicated as all directions along which the two doublets H_1 and H_2, respectively their eight field components, can tend to arbitrarily large values need to be considered. The conditions that need to be fulfilled to secure

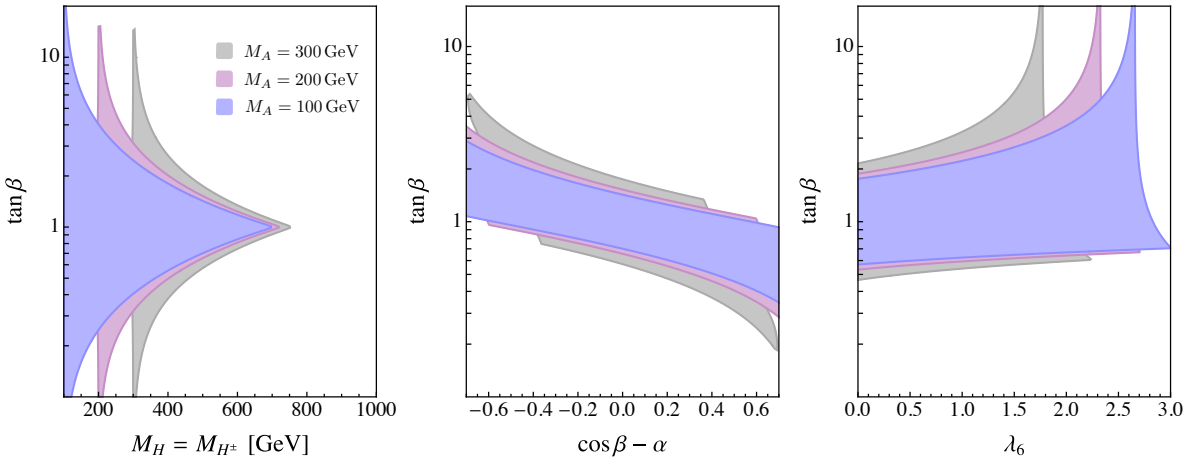

Figure 4.5: Left: Allowed mass splitting between the pseudoscalar mass and the masses of the heavy scalars $M_H = H_{H^\pm}$ depending on $\tan\beta$ for three different values of pseudoscalar mass $M_A = 100$ GeV (blue), 200 GeV (purple) and 300 GeV (gray). Middle: Parameter space allowed by stability, unitarity and perturbativity constraints in the $\cos(\beta-\alpha) - \tan\beta$ plane for $M_H = M_{H^\pm} = 500$ GeV and the three different pseudoscalar masses. Right: The effect of an additional non-vanishing quartic coupling λ_6 on the parameter space in the alignment limit $\cos(\beta-\alpha) = 0$. Figure taken from [15].

a proper minimum are the requirement that the quartic part of the scalar potential is positive for all field values, whereas the quadratic part can be negative for some values. All necessary conditions on the quartics can be derived from a study of the potential under specific directions of the fields. Such could be the direction $|H_1| \to \infty$ and $|H_2| = 0$ requiring $\lambda_1 \geq 0$, whereas the opposite direction leads to $\lambda_2 \geq 0$. Taking more directions into account one obtains the following conditions on the λ_is [58]

$$\lambda_1 \geq 0, \qquad \lambda_2 \geq 0, \qquad \lambda_3 \geq -\sqrt{\lambda_1\lambda_2}, \qquad \lambda_3 + \lambda_4 + \sqrt{\lambda_1\lambda_2} \geq 0, \tag{4.6}$$

where these four tree-level conditions are sufficient to ensure that the potential stays positive along all directions.

All quartic couplings need to respect their own perturbativity constraint $|\lambda_i| < 4\pi$ with $i \in \{1, ..., 4\}$ individually. Moreover, the requirement that the scattering amplitudes between the scalars preserve unitarity provides more bounds on the scalar potential than the limits from the stability of the scalar potential. Unitarity of the partial waves can be rephrased into the demand that the relevant submatrices of the scattering matrix have eigenvalues s_i with $|s_i| < 8\pi$ for all i [83].

The considered scalar potential (3.7) is in principle fixed by the masses of the spin-0 particles m_h, M_H, $M_A, M_{H^\pm}$ and the mixing angles $\tan\beta$ and $\cos(\beta-\alpha)$ as we have explicitly shown in equation (3.8) to (3.14). Hence setting $M_H = M_{H^\pm} = 500$ GeV provides strong constraints on the $\cos(\beta-\alpha) - \tan\beta$ plane emerging from stability, unitarity and perturbativity conditions. This results into the fact that a large mass splitting $M_A \ll M_H, M_{H^\pm}$ is widely constrained by perturbativity and unitarity as sizable quartic couplings would become necessary, see the left panel of Figure 4.5.

The allowed masses of the neutral and charged heavy scalars, which are by electroweak precision bounds forced to share the same mass, are shown in the left panel of Figure 4.5 depending on $\tan\beta$ for three different values of the pseudoscalar mass $M_A = 100$ GeV (blue), 200 GeV (purple) and 300 GeV (gray). It can be seen that the additional scalars cannot be arbitrary heavy for rather light pseudoscalar masses. This dependence emerges from the scalar potential (3.7) as the masses are related to the couplings in the potential and therefore are not free input parameters in our simplified model. Hence, no arbitrary large

mass splitting is allowed, and the additional scalar degrees of freedom cannot be shifted to heavier masses which can in principle be integrated out. In the middle panel of Figure 4.5, we present the parameter space allowed by stability, unitarity and perturbativity constraints in the $\cos(\beta-\alpha)-\tan\beta$ plane for $M_H = M_{H^\pm} = 500$ GeV and again three values for the pseudoscalar mass $M_A = 100$ GeV (blue), 200 GeV (purple) and 300 GeV (gray). By combining the constraints from the electroweak precision observables for the above masses, where we obtained a restriction close to the alignment limit $|\cos(\beta-\alpha)| \lesssim 0.2$, with the bounds derived in this section one obtains the constraint $0.4 \lesssim \tan\beta \lesssim 3$. This bound can be significantly relaxed in more general models where fewer symmetries are present allowing for the presence of additional quartic couplings. One example is given in the right panel of Figure 4.5 where we added the quartic coupling $\Delta V_H = \lambda_6 H_1^\dagger H_1\, H_1 H_2^\dagger + h.c.$ to the potential (3.7). We show the effect of this additional term in dependence of real values of λ_6 in the interval from 0 to 3 in the alignment limit $\cos(\beta-\alpha)=0$. Here, larger values for $\tan\beta$ are in general possible but are still disfavored in comparison to smaller values of $\tan\beta = \mathcal{O}(1)$.
One can derive additional perturbativity constraints by taking the Yukawa couplings presented in (2.28) into account. For both considered two Higgs doublet models the top Yukawa coupling sets a lower bound on $\tan\beta \gtrsim 0.3$ as below this limit the coupling becomes non-perturbative [84]. This constraint is already fulfilled once the stability, perturbativity and unitarity constraints on the scalar potential are taken into consideration and hence are not explicitly drawn.

4.5 Collider Searches for Heavy Partners of the Higgs

A different approach to search for physics beyond the Standard Model at the collider is the attempt to aim for a direct detection of the mediator to find evidence for the existence of the dark matter particle. Such mediator searches in particular become relevant if the dark matter mass is too heavy for a decay of the mediator into a dark matter pair. In our simplified model however the relic density prefers a dark matter mass which is below half of the mediator mass. Nevertheless, for some regions in the parameter space the mono-X searches in general might be less sensitive than a constraint coming from a search of the mediator. This turns out to be not the case for our simplified model as we will show later.
Collider searches for the heavy Higgs particles can be used to set limits on the masses as well as the couplings to the Standard Model of the various spin-0 states. If the masses of the extended Higgs sector are within reach of the LHC, limits on the mediator masses can be set by a number of analyses searching for possible signatures of decays of the heavy states. Anticipating that the current limits on the masses of the heavy Higgs bosons are less stringent than the ones obtained from flavor physics combined with the electroweak precision observables, we want to give a short overview of the different decay channels setting bounds on the scalars and pseudoscalars as well as on $\tan\beta$ which provides a measure of the coupling strength. Not being able to extract any sensitive constraints out of collider searches for the heavy Higgs bosons has several distinct reasons. For the pseudoscalar A the presence of an additional decay channel into dark matter with a branching ratio $\mathrm{Br}(A \to \chi\bar{\chi})$ reduces the decays into Standard Model fermions. Especially since it dominates over most of the relevant parameter space if values of $\tan\beta$ are of the order one. This is in a general two Higgs doublet model a sensitive decay channel for a pseudoscalar collider search. Other decays as into gauge bosons are not available in the alignment limit and hence cannot constrain the pseudoscalar of our simplified model. The masses of the heavy charged Higgs $H^\pm$ as well as the heavy neutral scalar H are required to be above 500 GeV because of flavor physics and electroweak precision observables. This results in the fact that for our model collider searches for such states are not sensitive enough to provide relevant bounds. Moreover, for the neutral heavy Higgs the decay channels into ZA and AA become accessible, whereas the charged Higgs can decay into $W^\pm A$. As further the

pseudoscalar has a large branching ratio to dark matter this weakens the mediator searches. Altogether we can conclude that the most stringent limits at colliders are obtained from the mono-X searches which we present in the following chapter. But before, we want to provide an overview of the searches for additional spin-0 particles.

Searches for the existence of a pseudoscalar A are the decay $A \to hZ$ [85–88] which is not present in the alignment limit, $A \to tt$ [89], $A \to \gamma\gamma$ [90] which both do not reach the required sensitivity, and $A \to \tau\tau$ [91–93] as well as the most sensitive channel $A \to bb$ [94] which can only set constraints on $\tan\beta \gtrsim 15$ for our simplified model. The neutral heavy scalar is searched in $H \to tt$ [95], in top or bottom quarks associated production [96] as well as for large values of $\tan\beta$ in $H \to \tau\tau$ [95, 97], whereas decays into gauge bosons as $H \to VV$ [98–100], $H \to hV$ [101] and $H \to hh$ [102] are not present in the alignment limit. Searches for the heavy charged scalar $H^\pm$ focus on $H^\pm \to tb$ [103], heavy quark associated production [96], whereas $H^\pm \to \tau\nu$ [104, 105], associated jet production [106] are less sensitive and $H^\pm \to W^\pm Z$ [107] not even occurs in our simplified model.

We have discussed all the relevant branching ratios of the additional spin-0 states in the end of the previous Chapter 3.3 in great detail where we only considered the alignment limit with $\cos(\beta - \alpha) = 0$.

5 Constraints Motivated by Exploring the Dark Sector

In this chapter we continue to discuss experimental bounds on our simplified model which are now derived from the study of the dark sector, whereas in the previous chapter the existence of dark matter was not necessary for setting the constraints as they entirely emerged from the scalar sector. We focus first on constraints which can be derived from the relic density which we already discussed from a theoretical perspective in Section 2.3 in terms of the thermal freezeout. Secondly we study the prospects of direct and indirect detection experiments. Thereby, we assume that the particle χ is the main part of the dark matter. As before the constraints we derive in this chapter are model dependent and may change in a complete model which can be expressed in an appropriate limit by the EFT (2.28). This chapter is partially based on [15, 63].
The numerical results obtained in this chapter are calculated with micrOmegas version 4.3.1 [108,109]. We must provide a CH file which we generated with FeynRules version 2.3.24 [110,111] using a modified copy of 'The general Two-Higgs Doublet Model' model file as it is found in the FeynRules model database [112]. We cross-checked our modifications of the Higgs basis rotation regarding the Yukawa couplings as well as trilinear and quartic Higgs self-interactions as presented in Section 3.1.

5.1 Relic Density

The overall relic dark matter abundance has been measured to be $(\Omega_\chi h^2)_{\text{Planck}} = 0.1198 \pm 0.0015$ [5] by the Planck collaboration. Our simplified dark matter model is therefore required to reproduce this measured quantity. Hereby we assume that the dark matter fermion χ in our simplified model (2.28) is the main dark matter candidate contributing to the relic density. This measurement translates into a relation between the mediator mass, the dark matter mass and the coupling strength of this interaction. In situations where the theory is not complete, as in our simplified model, this relation must be treated with caution regarding the obtained allowed parameter space. Here an under-abundance due to a too efficient annihilation can for example be explained by an additional stable particle occurring in the complete theory. On the contrary, an over-closure of the universe which could emerge from a too small predicted annihilation cross section could be explained by additional decay channels. For example, collider searches for mono-X signals could find such a dark matter candidate stable on collider time scales to which the mediator couples dominantly, but which can decay into a lighter and stable dark matter particle leading to a lower relic density. Even if these possibilities exist we want to concentrate on the situation where χ can explain most of the observed relic density. Anticipating the outcome of the work of this chapter, it bears mentioning that the parameter space in which we can reproduce the measured relic abundance coincides with the constraints obtained in the previous chapter which were independent from the dark matter and only derived from the two Higgs doublet phenomenology. There we have shown that dark matter interactions with scalar couplings are highly disfavored, compare with Section 4.1. As we have mentioned already in Section 2.6 direct detection experiments do not provide relevant bounds on the cross sections for pseudoscalar interactions due to the velocity suppression. Hence, we want to make use

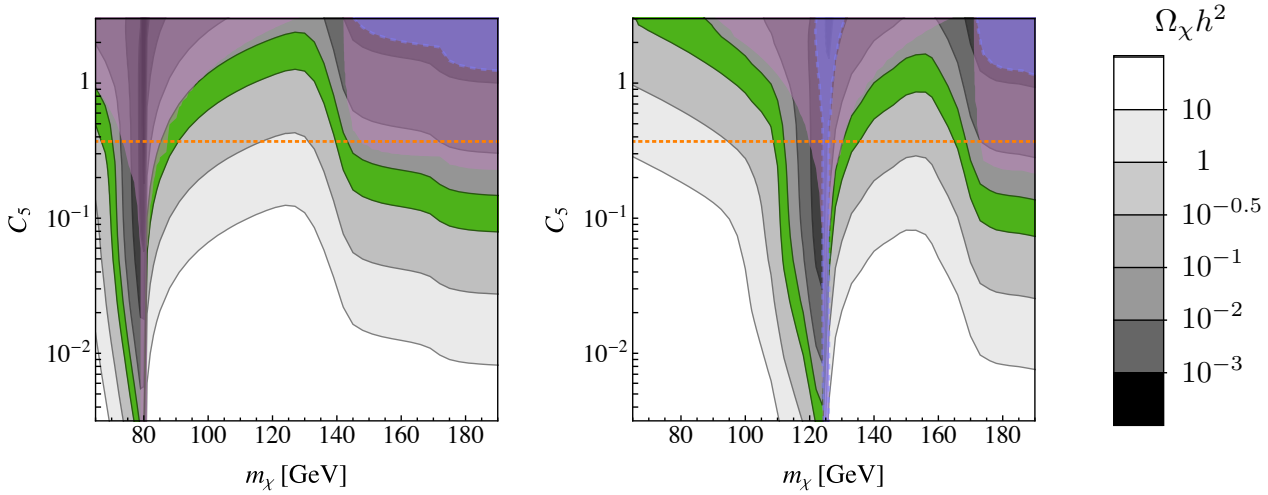

Figure 5.1: Contours of the dark matter annihilation cross section in units of the relic density $\Omega_\chi\, h^2$ are shown for $\tan\beta = 1$ and a mediator mass of M_A=160 GeV (left panel) as well as M_A=250 GeV (right panel) depending on m_χ and C_5. The green band corresponds to $0.04 > \Omega_\chi h^2 > 0.13$, whereas the purple region is excluded by the CMB-measurement from the Planck collaboration and the blue shaded area indicates the projections of the sensitivity expected from a CTA measurement. The dashed orange line corresponds to the chosen value of the pseudoscalar coupling strength for the analyses in the remainder of this thesis. Figures taken from [15].

of the condition that the measured relic density needs to be reproduced by our model to set limits on the dark matter mass m_χ as well as on the CP-conserving purely pseudoscalar coupling constant C_5. Thereby, we self-evidently take the constraints derived in the previous chapter into consideration.
A scan for natural values of the coupling strength C_5 and the dark matter mass m_χ between 70 and 190 GeV for various pseudoscalar masses M_A in the range of 80 to 350 GeV was performed. We fixed $\cos(\beta-\alpha) = 0$, $C_\chi = 0$, $M_H = M_{H^\pm} = 500$ GeV and $\tan\beta = 1$. The corresponding predictions of the relic abundance $\Omega_\chi h^2$ are shown in Figure 5.1 and are valid for both type I and II two Higgs doublet models. There the $m_\chi - C_5$ planes show the relic density depending on the pseudoscalar coupling strength and dark matter mass are presented for two different pseudoscalar masses of $M_A = 160$ GeV (left panel) and $M_A = 250$ GeV (right panel), respectively. The green shaded regions indicate the parameter space where the relic abundance lies within $0.13 > \Omega_\chi h^2 > 0.04$. This we consider as the allowed range in which χ is not the exclusive but still a significant contribution to the observed dark matter density. To gain a better understanding of the shape of these contours we will shortly discuss the velocity averaged cross section of the main annihilation channel of the dark matter, which is the decay into a pair of b-quarks for most of the considered parameter space where a decay into top quarks is kinematically forbidden. As we have seen before in (2.13) the annihilation cross section directly influences the relic density. More effective annihilation leads to lower dark matter abundance. The leading order cross section of $\chi\bar{\chi} \to A \to b\bar{b}$ for the non-relativistic limit can be approximated by

$$\langle \sigma_{ann} v \rangle \;\approx\; \sigma_{ann}\, v \;=\; \frac{N_c}{4\pi}\,\frac{\sqrt{s-4m_b^2}}{m_\chi}\,\left(\frac{g_{A5}\,\kappa_{Ad}\,m_b}{v}\right)^2 \frac{4m_\chi^2}{\left(4m_\chi^2 - M_A^2\right)^2 + M_A^2\,\Gamma_A^2}\,, \tag{5.1}$$

where N_c represents the color factor of the final state quarks and Γ_A the total decay width of the pseudoscalar which can be obtained from summing over all partial widths given in (B.5) - (B.8). The center of mass energy of the interaction is parametrized by s, whereas κ_{Ad} is the scale factor of the coupling. A detailed derivation of (5.1) can be found in [63]. With the above equation we are now able to understand the resonant enhancement of the annihilation cross sections at the pseudoscalar-pole $m_\chi = M_A/2$ where

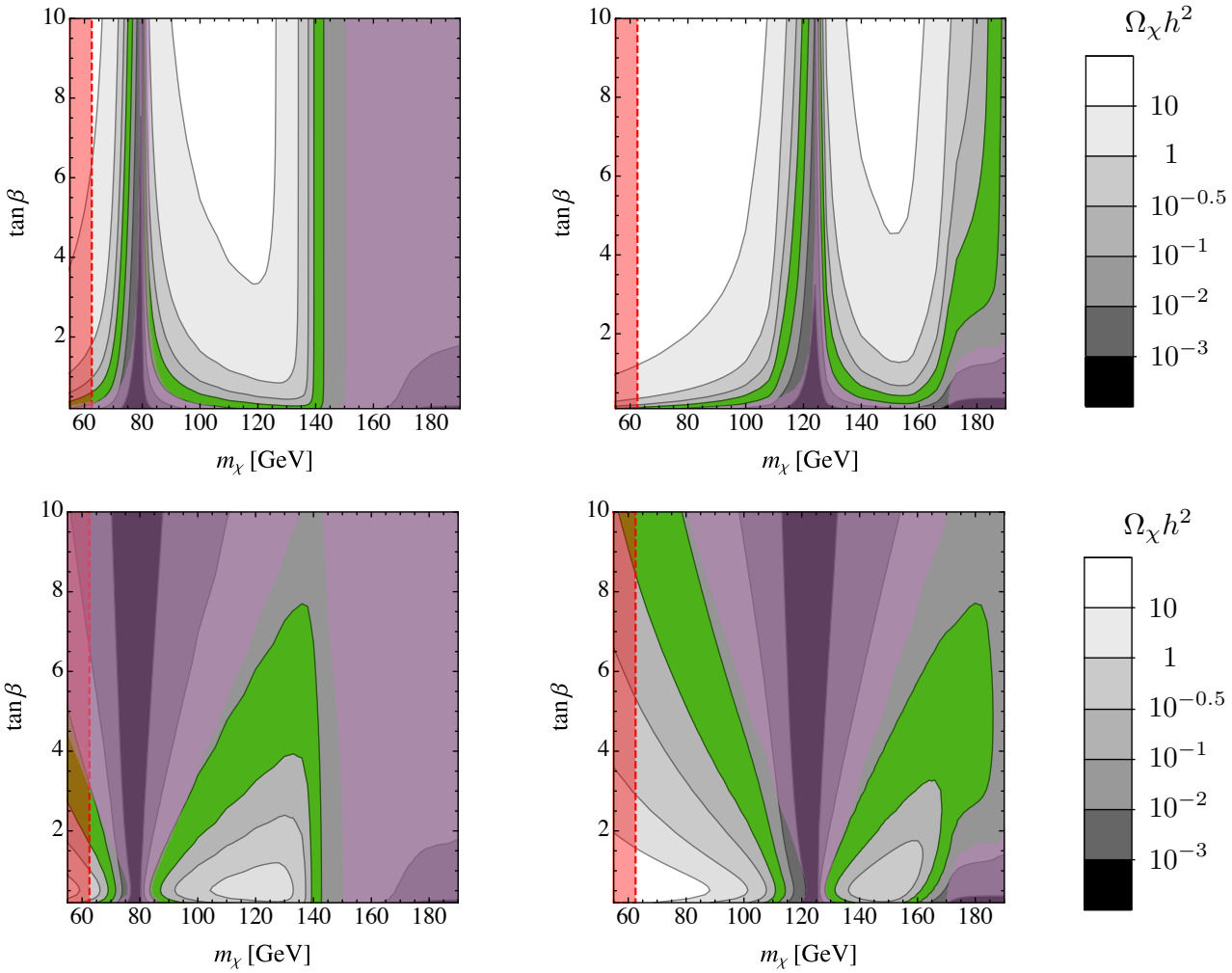

Figure 5.2: Contours of the dark matter relic density $\Omega_\chi h^2$ are shown for $C_5 = 0.37$ and a mediator mass of M_A=160 GeV (left panel) as well as M_A=250 GeV (right panel) depending on m_χ and $\tan\beta$. The contours in the upper (lower) panels present the different Yukawa sectors of type I (II) 2HDM. The green band corresponds to $0.04 > \Omega_\chi h^2 > 0.13$, whereas the purple region is excluded by the CMB-measurement from the Planck collaboration. The Higgs signal strength measurements disfavor the red shaded region. Figure taken from [15].

$\langle\sigma_{ann}v\rangle$ is maximal which leads to a minimal relic density. The corresponding coupling C_5 needs to be small to obtain the required relic density. One can as well consider the light Higgs h instead of the pseudoscalar as the mediator and obtain a minimum of the relic density at $m_\chi = m_h/2$ like in the prior case. The further behavior of the green contour representing a suitable relic abundance can be explained by the opening of the annihilation channels $\chi\bar{\chi} \to Ah$ and $\chi\bar{\chi} \to A \to t\bar{t}$ for $m_\chi \geq (M_A + m_h)/2$ and $m_\chi \geq m_t$, respectively. The request of feasible mono-X signatures at colliders, which we are going to study in the next chapter, requires that the pseudoscalar mediator A is able to decay on-shell into a pair of dark matter particles. Hence, we prefer $m_\chi \leq M_A/2$. For such masses no extreme fine-tuning of the coupling strength C_5 is necessary to get the correct relic density. The coupling constant C_5 can take values in the range of 0.25 to 2.5. For our further work we set $C_5 = 0.37$ which is indicated as the dashed orange line in Figure 5.1, corresponding to $c_5 = 1.5 \times 10^{-3}$ (Λ/GeV) with Λ =1 TeV.
The relic abundances are shown in the upper (lower) panels of Figure 5.2 for the Yukawa couplings of a type I (II) two Higgs doublet model in dependence of $\tan\beta$ and the dark matter mass. The left panels illustrate the relic density in the $m_\chi - \tan\beta$ plane for $M_A = 160$ GeV, whereas for the right-hand panels

we fix the pseudoscalar mass to $M_A = 250$ GeV. We further stay in the alignment limit $\cos(\beta-\alpha) = 0$, set $C_5 = 0.37$ and forbid scalar couplings as $C_\chi = 0$. The preferred parameter space, where the relic density takes values $0.13 > \Omega_\chi h^2 > 0.04$, is shaded in green. The regions excluded by the CMB-measurement are shaded purple. The region marked in red indicates the excluded parameter space where the Standard Model Higgs in principle can decay into a dark matter pair. For $\mathrm{Re}[C_\chi] = \mathrm{Im}[C_5] = 0$ this constraint vanishes, but already for couplings as small as $C_\chi = \mathcal{O}(10^{-4})$ and $m_\chi < m_h/2$ the fit to the Higgs signal strength measurements excludes most of the parameter space.
For the Yukawa couplings of type I two separate bands can be found. The first one occurs for $m_\chi < M_A/2$ and the second one for $m_\chi > M_A/2$, where the first one is favored as it allows on-shell decays. In case of a type II model the green contour is cut by the pseudoscalar pole and restricted for higher dark matter masses and large values of $\tan\beta$. The difference between the two types can be explained by the annihilation of χ via the mediator A into a pair of bottom quarks which leads to an inverted scaling with $\tan\beta$. In the upper panels, illustrating the type I couplings, $\tan\beta < 1$ is preferred which is mainly already restricted by various other experiments. It remain two rather narrow bands around the pseudoscalar pole for values of $\tan\beta > 1$. In the case of a type II model the parameter space is considerably less constraint where the contour of an appropriate dark matter abundance is broadened and $\left(\Omega_\chi h^2\right)_{\mathrm{Planck}}$ can be reproduced for $\tan\beta \gtrsim 1$. Here the highest possible value of $\tan\beta$ strongly depends on the mediator mass. Nevertheless, the relic abundance prefers $\tan\beta < 10$ and moreover is independent of $\cos(\beta-\alpha)$ as the pseudoscalar couplings have only a $\tan\beta$ dependence.
For larger dark matter masses than the one we require at our collider search $m_\chi < M_A/2$, additional annihilation channels open so that the relic density decreases. For $m_\chi \approx (M_A + m_h)/2$ the channel $\chi\bar{\chi} \to hA$ becomes available and the annihilation rate increases leading to the sharp cut-off in the relic abundance. For even larger masses where $m_\chi \approx m_t$ the dark matter can annihilate into a pair of top quarks, whereas the relic density drops, compare with Figure 5.2. For mediator masses $M_A \lesssim 215$ GeV the annihilation channel $\chi\bar{\chi} \to hA$ becomes most important, whereas for larger mediator masses $\chi\bar{\chi} \to t\bar{t}$ is the leading contribution.
For both type I and II and various mediator masses one can find regions in the parameter space where the relic density can be reproduced without huge fine-tuning . For the collider search we chose $C_5 = 0.37$ and fix the dark matter mass at $m_\chi = 70$ GeV and 100 GeV as we then can vary $\tan\beta$ in the requested range.

The influence of the different input parameters is widely discussed in [63], but we drop further treatment of the ones which are being set to zero in the further study. By shifting the pseudoscalar mass in the region where the relic density can be obtained, the pole is accordingly rearranged to the position where $m_\chi = M_A/2$. On the other hand, enlarging $\mathrm{Re}[C_5]$ displaces the bands slightly to the outer regions and broadens them. As a CP-violating coupling can be interesting for a phenomenology study of the influence of this dark matter model on baryogenesis the properties of such a coupling $\mathrm{Im}[C_\chi] \approx \mathrm{Re}[C_5]$ was investigated. It was found that this coupling affects the plotted relic abundance slightly. The possibility of a second pole due to the Standard Model Higgs was mentioned already above and requires the departure from zero of the real scalar coupling constant $\mathrm{Re}[C_\chi]$.
As the model was motivated originally by the Higgs doublet acting as a flavon we studied the behavior of the insertion of higher order operators, here the $n = 2$ case as defined in (3.40). Assuming again pure pseudoscalar couplings, the contour reproducing the relic density is almost vertical for $t_\beta > 3$, whereas it is flat in the presented $n = 1$ case.
Moreover, in our simplified model we dropped terms in the Lagrangian where two identical Higgs doublets interact with dark matter. These operators all lead to strongly constraint scalar couplings which in total

must respect the limit of $\mathrm{Re}[C_\chi] \lesssim 3.7 \times 10^{-4}$. The same influence can be observed by increasing the values of the coupling, so these additional operators do not contribute to a new phenomenology and only the Higgs pole is slightly distorted.

We showed that the relic density could be obtained within our simplified model and no fine-tuning of the input parameters is necessary. The coupling strength in the collider dark matter search will be set to $\mathrm{Re}[C_5] = 0.37$ and the mass of the dark matter will be set to m_χ =70 GeV and 100 GeV, respectively. We will continue to discuss the constraints derived from direct and indirect detection experiments which as well rely on the calculated annihilation cross sections.

5.2 Direct Detection

Direct detection experiments like XENON1T [113] or LUX [114] can set strong bounds on the cross section of the scattering between WIMPs and a nucleus of the detector measuring nuclear recoils. They are extremely sensitive to scalar dark matter couplings. In our case the constraints are considerable weaker as in our simplified model a pseudoscalar is the mediator. Hence, the dark matter to nucleon interaction is suppressed by the non-relativistic velocity of the dark matter [11]. As moreover the coupling of the pseudoscalar mediator to the nucleon in the detector is spin-dependent the enhancement factor of the used noble gases like Xenon is lost compared to the scalar spin-independent case which roughly leads to two orders of magnitude lower cross sections. In summary, we can state that direct detection experiments are not able to yield sensitive constraints to the dark matter-nucleon cross section for models containing a pseudoscalar mediator and no visible restrictions on the coupling strength $\mathrm{Re}[C_5]$ can be set. Stated differently the only reasonable constraints can be given for purely scalar currents where a h or H mediates the interaction between the dark sector and the Standard Model particles. The cross section in this case depends on the coupling strength $\mathrm{Re}[C_\chi]$. The currently strongest bounds on the spin-independent dark matter-nucleus scattering cross section are given by the exclusion limits of the XENON1T experiment at 90 % confidence level. Hence, we compare this obtained limit with our cross section calculated by micrOmegas. XENON1T is most sensitive to WIMP masses of roughly 30 GeV. In this case cross sections as low as $\sigma_{\chi-N}^{\mathrm{XENON1T}} \approx 10^{-47}\ \mathrm{cm}^2$ can be ruled out, compare to Figure 5.3. This limit can be translated into a constraint on the coupling constant $\mathrm{Re}[C_\chi] \lesssim 1.1 \times 10^{-2}$ where we assume an exchange of the Standard Model Higgs h for a maximal value of $g_{h\chi}$ in the alignment limit with $\cos(\beta-\alpha) = 0$ and $\tan\beta = 1$ [1] to get an upper bound on C_χ. As the dark matter mass in our model is usually assumed to be $m_\chi = 70$ GeV we overestimate the exclusion limit slightly as the sensitivity of the XENON1T experiment decreases for higher dark matter masses.
The derived constraint on $\mathrm{Re}[C_\chi]$ from the scalar nucleon scattering cross section is in agreement with the bounds obtained from the global Higgs signal strength measurement fit in Section 4.1. For dark matter masses $m_\chi < m_h/2$ the global fit leads to stronger bounds on $\mathrm{Re}[C_\chi]$ than direct detection experiments.

5.3 Indirect Detection

Indirect detection experiments aim to find further evidence for the existence and nature of dark matter. They investigate various observables like peaks in a photon or γ-ray spectrum or the distribution of anti-matter, which are again connected to the dark matter annihilation to Standard Model particles.
We start by considering constraints from distortions in the cosmic microwave background (CMB). To

[1] The constraint from the heavy scalar H acting as a mediator in the dark matter nucleus interaction is suppressed by a factor m_h^4/M_H^4 and $g_{H\chi}$ which tends to zero at $\tan\beta = 1$ in the alignment limit.

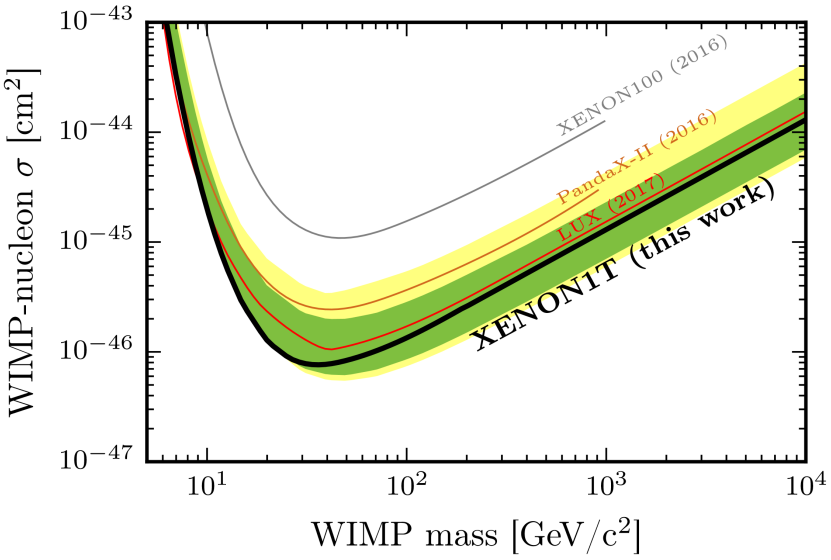

Figure 5.3: Current exclusion limit for the spin-independent WIMP-nucleon scattering cross section depending on the WIMP mass from various experiments as the XENON collaboration, LUX and PandaX-II. The strongest bounds are given by the XENON1T experiment. Figure taken from [113].

ensure the absence of a significant reheating process of the CMB the effective annihilation cross section of dark matter to photons is required to be small at the time they decouple from the early thermal bath. The recent measurement of Planck [5] results in the following bound [42]

$$f_{\text{eff}} \frac{(\sigma v)_{\text{ann}}}{m_\chi} \lesssim 3 \times 10^{-28} \frac{\text{cm}^3}{\text{s GeV}}, \tag{5.2}$$

where $f_{\text{eff}} = 0.35$ represents the redshift-dependent efficiency factor. It is evaluated at the time of the last scattering for the leading annihilation process $\chi\bar{\chi} \to b\bar{b}$ for most of the parameter space [41]. The corresponding velocity averaged annihilation cross section is denoted as $(\sigma v)_{\text{ann}}$. In our simplified model this is almost independent of the mean velocity v. As the velocity is the only relevant variable varying during the evolution of the universe, we can approximate $(\sigma v)_{\text{ann}}$ by the annihilation cross section obtained by micrOmegas for today. The parameter space which is excluded by this constraint is shaded purple in Figure 5.1.

A further, but weaker bound can be derived from the projected limits of the Cherenkov Telescope Array (CTA) which is currently constructed to observe the photon flux. In this case the absence of a gamma ray signal can be translated into a constraint on the annihilation cross section of the dark matter. The expected bounds obtained from a projection of the experimental reach of CTA is shown in Figure 5.4. To compare these limits with our model we calculated the dark matter annihilation cross section in the simplified model with micrOmegas. As a check we match the parameters of our model to the coefficients of the simplified model containing Dirac dark matter and a pseudoscalar mediator as given in [40]. For dark matter masses $m_\chi \lesssim M_A/2$ we are able to reproduce the cross sections shown in the upper right of Figure 5.4 as the black dashed line. If we consider larger dark matter masses the annihilation channel $\Gamma(\chi\bar{\chi} \to hA)$ becomes more relevant and increases the dark matter annihilation cross section. This effect is not present in their study as well as the strong dependence on $\tan\beta$. For the simplified model both rather small and rather large values of $\tan\beta$ can be ruled out due to the minimum at $\tan\beta = 1$.

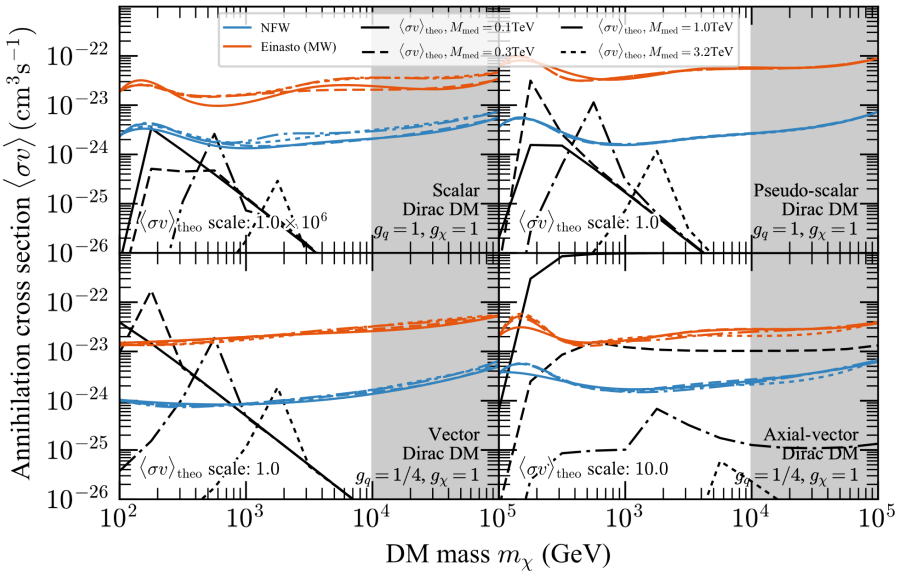

Figure 5.4: Projected limits for the future CTA experiment on the annihilation cross sections for various simplified models. Bounds are presented for two considered dark matter density profiles, the blue and the orange lines, and for various mediator masses $M_{med} = M_A = 0.1$, 0.3, 1, and 3.2 TeV. Theoretical cross sections represented by the black lines are upscaled by a factor of 10^6 respectively 10 for the scalar and axial-vector dark matter. For the pseudoscalar case they could be reproduced with the simplified model (2.28). The gray shaded region on the right indicates the breakdown of their NLO approximation for $m_\chi > 10$ TeV. Figure taken from [40].

The two discussed constraints from indirect detection experiments are presented in the figures showing the calculated relic densities. The parameter space excluded by the CMB study is shaded purple in the Figures 5.2 and 5.1. As the projected limits from the CTA experiment are roughly one order of magnitude weaker than the ones derived from the CMB spectrum they are only shown in Figure 5.1 as the blue shaded region.

Both constraints from CMB and CTA exclude regions in the parameter space which are not preferred by the measured relic density. Hence, the collider searches focusing on mono-X final state signatures are expected to be most sensitive in the parameter space where the resonant decay of the mediator into dark matter is kinematically allowed, hence $m_\chi < M_A/2$ is fulfilled.

6 Mono-X Dark Matter Searches at the LHC

In this chapter we will concentrate on a detailed study of the reach of mono-jet, mono-Z and $t\bar{t} + E_T^{\text{miss}}$ dark matter searches for the simplified model (2.28) at the LHC [15]. We have already stated that such signatures can be complementary to direct and indirect searches which we are going to reaffirm now more qualitatively. Therefore, we define two benchmark sets by considering the prior obtained constraints,

$$\text{Benchmark 1} \quad M_A = 160 \text{ GeV}, M_H = M_{H^\pm} = 500 \text{ GeV}, m_\chi = 70 \text{ GeV}, C_5 = 0.37, C_\chi = 0, \quad (6.1)$$

$$\text{Benchmark 2} \quad M_A = 250 \text{ GeV}, M_H = M_{H^\pm} = 500 \text{ GeV}, m_\chi = 100 \text{ GeV}, C_5 = 0.37, C_\chi = 0. \quad (6.2)$$

The main difference between the two scenarios is the presence of the decay $H \to AA$ in the first benchmark, whereas in the second benchmark this decay is kinematically not possible. On the other hand, in the second benchmark the decay $A \to hZ$ is present outside the alignment limit, i.e. $\cos(\beta - \alpha) \neq 0$, but it is kinematically forbidden for $M_A = 160$ GeV. It is worth mentioning that the results obtained in this chapter are mainly independent of the dark matter mass m_χ as long as the pseudoscalar can decay into a dark matter pair which requires $m_\chi < M_A/2$. The relic density can be reproduced for both benchmarks in a considerably broad range of values for $\tan\beta$ as shown in the previous chapter.
The remainder of this chapter is structured as follows: we start by reviewing the method used for generating the analyzed Monte Carlo events where we focus on the different exploit tools. Next, we present the main backgrounds for the mono-jet, mono-Z and $t\bar{t} + E_T^{\text{miss}}$ searches which were generated to crosscheck the correct implantation of the cuts used by the experimental analyses. We continue with providing an overview of these cuts which were inserted to reproduce the analyses performed by ATLAS and CMS. It follows a detailed description of each of the performed analyses for the three main dark matter signatures we studied, as well as a brief outlook to further possible mono-X signals. Finally, we summarize the main results of the collider search, where we concentrate on the broken hierarchy of mono-X signatures and conclude with a projection of the reach at a high luminosity LHC run.

6.1 Event Generation and the Underlying Monte Carlo Chain

To derive constraints from the mono-X searches on the remaining dark matter parameter space, we need to simulate dark matter signal events which we then compare to the limits provided by the experimental groups at the LHC. We base our Monte Carlo simulation on a Universal FeynRules Output (UFO) implementation of the simplified model described in (2.28). We use FeynRules 2 [110, 111] and the NLOCT package [112] embedded in FeynArts 3.9 [115]. Some of the mono-X signals are produced by 1-loop diagrams at leading order. As the main production of the heavy Higgs or the pseudoscalar is loop-induced, we build our analysis on the FeynRules model file 'The general Two-Higgs Doublet Model' [112]. We rotate the scalar potential from the Higgs to the physical mass basis [59], impose a discrete symmetry of the potential and add the dark matter term to the Lagrangian. We validate the implementation of our model by comparing the Higgs tree-level couplings to the literature [59]. We export the UFO file to Madgraph5_aMC@NLO 2.5.5 [116] for calculating the hard matrix elements. As the mono-Z and mono-jets processes are at leading order already loop-induced, there are currently no tools for calculating

the NLO corrections available. For the generation of these processes MADLOOP [117] with its OPP integrand reduction method [118] inherited from CUTTOOLS [119] is used. The computation of the associated top production amplitude is also performed at leading order with Madgraph5_aMC@NLO 2.5.5. The showering is performed with the Pythia 8.226 [120] interface for Madgraph and the fast detector simulation with Delphes 3.4.0 [121]. For the event generation the NNPDF23_lo_as_130 set of parton distribution functions is used [122].
For the mono-jets study we perform a Matrix Element and Parton Shower (ME+PS) merging between the zero- and the one-jet sample, where the numbers refer to the required hard jets in the matrix element. Hence, we generate the signal processes $pp \to A$ and $pp \to A + j$ with Madgraph5_aMC@NLO 2.5.5. We obtain our event sample by employing the $k_T - MLM$ scheme [123] for 0- and 1-jet multiplicities within Pythia8. We set *xqcut* accordingly to a quarter of the hard scale in each process. This variable parametrizes the minimal distance in phase space between the QCD partons. The merging scale Q_{Cut} is chosen to be 1.5 times this distance to guarantee a smooth jet measure cut-off. For the rescaling of α_s 5 flavors are considered [124]. As in principle this merging procedure could be done for any of the mono-X signatures we restricted ourselves to the mono-jets as the ME +PS merging is expected to have a strong influence only in this case. The other two processes are presented on parton-level due to simplicity.
For the selected benchmark points we keep the mass of the pseudoscalar m_A and $\tan\beta$ free and fix the other parameters accordingly to the above discussion. For the two heavy Higgs partners H and $H^\pm$ we choose masses of 500 GeV and restrict ourselves to the alignment limit where $\cos(\beta - \alpha) = 0$.
The energy scale Λ, where we expect new physics, is set to 1 TeV and for the pure pseudoscalar coupling between the Standard Model and the dark sector we choose $\mathrm{Re}[C_5] = 0.37$ as suggested in Section 5.2, whereas the other scalar as well as the two CP-violating couplings are switched off. We want to avoid these CP-violating couplings to assure the absence of FCNCs and for the scalar coupling we must take the constraints from the Higgs signal strength fit as well as the direct detection measurements into account. Predictions for signals based on these couplings can be obtained merely by rescaling the cross sections with the corresponding modified branching ratios.

6.2 Production of the Main Backgrounds

One can check if a certain parameter set of a simplified dark matter model can be excluded with a missing transverse energy collider search by comparing the number of generated signal events with the number of allowed background events for the corresponding luminosity. More specifically, if the signal events exceed the 2σ bound of the uncertainty on the measured Standard Model background, the parameter space is excluded by the 95 % confidence level. The performed analyses require certain cuts to be sensitive to a dark matter signal. As these searches consider a different dark matter model, we cannot simply compare the number of signal events they obtained for their model. Hence, we are required to reconstruct their analyses and check if we correctly implemented the cuts, used by the experimental collaborations. Moreover, we need to generate the corresponding leading Standard Model backgrounds, apply our cuts and then check the number of obtained background events where we only consider the main background for each analysis. We perform the analyses within the MADANALYSIS5 framework [125] where we partially must use the expert mode and write a Root analysis files [126]. The implemented cuts are based on mono-X searches from ATLAS [127] and CMS [128, 129] for the mono-jets, mono-Z and $t\bar{t} + E_T^{\mathrm{miss}}$.
To crosscheck the implementation of the cuts for the various searches we generate the following background events and compare them to the measured number of events of the experiments. The mono-jets background is validated with $Z \to \nu\nu$+jets which in the ATLAS search at 36.1 fb^{-1} provides about 60 % of the total background [127]. We use the k_t-MLM jet merging scheme for up to 4 jets which provides

ATLAS Mono-Jet	CMS Mono-Z	CMS $t\bar{t} + E_T^{\text{miss}}$
$E_T^{\text{miss}} > 250$ GeV	$p_T^l > 25$ (20)/20 GeV	$E_T^{\text{miss}} > 200$ GeV
$p_T^j > 250$ GeV	$m_Z - 15 < m_{ll} < m_Z + 10$ GeV	lepton veto $p_T^l > 10$ GeV
$\lvert\eta_j\rvert < 2.4$	$\lvert\eta_l\rvert < 2.4$	Jets ≥ 4 with $p_T^j > 20$ GeV
lepton veto $p_T^e > 20$ GeV	3^{rd}-lepton veto $p_T^{e,\mu} > 10$ GeV	number b-tags ≥ 2
lepton veto $p_T^\mu > 10$ GeV	3^{rd}-lepton veto $p_T^\tau > 18$ GeV	$\Delta\phi\left(\text{jet}, E_T^{\text{miss}}\right) > 1.0$ radians
Jets ≤ 4 with $p_T^j > 30$ GeV	$p_T^{ll} > 60$ GeV	
$\Delta\phi\left(\text{jet}, p_T^{\text{miss}}\right) > 0.4$ radians	Jets ≤ 1 with $p_T^j > 30$ GeV	
	Top quark veto $p_T^b > 20$ GeV	
	$E_T^{\text{miss}} > 100$ GeV	
	$\left\lvert E_T^{\text{miss}} - p_T^{ll}\right\rvert / p_T^{ll} < 0.4$	
	$\Delta\phi\left(ll, \vec{p}_T^{\text{miss}}\right) > 2.8$ radians	
	$\Delta\phi\left(\text{jet}, E_T^{\text{miss}}\right) > 0.5$ radians	

Table 6.1: Cuts applied in the various mono-X channels based on the ATLAS mono-jet search [127], and the CMS searches for mono-Z [128] and $t\bar{t} + E_T^{\text{miss}}$ final states [129].

roughly the correct number of expected background events. The disagreement results from the fact that some applied cuts are not reproducible. An example would be cuts on the shape of the jets, but they are dominated by statistical fluctuations of our event generation. As an estimate of the validity of the implemented cuts the obtained precision is sufficient. The above argumentation also applies to $ZZ \to \nu\nu l^+ l^-$, the dominant background for mono-Z in the CMS search at 12.9 fb^{-1} [128] which is matched rather well. In case of the $t\bar{t}-$associated production we use the $VV \to t\bar{t} + E_T^{\text{miss}}$ channel which is subdominant but quite clean compared to the leading $t\bar{t}$ background where the top quarks must be reconstructed. Here we overestimate the background by about 20 % as we are missing again some non-reproducible cuts of the CMS search at 2.2 fb^{-1} [129].

6.3 Overview of the Various Cuts in the LHC Searches

Reproducing the distinct collider searches for dark matter at the LHC requires the implementation of the cuts applied by ATLAS respective CMS in their analyses. Every potential discovery channel necessitates specific cuts optimized for the characteristic signatures of the different processes. We are going to present the cuts implemented in our analyses and point out where we had difficulties to take some of the cuts into consideration.

As the fast detector simulation with Delphes, which we use in our framework, is an oversimplification of the full detector simulation performed by the LHC experiments we are not able to reproduce every single cut. For example, missing restrictions on the jet shapes and a study of the constituents of the jets are not considered.

For all three processes we consider cuts on the leading transverse momentum p_T as well as on the missing transverse energy (MET) in an event. In general, if one produces dark matter at a collider from an interaction of two Standard Model particles one would expect no signature at the detector as the dark matter is assumed to be extremely weakly coupled to the Standard Model and stable on timescales of the universe. Hence, MET is a strong indicator of signal events as the dark matter particles escape from the detector without leaving any tracks. Initial state radiation ensures that the event finally becomes visible for the detectors. Possible MET+X-signatures are mono-jets/Z , heavy fermion associated production, mono-$W/h/\gamma$ - from which we analyze the first three. Strongly boosted particles recoiling against the dark matter can then be detected in the experiments. Backgrounds which can fake these signals are mainly decays into neutrinos as well as miss-measured particles.

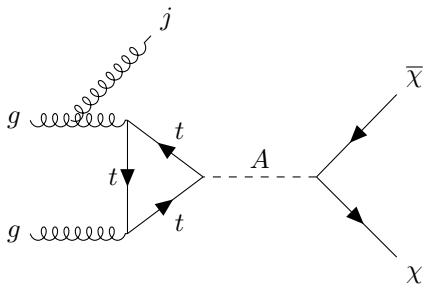

Figure 6.1: Feynman diagram contributing to mono-jet production from initial state radiation. Diagram generated with [73].

In the mono-jet analysis performed by ATLAS, a $E_T^{\text{miss}} > 250$ GeV is required as well as a leading jet transverse momentum of $p_T > 250$ GeV. Only leading jets with a pseudorapidity $|\eta_j| < 2.4$ are considered. Events with more than four jets with $p_T > 30$ GeV are rejected. To reduce the background of multi-jet events, where MET can result from miss-measuring the jet energies, all jets need to be separated by at least $\Delta\phi(jet, p_T^{\text{miss}}) > 0.4$ radians in the azimuthal plane from the missing transverse momentum. As the event is expected to be exclusively hadronic all events with electrons (muons) with $p_T > 20$ (10) GeV are discarded.
In the mono-Z study of CMS, one lepton pair with opposite electrical charges is requested with the leading transverse momentum $p_T > 25$ (20) GeV for electrons (muons), whereas the sub-leading lepton in both cases is required to have $p_T > 20$ GeV. The pseudorapidity of the leading lepton should be smaller than $|\eta_l| < 2.4$. To ensure that the leptons originate from a decay of a Z boson the invariant mass is narrowed to the range of 75-101 GeV and a combined transverse momentum larger than 60 GeV is required. Third leptons are vetoed with a p_t greater than 10 GeV for electrons and muons, whereas for taus the limit is 18 GeV. A maximum of one jet with a $p_T > 30$ GeV is allowed which needs to be separated from the missing transverse energy by $\Delta\phi\left(\text{jet}, E_T^{\text{miss}}\right)$ at least 0.5 radians. Since no hadronic decays are expected, a top quark veto is applied as events containing a b-jet with $p_T > 30$ GeV are rejected. Furthermore, direct cuts on the missing transverse energy are introduced requiring $E_T^{\text{miss}} > 100$ GeV and two cuts securing that the MET and the lepton pair are geometrically recoiling against each other which is taken into consideration by $\left|E_T^{\text{miss}} - p_T^{ll}\right| / p_T^{ll} < 0.4$ and $\Delta\phi\left(ll, \vec{p}_T^{\text{miss}}\right) > 2.8$ radians.
In case of the top associated production of dark matter as analyzed by the CMS collaboration, a missing transverse energy cut of 200 GeV is applied. A minimum of 4 jets with transverse energies above 20 GeV are necessary of which at least two must be b-tagged. As the jets are supposed to recoil against the dark matter $\Delta\phi\left(\text{jet}, E_T^{\text{miss}}\right)$ above 1 radians is required. Leptons with a p_T larger than 10 GeV are once again vetoed as the process should be mainly hadronic.
An overview of the discussed cuts for the various searches is given in Table 6.1. Since we have investigated the construction of the three analyses, we continue with a presentation of the corresponding results.

6.4 Mono-Jets

One attempt to detect dark matter at a collider is the search for missing transverse energy accompanied by mono-jets. These jets can be radiated of the initial or final state. An example for such a process is shown in Figure 6.1. In the analysis we implement cuts according to the ATLAS mono-jet search [127] and validate the results with the rescaled projections of the simplified model used by the LHC Dark Matter Forum [130]. The applied cuts are selected in the left column of Table 6.1.
For the signal generation we use Madgraph5_aMC@NLO where we require one jet being radiated of the

initial state besides the production of a pseudoscalar A from a gluon fusion loop. The mediator then decays further into a pair of dark matter fermions χ. The jet can emerge either from the hard matrix element directly or from the showering process performed within Pythia8. The two dark matter particles provide the missing transverse energy required to detect the event and to classify it as a signal event.
Taking only the contribution from the top-quark in the loop into account increases the runtime tremendously and affects the cross section only by a factor of up to 2 % for a light pseudoscalar mass and considerable large $\tan\beta$. Neglecting the b quark in the loop for low values of $\tan\beta$ is justified as this error is considerably smaller than the statistical one, which is of the order of approximately 10 %. The systematic signal uncertainty, due to different choices for the PDFs, is approximately 3.7 % and for the variation of the renormalization and factorization scales we find about 30 % at leading order which is expected to decrease tremendously as soon as NLO corrections are taken into account. In this analysis a systematic uncertainty of 5 % is assumed. We account for higher order corrections by applying a mass-dependent N^{2}LO K-factor at $\sqrt{s} = 13$ TeV. This K-factor is in the range of 2.1 to 2.37 for pseudoscalar masses between 150 to 430 GeV [131].
With the current data set of 36.1 fb^{-1} values of $\tan\beta$ below 0.5 can be excluded up to a pseudoscalar mediator mass of 340 GeV, compare Figure 6.5. This sharp cut-off can be explained by the opening of the top-decay channel where the pseudoscalar dominantly decays into a pair of top quarks, see the left plot of Figure 3.1.
In Figure 6.6 the exclusion limits for the mono-X searches are presented in the $\cos(\beta-\alpha) - \tan\beta$ plane for a pseudoscalar mass of 160 GeV (left) and 250 GeV (right), respectively. As on the right plot the decay of the mediator into the Standard Model Higgs and a Z boson becomes present for $(\cos\beta - \alpha) \neq 0$, the bounds become slightly weaker to the edges due to the opening of the decay channel $A \to hZ$. This decay is kinematically not allowed for $M_A = 160$ GeV because the mediator is too light to decay into a Higgs and a Z boson.
Since the uncertainty for the Standard Model prediction for the total number of events in the inclusive signal region is mainly restricted by systematic uncertainties, the reach of this study for higher luminosity is limited by those. Therefore, higher statistics only slightly improve the exclusion bounds of this search channel.

6.5 Mono-Z

Initial state radiation of the Z boson is almost negligible compared to mono-jets as this process is suppressed by the weak coupling besides the production of the Z boson mass [132]. The simplified model with a pseudoscalar mediator requires the presence of an additional heavy scalar which cannot be decoupled without violating the stability and unitarity constraints derived in Section 4.4. The existence of this heavy scalar besides the pseudoscalar mediator allows for a resonantly enhanced mono-Z final state,

$$pp \to H \to AZ \to \chi\bar{\chi}Z, \tag{6.3}$$

where the heavy Higgs H can decay into a pseudoscalar A and a Z boson, as it is shown in Figure 6.2. The signature in (6.3) is identified to be a universal signal for all simplified models with pseudoscalar mediators.
For our parameter space with small values for $\tan\beta$ the contribution of the lighter quarks gives only a small correction to the total production cross section. Therefore, in our analysis H is generated via a fermion loop where only the top quark is considered. The mono-Z signal is hence directly proportional

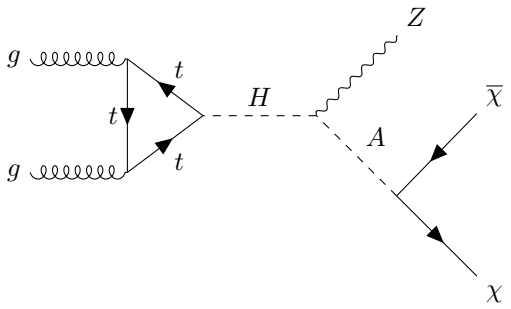

Figure 6.2: Feynman diagram contributing to resonant mono-Z production. Diagram generated with [73].

to the production cross section of the heavy scalar. The signal is generated with Madgraph5_aMC@NLO at leading order and require the Z boson to decay leptonically. The mediator then should decay into dark matter to provide the necessary missing transverse energy. The cuts are applied accordingly to the CMS mono-Z search [128] and are shown in the central column of Table 6.1.

Statistical uncertainties of the signal generation and the analysis are of the order of 1-2 % and therefore rather small compared to the ones of the mono-jet study. The scale variation for the leading order is approximately 20 % and expected to be significantly smaller at NLO. PDF uncertainties are of the order of about 4.9 %. We assume a systematic error of 7 % to generate the corresponding exclusion limits and apply a N^{2}LO K-factor of 2.3 for $M_H = 500$ GeV at $\sqrt{s} = 13$ TeV [133, 134] to account for higher order corrections.

The branching ratio BR($H \to AZ$) dominates over BR($H \to AA$) for $\tan\beta \approx 1$. This is due to the fact that the later branching ratio has a pole at $\tan\beta = 1$, which can be seen in Figure 3.2. Already at values of $\tan\beta \approx 1.5$, which corresponds to the considered parameter space, these two branching ratios are comparable. Hence, a remarkable bump in the mono-Z spectrum becomes visible and can be explained by the prompt closing of the decay channel $H \to AA$. At at 250 GeV this decay is kinematically no longer accessible as the pseudoscalar mass becomes larger than half the heavy Higgs mass. This results in a sudden increase of the branching ratio BR($H \to AZ$). At this transition point we can exclude values up to $\tan\beta \approx 2$ as shown in Figure 6.5.

For light pseudoscalar masses M_A, values for $\tan\beta$ up to 1.85 can be excluded. From there on the signal remains on a plateau before it increases up to values of $\tan\beta \approx 2$ as the decay channel $H \to AA$ closes. For further increasing masses sensitivity is decreasing since the heavy Higgs tends to decay more likely into a pair of top quarks and furthermore the pseudoscalar begins to decay into an off-shell pair of top quarks. Sensitivity is finally completely lost at 340 GeV where the decay of A into a top quark pair becomes available. In Figure 6.6 the dependence of the signal strength on $\cos(\beta - \alpha)$ is shown. On the left plot M_A is set to 160 GeV. The strongest bounds of the mono-Z are obtained in the alignment limit as the branching ratio $H \to AZ$ is maximal, whereas it vanishes for $\cos(\beta - \alpha) = \pm 1$. On the right-hand side the behavior changes slightly since $M_A = 250$ GeV is heavy enough to access the decay channel $A \to hZ$, which reduces the signal strength to larger absolute values of $\cos(\beta - \alpha)$. Both searches can cover most of the remaining parameter space and strongly constrain the preferred alignment limit.

We expect that this search at 12.9 fb^{-1} is not yet at its full potential and slightly stronger limits from the high luminosity run at the LHC can be predicted.

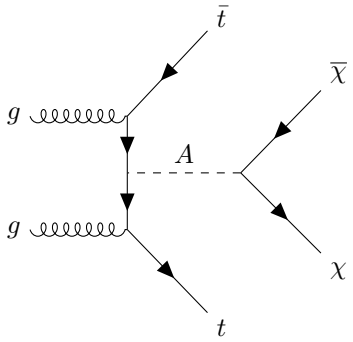

Figure 6.3: Feynman diagram contributing to $t\bar{t}$ - associated dark matter production. Diagram generated with [73].

6.6 Dark Matter Associated with Heavy Flavor

In the simplified model the couplings of spin-0 mediators are flavor dependent. This particularly motivates missing energy searches associated with heavy flavor production. In the case of the type II two Higgs doublet simplified model discussed in this chapter and the rather low values of $\tan\beta$ the $t\bar{t}+E_T^{\text{miss}}$ signature is strongly favored over the $b\bar{b}+E_T^{\text{miss}}$ final state. The two top quarks mainly emerge from gluon-splitting and the corresponding Feynman diagram for the process $pp \to At\bar{t} \to t\bar{t}+E_T^{\text{miss}}$ is presented in Figure 6.3.

The events are generated at leading order and along with the analysis have a statistical uncertainty of about 10 % if we apply the cuts collected in the right column of Table 6.1 as used in the CMS search [129]. The PDFs obey an uncertainty of 8.1 % and the scaling at leading order contributes about 25 % but is expected to decrease by considering higher order corrections. For obtaining the exclusion limits we neglect the systematic uncertainties and apply a mass independent K-factor of 1.1 for the $t\bar{t}+A$ production at $\sqrt{s} = 13$ TeV [135].
The search is most sensitive for small masses of the mediator as the pseudoscalar needs to be produced and does not emerge from a resonant decay. As soon as the top-threshold for the mediator is reached sensitivity is lost. This channel is comparable to the mono-jets signal and excludes $\tan\beta < 0.5$ for most of the mediator masses. As it is shown in Figure 6.6 for a light mediator of 160 GeV this process is independent of $\cos(\beta-\alpha)$, whereas for 250 GeV the bounds become slightly weaker for increasing $\cos(\beta-\alpha)$ as the channel $A \to hZ$ becomes accessible. This search at 2.2 fb^{-1} is limited at the current state mostly by statistics and is expected to reveal its full potential at the HL-LHC.

6.7 Other Mono-X Signatures

Besides mono-jet, mono-Z and $t\bar{t}+E_T^{\text{miss}}$ searches, possible collider signatures are mono-W, mono-photon and mono-Higgs final states. In the discussed simplified model, the last two only occur through initial state radiation, whereas the mono-W in principle can also be enhanced. In the Figures 3.3, 3.2 the branching ratio $\text{BR}(H^\pm \to W^\pm Z)$ seems to be comparable to $\text{BR}(H \to AZ)$ which indicates that mono-W searches are worth to discuss. We note that the production rates of $H^\pm$ $\sigma(pp \to H^\pm) \approx 0.5$ fb and $\sigma(gg \to W^- H^\pm) \approx 0.01$ pb are considerably smaller than $\sigma(gg \to H) \approx 1.77$ pb. This indicates that it is challenging to detect events with only a single W boson and missing transverse energy. However, signatures with additional quarks as $\sigma(g\bar{b} \to H^\pm\bar{t}) \approx 0.17$ pb or $\sigma(gg \to H^\pm\bar{t}b) \approx 0.21$ pb seem to be more promising to investigate. Nevertheless, compared to the mono-Z search the signals are harder to identify as the hadronic decays of the W boson need to be analyzed. This results from the fact that in

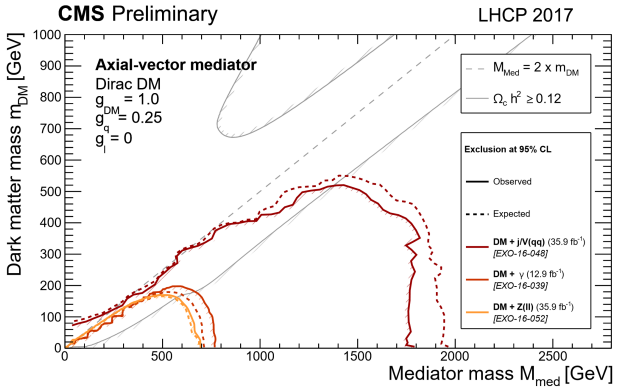

Figure 6.4: Exclusion limits for various mono-X searches. Here initial state radiation of the mono-jet search provides the most stringent constraint followed by mono-photon and mono-Z. Figure taken from [53].

the leptonic decays additional missing transverse energy would occur from the neutrinos. Hence, these searches are way more challenging compared to the mono-Z case.
Another possible signature for dark matter at a collider is a mono-Higgs. Since the Higgs is a scalar and couples only via its mass to the Standard Model fermions it is rarely radiated because two massive spin-0 bosons need to be produced. Even if a Higgs can occasionally occur as initial state radiation besides dark matter it is difficult to reconstruct the Higgs in a detector. This leads to the expectation that in general mono-Higgs signatures rarely play a role in collider dark matter searches. Nevertheless, in certain UV completions, as in (2.29), a resonant enhancement similar to the mono-Z signature can occur for the mono-Higgs if the effective coupling of the pseudoscalar to the dark matter is resolved. Then the mono-Higgs can even provide the strongest bounds. However, this signal strongly depends on the UV complete theory, whereas the resonant enhancement of the mono-Z signal is a universal feature of all simplified theories with pseudoscalar mediators. The discussion should be kept as general as possible, which is why the mono-Higgs search is not performed in detail.
A further search at the LHC experiments is a mono-photon signal. However, these searches provide weaker bounds than the mono-jets due to the weak coupling even if their energies can be measured way more precisely in the electric calorimeter. The mono-photon production compared to the mono-jet signal is suppressed by $Q_f^2 N_C \alpha_e / \alpha_s$. As there is no resonant enhancement present in our simplified model we skip a further discussion of this channel.

6.8 Summary of the Results of the Mono-X Searches and Their Future Reach

To gain a better understanding of the results obtained in this chapter, we first discuss the naive expectation of the reach of the distinct mono-X searches. Neglecting the enriched phenomenology of the studied consistent simplified model and instead turning to the models suggested by the LHC Dark Matter Forum and used in the analyses of the experiments, the strongest bounds are expected to emerge from the mono-jet searches as can be found in Figure 6.4. In these models only a coupling constant between the mediator and the Standard Model $g_q = 1$ as well as the dark matter $g_{\mathrm{DM}} = 0.25$ are assumed to set constraints in the parameter space spanned by the masses of the mediator and the dark matter. Hence, only initial or final state radiation can lead to missing transverse energy signatures. The stringent constraints coming from the mono-jet searches can now be explained by the hierarchy of the coupling strengths. Jets are radiated from the process of the dark matter production with the strong coupling, whereas photons are

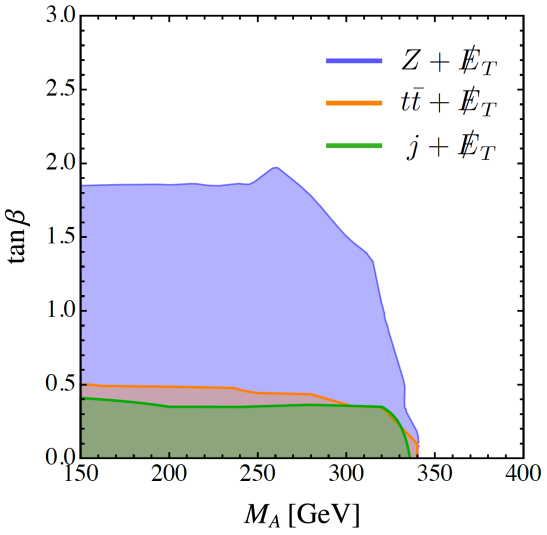

Figure 6.5: Exclusion limits in the $M_A - \tan\beta$ plane for mono-Z (blue), $t\bar{t} + E_T^{\text{miss}}$ (orange), and mono-jet (green) searches at the LHC for $\cos(\beta - \alpha) = 0$. Figure taken from [15].

suppressed by the weak coupling. In case of the mono-Z signals besides the suppression from the weak scale, the production of the mass of the Z boson further limits the reach of this search. Hence, we end up with the following hierarchy of initial state radiation: mono-jet > mono-photon > mono-Z.
The extensive study of the consistent simplified model (2.28) with a pseudoscalar mediator shows however that this hierarchy might be broken. In particular, the resonant enhancement of the mono-Z via a decay of the heavy scalar H leads to this highly non-trivial result that the strongest bounds are obtained for signatures with a Z boson and missing transverse energy, compare Figure 6.5. That the $t\bar{t}$ associated production slightly exceeds the mono-jets can be explained by the fact that the production of the pseudoscalar A does not require the radiation of an additional particle. Nevertheless, due to the small gluon splitting function into top quarks, this process with the current statistics cannot compete with the enhanced mono-Z signature. The reach of the exclusion limits at 95 %C.L. in the $M_A - \tan\beta$ plane for mono-Z (blue), $t\bar{t} + E_T^{\text{miss}}$ (orange) and mono-jet (green) are shown in Figure 6.5. We have fixed $M_H = M_{H^\pm} = 500$ GeV, $\cos(\beta - \alpha) = 0$ and $c_5 = 1.5 \times 10^{-3}$ (Λ/GeV), $c_\chi = 0$. The mono-Z searches for rather light pseudoscalar masses can exclude values of $\tan\beta \approx 1.85$ and at $M_A = 250$ GeV even up to $\tan\beta \approx 2$, whereas the mono-jet and $t\bar{t} + E_T^{\text{miss}}$ searches lose sensitivity at roughly $\tan\beta = 0.4$ and 0.5. This can be explained as both searches are suppressed by phase space and the $1/\tan\beta^4$ scaling of the $t\bar{t}A$ coupling. There is a lower constraint coming from the requirement that the top-Yukawa stays perturbative which excludes values of $\tan\beta \lesssim 0.3$ in both types of two Higgs doublet models [84]. All three searches for missing transverse energy lose sensitivity shortly before the top-threshold where the mediator A dominantly decays into a pair of top quarks. As Madgraph allows for virtual decays there is no sharp edge at a pseudoscalar mass of twice the top mass, but this cut-off is smeared out due to the virtual decay $A \to t\bar{t}^*(\bar{t}^* \to W^-\bar{b})$.
In Figure 6.6 the exclusion limits of the performed LHC dark matter searches are now presented in the $\cos(\beta - \alpha) - \tan\beta$ plane for $M_A = 160$ GeV (left panel) and $M_A = 250$ GeV (right panel). The gray shaded region in both panels represents the excluded parameter space which was constraint by the study of the scalar potential in Chapter 4. Thereby it was assumed that the additional particles of the UV complete theory, which are integrated out, are so heavy that they do not affect the derived bounds. As one can show that this is not always a valid assumption, these bounds could be in principle relaxed. Reasons can for example be the relaxation of the flavor bounds due to an additional charged particle being

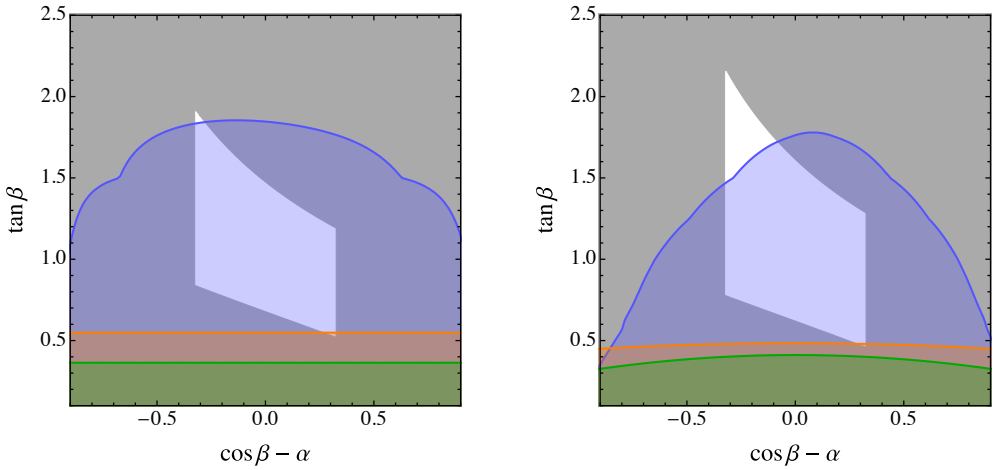

Figure 6.6: Exclusion limits in the $\cos(\beta-\alpha)-\tan\beta$ plane for $M_A = 160$ GeV (left) and 250 GeV (right) for mono-Z (blue), $t\bar{t}+E_T^{\text{miss}}$ (orange), and mono-jet (green) searches at the LHC. The gray shaded region is excluded by the prior constraints, mainly electroweak precision observables and stability requirements of the scalar potential. Figure taken from [15].

present in the corresponding loop, or a weakening of the stability requirements of the scalar potential due to the presence of further quartic couplings, which are currently forbidden by the applied symmetries. Nevertheless, it is remarkable that even under our simplest assumptions we find a region in the parameter space which is still allowed. Hence, we interpret these constraints more as guide. The white area is the remaining parameter space which spreads around the alignment limit. This region is slightly larger on the right panel due to the larger mediator mass relaxing the bound on $\tan\beta$ in the stability requirements as can be seen in the central panel in Figure 4.5. Both benchmark scenarios strongly constrain the remaining parameter space, especially the alignment limit. As we have stated above the upper limits on $\tan\beta$ are likely to change in the presence of additional states which makes a general exclusion rather challenging.
For $M_A = 160$ GeV (left panel) the mono-jet and $t\bar{t}+E_T^{\text{miss}}$ searches show no dependence on $\cos(\beta-\alpha)$, whereas the mono-Z loses sensitivity for larger absolute values of the mixing angle and completely vanishes at $|\cos(\beta-\alpha)| = 1$. This can be explained by the parametric dependence of the width $\Gamma(H \to AZ) \propto \sin^2(\beta-\alpha)$. Additionally, we neglect mono-Z initial state radiation which is suppressed compared to the mono-jet signature by both its mass and the weak coupling.
In the case of a pseudoscalar mass of 250 GeV (right panel) the $t\bar{t}+E_T^{\text{miss}}$ and mono-jet searches yield slightly weaker exclusion limits, whereas the mono-Z search is slightly stronger for $\cos(\beta-\alpha) \approx 0$. The mono-$Z$ signal falls off way steeper than in the left panel as outside the alignment limit the decay $A \to hZ$ becomes accessible, which leads to a smaller branching ratio for $A \to \chi\bar{\chi}$. This new decay channel influences the mono-jet and $t\bar{t}+E_T^{\text{miss}}$ searches as well. However, this can only hardly be seen in Figure 6.6. Nevertheless, the presence of this new decay channel could be used as a signature to search dark matter at the LHC even if it decreases the sensitivities of the studied mono-X signatures to large $|\cos(\beta-\alpha)|$. A possible signature can be a mono-hZ where the second pseudoscalars decays to dark matter.
From a still ongoing study of the potential reach of the three different searches at a high luminosity run at the LHC with 300 fb^{-1}, only the $t\bar{t}+E_T^{\text{miss}}$ is expected to get a large boost. The mono-jet study is already now mainly limited by systematic uncertainties and similarly holds true for the mono-Z search, which exclusion bounds are expected to increase only slightly. One word of caution needs to be stressed as the current $t\bar{t}+E_T^{\text{miss}}$ search is evaluated at 2.2 fb^{-1}, whereas the mono-Z is already at 12.9 fb^{-1} and the mono-jet data set is even at 36.1 fb^{-1}. This large enhancement of the heavy quark associate production can be explained by its current rather low statistics.

7 Conclusion

Collider searches turn out to be very powerful in probing pseudoscalar mediated interactions to the dark sector. This is especially useful since these models are extremely challenging to constrain by direct detection experiments as the cross sections are suppressed by the non-relativistic dark matter velocities. Extending the Standard Model by a pseudoscalar in a consistent gauge-invariant way requires an enlarged Higgs sector as no renormalizable coupling to the Higgs or the gauge bosons is possible. Adding a second Higgs doublet is a feasible and frequently discussed solution. In such a two Higgs doublet model the pseudoscalar is embedded in the theory as one of the additional four degrees of freedom emerging from the second $SU(2)_L$ doublet. The stability requirements on the scalar potential combined with the unitarity bounds of scalar scattering amplitudes lead to a strong limit on the mass splitting between the added spin-0 states. Hence, the additional particles aside the requested pseudoscalar cannot be integrated out resulting in a rich phenomenology. In the simplified model (2.28) the pseudoscalar mediator is part of a second Higgs doublet coupling to Dirac dark matter fermions. The coupling to the dark matter is left effective to remain the discussion as general as possible. Potential UV completions with either an enlarged mediator sector [14] or a dark matter particle being part of an electroweak multiplet [57] can be matched on the discussed model. A generic feature of all models containing a pseudoscalar mediator is the presence of a mono-Z final state signature. This universal signal is providing the most stringent exclusion limits in the parameter space in which mono-X searches are most powerful, because of the resonant decay chain $pp \to H \to AZ \to \chi\bar{\chi}Z$. In contrast, in an effective field theory approach one would expect that the constraint from a mono-Z signal would be subleading to the mono-jet constraint as the resonant enhancement will not be present. This indicates the importance of the treatment of self-consistent simplified models at the LHC which allows to obtain the correct hierarchy of the various dark matter signatures.

Bounds from the global fit to the Higgs signal strength measurements as well as direct detection experiments strongly constrain interactions with the dark matter mediated by the scalars h and H and favor purely pseudoscalar couplings. Moreover, values of the mixing angles $\cos(\beta - \alpha)$ towards the alignment limit are preferred. The absence of flavor changing neutral currents at tree-level leads to a constraint of $M_{H^\pm} > 500\,\text{GeV}$, whereas the conservation of the ρ parameter in electroweak precision observables demands $M_H \approx M_{H^\pm}$. As the scalar potential is assumed to conserve CP the requirements on stability, unitary and perturbativity restrict $\tan\beta$ to be of order one. These constraints can be relaxed by the presence of the additional states of a complete theory or further operators occurring in the scalar potential by dropping the CP symmetry, i.e. the bounds derived from flavor physics and the stability of the scalar potential. Hence, they are interpreted more as a guidance than stringent restrictions. Nevertheless, so far none of the expected heavy partners of the Higgs could be found at the LHC and the obtained mass limits are weakened by their additional decay channels to dark matter.

Remarkably, the remaining parameter space coincides with the region in which the correct relic density can be reproduced without a huge amount of fine-tuning being necessary. Exclusion bounds from direct and indirect detection experiments are considered to obtain the relic abundance where the strongest constraint emerges from the study of anisotropies in the cosmic microwave background. Combining these various constraints leaves a well-motivated region in the parameter space which can be almost entirely

probed by future LHC mono-Z searches.
The enhancement of the mono-Z signal can be explained by the dominant branching ratio of the heavy scalar H ,Br($H \to AZ$), in the relevant parameter space. The pseudoscalar A preferably decays into a pair of dark matter if $2m_\chi < M_A < 2m_t$ as the only competing decay channel is $A \to b\bar{b}$ which is small for values of $\tan\beta$ close to one. For mediator masses above the top threshold the decay of $A \to t\bar{t}$ becomes the dominant decay channel of the pseudoscalar and all three mono-X searches lose sensitivity. Outside the alignment limit the decay $A \to hZ$ becomes accessible for $M_A > m_h + m_Z$, but this region is strongly constrained by the global fit to the Higgs signal strength measurements. On the contrary to the mono-Z final state, the mono-jet signal entirely emerges from initial state radiation. Hence, in the studied simplified model the mono-jet as well as the heavy top quark associated production signals are not enhanced by any resonance and therefore the reach of these two signatures is restricted to values of $\tan\beta$ below 0.5 and 0.7, respectively. On the other hand, mono-Z can constrain a huge part of the remaining parameter space and obtains limits of $\tan\beta$ up to 1.85 for light pseudoscalar mediators. In the region where the decay $H \to AA$ becomes inaccessible the bound can even reach $\tan\beta = 2$ for the mono-Z search which allows to cover almost the entire preferred parameter space in both benchmarks scenarios. For the high luminosity run of the LHC the $t\bar{t} + E_T^{\text{miss}}$ search is expected to get a sizable boost, whereas already at the current state mono-Z and especially mono-jet searches are restricted by the systematic uncertainties.
The WIMP remains a likely dark matter candidate even if a broad class of pseudoscalar mediator dark matter models are already within reach of mono-Z collider searches. The mono-X searches are complementary to the measurements of direct and indirect detection experiments and are an important tool to further constrain the dark matter parameter space.

Relaxing the restriction on $\cos(\beta - \alpha)$ being in the alignment limit leads to the presence of an additional decay channel of the pseudoscalar $A \to hZ$. For light mediators the decay $H \to AA$ is accessible which can provide an entirely new signature if one pseudoscalar decays to dark matter and the other one to a Standard Model Higgs h and a Z boson. This would lead to a mono-hZ signal which would be a clear indicator for the existence of new physics.
As the model is originally inspired by a theory aiming at an explanation of the mass hierarchy in the fermion sector the $H_1^\dagger H_2$ operator can be interpreted as a flavon [56]. It would be an interesting challenge to combine these two approaches and expand the $\mathbb{Z}_2$ symmetry to allow for higher order insertions of the operator. One expects that the presence of dark matter relaxes the constraints derived in the flavon model and leads to an enriched phenomenology.
So far only CP-conserving couplings are allowed between the Standard Model and the dark sector. It would be natural to explore the influence of the CP-violating interactions as well as the additional terms in the scalar potential. For example, there could be implications on baryogenesis.
One can study the effect of the additional particles that are expected in the various UV completions of the simplified model. These will extend the parameter space and could provide further signatures as a mono-Higgs final state [14]. Nevertheless, the mono-Z signature is the only universal signal for consistent simplified models with a pseudoscalar mediator and should be studied more intensely.

Appendices

A Rotation from Interaction to Higgs Basis

First we note some helpful identities,

$$\frac{\cos\alpha}{\sin\beta} = s_{\beta-\alpha} + \cot\beta c_{\beta-\alpha} \ , \tag{A.1}$$

$$\frac{-\sin\alpha}{\cos\beta} = s_{\beta-\alpha} - \tan\beta c_{\beta-\alpha} \ , \tag{A.2}$$

$$\frac{\sin\alpha}{\sin\beta} = c_{\beta-\alpha} - \cot\beta s_{\beta-\alpha} \ , \tag{A.3}$$

$$\frac{\cos\alpha}{\cos\beta} = c_{\beta-\alpha} + \tan\beta s_{\beta-\alpha} \ , \tag{A.4}$$

Now we can provide the tree-level vector boson couplings C_V with $V = (W, Z)$ and fermionic couplings normalized to the Standard Model values in the two Higgs doublet models of type I and II as

	Type I and II	Type I		Type II	
Higgs	VV	up quarks	down quarks and leptons	up quarks	down quarks and leptons
h	$\sin(\beta-\alpha)$	$\cos\alpha/\sin\beta$	$\cos\alpha/\sin\beta$	$\cos\alpha/\sin\beta$	$-\sin\alpha/\cos\beta$
H	$\cos(\beta-\alpha)$	$\sin\alpha/\cos\beta$	$\sin\alpha/\cos\beta$	$\sin\alpha/\cos\beta$	$\cos\alpha/\sin\beta$
A	0	$\cot\beta$	$-\cot\beta$	$\cot\beta$	$\tan\beta$

Table A.1: Scaling factors of the couplings of the Higgs scalars to vector bosons and fermions [136]

We can write the two Higgs doublets both in the interaction basis H_a with $a \in 1, 2$ and in the Higgs basis where only one Higgs aquires a vacuum expectation value [58]. The scalar doublets are hence given as

$$\begin{aligned} H_1^{\mathrm{HB}} &= \cos\beta H_1 + \sin\beta H_2 = \begin{pmatrix} \cos\beta\phi_1^{\pm} + \sin\beta\phi_2^{\pm} \\ \frac{1}{\sqrt{2}}\left[\cos\beta(v_1+\rho_1+i\eta_1) + \sin\beta(v_2+\rho_2+i\eta_2)\right] \end{pmatrix} \\ &= \begin{pmatrix} G^{\pm} \\ \frac{1}{\sqrt{2}}\left[iG^0 + (\cos\beta\rho_1 + \sin\beta\rho_2) + v\right] \end{pmatrix} := \begin{pmatrix} G^{\pm} \\ \frac{1}{\sqrt{2}}\left[iG^0 + S_1 + v\right] \end{pmatrix} \ , \end{aligned} \tag{A.5}$$

$$\begin{aligned} H_2^{\mathrm{HB}} &= -\sin\beta H_1 + \cos\beta H_2 = \begin{pmatrix} -\sin\beta\phi_1^{\pm} + \cos\beta\phi_2^{\pm} \\ \frac{1}{\sqrt{2}}\left[-\sin\beta(v_1+\rho_1+i\eta_1) + \cos\beta(v_2+\rho_2+i\eta_2)\right] \end{pmatrix} \\ &= \begin{pmatrix} H^{\pm} \\ \frac{1}{\sqrt{2}}(-\sin\beta\rho_1 + \cos\beta\rho_2) + \frac{i}{\sqrt{2}}(-\sin\beta\eta_1 + \cos\beta\eta_2) \end{pmatrix} := \begin{pmatrix} H^{\pm} \\ \frac{S_2+iS_3}{\sqrt{2}} \end{pmatrix} \ , \end{aligned} \tag{A.6}$$

The Higgs basis has the attractive feature that the three Goldstone fields $G^{\pm}$ and G^0 get separated as components of H_1^{HB}. On the other hand, the three neutral scalar mass eigenstates $\varphi_i = (h, H, A)^T$ can be obtained by an orthogonal transformation $\mathcal{R}$ from the S_i fields as $\varphi = \mathcal{R}_{ij}S_j$. In the most general

case the CP-odd state S_3 can mix with the CP-even states and hence they are no eigenstates under CP. For CP-conserving potentials however the mixing disappears and A can be associated with the state S_3.

B Decay Widths of the Higgs Bosons

We give an overview of the most important partial decay widths for the heavy scalar H, the pseudoscalar A and the charged scalar $H^\pm$ in the alignment limit where $\cos(\beta-\alpha)=0$ as given in [15]. As for the light Higgs h which we interpret in the alignment limit as the Standard Model Higgs we limit ourselves to present the partial decay width into dark matter as the other partial widths stay the same as in the Standard Model even if the total width changes. We do not discuss decays which occur at off-shell processes or become relevant outside of the alignment limit where $\cos(\beta-\alpha)>0$. They can be found in [137]. The relevant partial widths for the scalar H are

$$\Gamma(H\to t\bar{t}) = \frac{3}{8\pi}\frac{m_t^2}{v^2}\kappa_{H_u}^2 M_H\left(1-\frac{4m_t^2}{M_H^2}\right)^{3/2}, \tag{B.1}$$

$$\Gamma(H\to \chi\bar{\chi}) = \frac{1}{8\pi}g_{H\chi}^2 M_H\left(1-\frac{4m_\chi^2}{M_H^2}\right)^{3/2}, \tag{B.2}$$

$$\Gamma(H\to ZA) = \frac{1}{16\pi}s_{\beta-\alpha}^2\frac{M_Z^4}{v^2 M_H}\lambda(M_A^2,M_Z^2,M_H^2)^{1/2}\lambda(M_A^2,M_H^2,M_W^2), \tag{B.3}$$

$$\Gamma(H\to AA) = \frac{1}{32\pi}\frac{(M_A^2-M_H^2)^2}{v^2 M_H}\frac{(t_\beta^2-1)^2}{t_\beta}\left(1-\frac{4M_A^2}{M_H^2}\right)^{1/2}, \tag{B.4}$$

where $\lambda(x,y,z)=((x+y-z)^2-4xy)/z$ and the scaled couplings κ_{H_u} as well as $g_{H\chi}$ are given in Table 3.2 receptively (3.31). For the pseudoscalar A, the following partial decay widths are the dominant ones

$$\Gamma(A\to t\bar{t}) = \frac{3}{8\pi}\frac{m_t^2}{v^2}\kappa_{A_u}^2 M_A\left(1-\frac{4m_t^2}{M_A^2}\right)^{1/2}, \tag{B.5}$$

$$\Gamma(A\to b\bar{b}) = \frac{3}{8\pi}\frac{m_b^2}{v^2}\kappa_{A_d}^2 M_A\left(1-\frac{4m_b^2}{M_A^2}\right)^{1/2}, \tag{B.6}$$

$$\Gamma(A\to \tau^+\tau^-) = \frac{1}{8\pi}\frac{m_\tau^2}{v^2}\kappa_{A_\ell}^2 M_A\left(1-\frac{4m_\tau^2}{M_A^2}\right)^{1/2}, \tag{B.7}$$

$$\Gamma(A\to \chi\bar{\chi}) = \frac{1}{8\pi}g_{A5}^2 M_A\left(1-\frac{4m_\chi^2}{M_A^2}\right)^{1/2}, \tag{B.8}$$

where $\Gamma(A\to c\bar{c})$ can be derived from $\Gamma(A\to t\bar{t})$ by replacing $m_t\to m_c$. For the charged scalar $H^\pm$ the following partial widths can be calculated

$$\Gamma(H^+\to t\bar{b}) = \frac{3}{8\pi}\frac{|V_{tb}|^2}{M_{H^\pm}v^2}\lambda(m_t^2,m_b^2,M_{H^\pm}^2)^{1/2}\left((M_{H^\pm}^2-m_t^2-m_b^2)(m_b^2\kappa_{A_d}^2+m_t^2\kappa_{A_t}^2)-4m_t^2m_b^2\right), \tag{B.9}$$

$$\Gamma(H^+\to \tau^+\nu) = \frac{1}{8\pi}\frac{1}{M_{H^\pm}v^2}m_\tau^2\kappa_{A_\ell}^2\left(1-\frac{m_\tau^2}{M_{H^\pm}^2}\right)^3, \tag{B.10}$$

$$\Gamma(H^+\to AW^+) = \frac{1}{16\pi c_W^2}\frac{M_W^4}{M_{H^\pm}v^2}\lambda(M_A^2,M_W^2,M_{H^\pm}^2)^{1/2}\lambda(M_A^2,M_{H^\pm}^2,M_W^2). \tag{B.11}$$

In the alignment limit the decay widths of the Standard Model Higgs to fermions and gauge bosons are preserved. Therefore we only give the new contribution of h decaying into a pair of dark matter

$$\Gamma(h \to \chi\bar{\chi}) \;=\; \frac{1}{8\pi}\, g_{h\chi}^2\, m_h \left(1 - \frac{4m_\chi^2}{m_h^2}\right)^{3/2} . \tag{B.12}$$

As the dark matter is lighter than $m_h/2$ but heavier than the mass of the bottom quark the Higgs would dominantly decay into dark matter. As the branching ratio of Higgs decaying into invisibles is rather well known this gives stringent limits on the dark matter mass.

Bibliography

[1] Zwicky, F., Die Rotverschiebung von extragalaktischen Nebeln, Helvetica Physica Acta 6, 110-127 (1933).

[2] Freeman, K. C., Astrophys. J. 160, 811 (1970).

[3] Zwicky, F., On the Masses of Nebulae and of Clusters of Nebulae, Astrophys. J. 86, 217 (1937)

[4] Springel, Volker and others, Simulating the joint evolution of quasars, galaxies and their large-scale distribution, Nature 435, 629-636 (2005) [arXiv:0504097 [astro-ph]].

[5] Ade, P. A. R. and others, Planck 2015 results. XIII. Cosmological parameters, Astron. Astrophys. 594 (2016) [arXiv:1502.01589 [hep-ph]].

[6] Kahlhoefer, Felix, Review of LHC Dark Matter Searches, Int. J. Mod. Phys. 13 (2017) [arXiv:1702.02430 [hep-ph]].

[7] M. J. Dolan, F. Kahlhoefer, C. McCabe and K. Schmidt-Hoberg, JHEP 1503, 171 (2015) Erratum: [JHEP 1507, 103 (2015)] [arXiv:1412.5174 [hep-ph]].

[8] F. Kahlhoefer, K. Schmidt-Hoberg, T. Schwetz and S. Vogl, JHEP 1602, 016 (2016) [arXiv:1510.02110 [hep-ph]].

[9] M. Fairbairn, J. Heal, F. Kahlhoefer and P. Tunney, JHEP 1609, 018 (2016) [arXiv:1605.07940 [hep-ph]].

[10] N. Okada and S. Okada, Phys. Rev. D 93, no. 7, 075003 (2016) [arXiv:1601.07526 [hep-ph]]. 22

[11] J. M. Zheng, Z. H. Yu, J. W. Shao, X. J. Bi, Z. Li and H. H. Zhang, Nucl. Phys. B 854, 350 (2012) [arXiv:1012.2022 [hep-ph]].

[12] D. Goncalves, P. A. N. Machado and J. M. No, Phys. Rev. D 95, no. 5, 055027 (2017) [arXiv:1611.04593 [hep-ph]].

[13] M. Bauer, U. Haisch and F. Kahlhoefer, JHEP 1705, 138 (2017) [arXiv:1701.07427 [hep-ph]].

[14] Bauer, Martin, Haisch, Ulrich and Kahlhoefer, Felix, Simplified dark matter models with two Higgs doublets: I. Pseudoscalar mediators, JHEP 05, 138 (2017) [arXiv:1701.07427 [hep-ph]].

[15] M. Bauer, M.Klassen, V.Tenorth, Universal Properties of Pseudoscalar Mediators, in preparation

[16] Bertone, Gianfranco and Hooper, Dan, A History of Dark Matter, Submitted to: Rev. Mod. Phys. (2016) [arXiv:1605.04909 [hep-ph]].

[17] Kapteyn, J. C., First Attempt at a Theory of the Arrangement and Motion of the Sidereal System Astrophys. J. 55, 302 (1922)

[18] Oort, J. H., The force exerted by the stellar system in the direction perpendicular to the galactic plane and some related problems, bain J. 6, 249 (1932).

[19] Jeans, J. H., The Motions of Stars in a Kapteyn Universe, mnras 82, 122-132 (1922)

[20] Bosma, A. (1978), The distribution and kinematics of neutral hydrogen in spiral galaxies of various morphological types, Ph.D. thesis (PhD Thesis, Groningen Univ., (1978)).

[21] Alpher, R. A., Bethe, H. and Gamow, G., The Origin of Chemical Elements, Physical Review 73, 803-804 (1948)

[22] Y. Mambrini, Histories of Dark Matter in the Universe, http://www.ymambrini.com/My_World/Physics_files/Universe.pdf

[23] Penzias, A. A. and Wilson, R. W., A Measurement of Excess Antenna Temperature at 4080 Mc/s., Astrophys. J. 142, 419-421 (1965)

[24] Planck Collaboration, "Planck 2015 results. XI. CMB power spectra, likelihoods, and robustness of parameters," Submitted to: Astron.Astrophys. [arXiv:1507.02704 [astro-ph]].

[25] Chandra X-Ray Observatory, http://chandra.harvard.edu/photo/2006/1e0657/more.html

[26] W-M Yao et al, Review of Particle Physics, Journal of Physics G: Nuclear and Particle Physics 33, 1 (2006).

[27] Plehn, Tilman, Yet Another Introduction to Dark Matter, (2017) [arXiv:1705.01987 [hep-ph]].

[28] Aprahamian, A. and others, Fundamental symmetries, neutrinos, neutrons, and astrophysics: a White Paper on progress and prospects, (2015).

[29] Peccei, R. D. and Quinn, H. R., CP conservation in the presence of pseudoparticles, Physical Review Letters 38, 1440-1443 (1977)

[30] Baer, H. and Tata, Xerxes, Dark matter and the LHC, (2009) [arXiv:0805.1905 [hep-ph]].

[31] Graham, Peter W., Irastorza, Igor G., Lamoreaux, Steven K., Lindner, Axel and van Bibber, Karl A., Experimental Searches for the Axion and Axion-Like Particles, Ann. Rev. Nucl. Part. Sci. 65, 485-514 (2015) [arXiv:1602.00039[hep-ex]].

[32] Nishikawa, Hiroya and Kovetz, Ely D. and Kamionkowski, Marc and Silk, Joseph, Primordial-black-hole mergers in dark-matter spikes, (2017) [arXiv:1708.08449 [astro-ph]].

[33] Bramante, Joseph, Desai, Nishita, Fox, Patrick, Martin, Adam, Ostdiek, Bryan and Plehn, Tilman, Towards the Final Word on Neutralino Dark Matter, Phys. Rev. D93 6, 063525 (2016) [arXiv:1510.03460 [hep-ph]].

[34] Max-Planck-Institut für Kernphysik, url="https://www.mpi-hd.mpg.de/lin/research_DM.en.html"

[35] Hooper, Dan, Particle Dark Matter, (2010) [arXiv:0901.4090 [hep-ph]].

[36] Kolb, Edward W. and Turner, Michael S., The Early Universe, Front. Phys. 69, 1-547 (1990)

[37] Bergström, L. and Goobar, A., Cosmology and particle astrophysics, (1999) https://books.google.de/books?id=Mc61QgAACAAJ,

[38] Feng, J. L. and others, Planning the Future of U.S. Particle Physics (Snowmass 2013): Chapter 4: Cosmic Frontier, [arXiv:1401.6085 [hep-ex]].

[39] Conrad, Jan, Indirect Detection of WIMP Dark Matter: a compact review, (2014) [arXiv:1411.1925 [hep-ph]].

[40] C. Balzs, J. Conrad, B. Farmer, T. Jacques, T. Li, M. Meyer, F. S. Queiroz and M. A. Snchez-Conde, [arXiv:1706.01505 [astro-ph.HE]].

[41] T. R. Slatyer, N. Padmanabhan and D. P. Finkbeiner, Phys. Rev. D 80, 043526 (2009)

[42] W. Altmannshofer, S. Gori, S. Profumo and F. S. Queiroz, JHEP 1612, 106 (2016) doi:10.1007/JHEP12(2016)106 [arXiv:1609.04026 [hep-ph]].

[43] Actis, M. et al., Design concepts for the Cherenkov Telescope Array CTA: an advanced facility for ground-based high-energy gamma-ray astronomy, Experimental Astronomy 32, 193-316 (2011) [arXiv:1008.3703 [astro-ph]].

[44] Klasen, Michael, Pohl, Martin and Sigl, Günter, Indirect and direct search for dark matter, Prog. Part. Nucl. Phys. 85, 1-32 (2015) [arXiv:1507.03800 [hep-ph]].

[45] Duerr, Michael, Fileviez Pérez, Pavel and Smirnov,Juri, Scalar Dark Matter: Direct vs. Indirect Detection, JHEP 06, 152 (2016) [arXiv:1509.04282 [hep-ph]].

[46] Bauer, Martin, Butter, Anja, Desai, Nishita, Gonzalez-Fraile, Juan and Plehn, Tilman, Validity of dark matter effective theory, Phys. Rev. D95, 075036 (2017) [arXiv:1611.09908 [hep-ph]].

[47] Abercrombie, Daniel and others, Dark Matter Benchmark Models for Early LHC Run-2 Searches: Report of the ATLAS/CMS Dark Matter Forum, (2015) [arXiv:1507.00966 [hep-ex]].

[48] Ilten, Philip, Soreq, Yotam, Thaler, Jesse, Williams, Mike and Xue, Wei, Proposed Inclusive Dark Photon Search at LHCb, Phys. Rev. Lett. 116, 251803 (2016) [arXiv:1603.08926 [hep-ph]].

[49] De Simone, Andrea and Jacques, Thomas, Simplified models vs. effective field theory approaches in dark matter searches, Eur. Phys. J. C76, 367 (2016) [arXiv:1603.08002 [hep-ph]].

[50] Abdallah, Jalal and others, Simplified Models for Dark Matter and Missing Energy Searches at the LHC, (2014) [arXiv:1409.2893 [hep-ph]].

[51] G. Aad et al., JHEP 1511, 206 (2015) [arXiv:1509.00672 [hepex]].

[52] V. Khachatryan et al., JHEP 1702, 135 (2017) [arXiv:1610.09218 [hep-ex]].

[53] CMS Collaboration, Dark Matter Summary Plots from CMS for LHCP and EPS 2017, https://twiki.cern.ch/twiki/pub/CMSPublic/PhysicsResultsEXO/DM-summary-plots-Jul17.pdf

[54] Sirunyan, Albert M and others, Search for dark matter produced with an energetic jet or a hadronically decaying W or Z boson at $\sqrt{s} = 13$ TeV, JHEP 07, 014 (2017) [arXiv:1703.01651 [hep-ex]].

[55] C. Froggatt and H. B. Nielsen, Hierarchy of Quark Masses, Cabibbo Angles and CP Violation, Nucl.Phys. B147, 277 (1979).

[56] Bauer, Martin, Carena, Marcela and Gemmler, Katrin, Flavor from the Electroweak Scale, JHEP 11, 016 (2015) [arXiv:1506.01719 [hep-ph]].

[57] Freitas, Ayres, Westhoff, Susanne and Zupan, Jure, Integrating in the Higgs Portal to Fermion Dark Matter, JHEP 09, 015 (2015) [arXiv:1506.04149 [hep-ph]].

[58] M. M. Mühlleitner, Lecture Notes 'Beyond the Standard Model Physics', KIT WS2014/15

[59] J.F. Gunion and H.E. Haber, The CP conserving two Higgs doublet model: The Approach to the decoupling limit, Phys. Rev. D67 (2003) [arXiv:0207010 [hep-ph]].

[60] Aoki, Mayumi, Kanemura, Shinya, Tsumura, Koji and Yagyu, Kei, Models of Yukawa interaction in the two Higgs doublet model, and their collider phenomenology, Phys. Rev. D80, 015017 (2009) [arXiv:0902.4665 [hep-ph]].

[61] Branco, G. C., Ferreira, P. M., Lavoura, L., Rebelo, M. N., Sher, Marc and Silva, Joao P., Theory and phenomenology of two-Higgs-doublet models, Phys. Rept. 516, 1-102 (2012) [arXiv:1106.0034 [hep-ph]].

[62] Michael A. Fedderke et al., The fermionic dark matter Higgs portal: an effective field theory approach, JHEP 8, 122. (2014), [arXiv: 1404.2283 [hep-ph].

[63] Valentin Tenorth, Master Thesis: Consistent Models of Dark Matter at the LHC (2017).

[64] S. L. Glashow and S. Weinberg, Natural conservation laws for neutral currents, Phys. Rev. D 15 (1977) 1958.

[65] E. A. Paschos, Diagonal neutral currents, Phys. Rev. D 15 (1977) 1966.

[66] Aad, Georges and others, Constraints on new phenomena via Higgs boson couplings and invisible decays with the ATLAS detector, JHEP 11, 206 (2015) [arXiv:1509.00672 [hep-ex]].

[67] G. Aad et al. [ATLAS and CMS Collaborations], Measurements of the Higgs boson production and decay rates and constraints on its couplings from a combined ATLAS and CMS analysis of the LHC pp collision data at ps = 7 and 8 TeV, JHEP 1608 (2016) 045 [arXiv:1606.02266 [hep-ex]].

[68] G. Aad et al. [ATLAS Collaboration], JHEP 1511, 206 (2015) [arXiv:1509.00672 [hep-ex]].

[69] V. Khachatryan et al. [CMS Collaboration], JHEP 1702, 135 (2017) [arXiv:1610.09218 [hep-ex]].

[70] Misiak, Mikolaj and Steinhauser, Matthias, Weak radiative decays of the B meson and bounds on $M_{H^\pm}$ in the Two-Higgs-Doublet Model, Eur. Phys. J. C77, 201 (2017) [arXiv:1702.04571 [hep-ph]].

[71] T. Hermann, M. Misiak and M. Steinhauser, JHEP 1211, 036 (2012) [arXiv:1208.2788 [hep-ph]].

[72] M. Czakon, P. Fiedler, T. Huber, M. Misiak, T. Schutzmeier and M. Steinhauser, JHEP 1504, 168 (2015) [arXiv:1503.01791 [hep-ph]].

[73] Ellis, Joshua, TikZ-Feynman: Feynman diagrams with TikZ, Comput. Phys. Commun. 210, 103-123 (2017) do:10.1016/j.cpc.2016.08.019, [arXiv:1601.05437[hep-ph]].

[74] A. Denner, R. J. Guth, W. Hollik and J. H. Kühn, Z. Phys. C 51, 695 (1991).

[75] U. Haisch and A. Weiler, Phys. Rev. D 76, 074027 (2007) [arXiv:0706.2054 [hep-ph]].

[76] A. Freitas and Y. C. Huang, JHEP 1208, 050 (2012) Erratum: [JHEP 1305, 074 (2013)] Erratum: [JHEP 1310, 044 (2013)] [arXiv:1205.0299 [hep-ph]].

[77] L. F. Abbott, P. Sikivie and M. B. Wise, Phys. Rev. D 21, 1393 (1980).

[78] C. Q. Geng and J. N. Ng, Phys. Rev. D 38, 2857 (1988) Erratum: [Phys. Rev. D 41, 1715 (1990)].

[79] A. J. Buras, P. Krawczyk, M. E. Lautenbacher and C. Salazar, Nucl. Phys. B 337, 284 (1990).

[80] O. Eberhardt, U. Nierste and M. Wiebusch, JHEP 1307, 118 (2013) [arXiv:1305.1649 [hep-ph]].

[81] J.-M. Gerard and M. Herquet, Phys. Rev. Lett. 98, 251802 (2007) [arXiv:0703.051 [hep-ph]].

[82] B. Grzadkowski, M. Maniatis and J. Wudka, JHEP 1111, 030 (2011) [arXiv:1011.5228 [hep-ph]].

[83] I. F. Ginzburg and I. P. Ivanov, Phys. Rev. D 72, 115010 (2005) [arXiv:0508020 [hep-ph]].

[84] G. C. Branco, P. M. Ferreira, L. Lavoura, M. N. Rebelo, M. Sher and J. P. Silva, Phys. Rept. 516, 1 (2012) [arXiv:1106.0034 [hep-ph]].

[85] Aad, Georges and others, Search for a CP-odd Higgs boson decaying to Zh in pp collisions at $\sqrt{s} = 8$ TeV with the ATLAS detector, Phys. Lett.B744, 163-183 (2015) [arXiv:1502.04478 [hep-ex]].

[86] ATLAS Collaboration, Search for a CP-odd Higgs boson decaying to Zh in pp collisions at $\sqrt{s} = 13$ TeV with the ATLAS detector, (2016) ATLAS-CONF-2016-015 https://cds.cern.ch/record/2141003

[87] Khachatryan, Vardan and others, Search for a pseudoscalar boson decaying into a Z boson and the 125 GeV Higgs boson in $l^+l^-b\bar{b}$ final states, Phys. Lett. B748, 221-243 (2015) [arXiv:1504.04710 [hep-ex]].

[88] CMS Collaboration, Search for H/A decaying into Z+A/H, with Z to ll and A/H to fermion pair, (2015) CMS-PAS-HIG-15-001

[89] ATLAS Collaboration, Search for heavy Higgs bosons A/H decaying to a top-quark pair in pp collisions at $\sqrt{s} = 8$ TeV with the ATLAS detector, ATLAS-CONF-2016-073 (2016).

[90] Khachatryan, Vardan and others, Search for diphoton resonances in the mass range from 150 to 850 GeV in pp collisions at $\sqrt{s} = 8$ TeV,Phys. Lett. B750, 494-519 (2015) [arXiv:1506.02301 [hep-ex]].

[91] Aaboud, Morad and others, Search for Minimal Supersymmetric Standard Model Higgs bosons H/A and for a Z' boson in the $\tau\tau$ final state produced in pp collisions at $\sqrt{s} = 13$ TeV with the ATLAS Detector, Eur. Phys. J. C76, 585 (2016) [arXiv:1608.00890 [hep-ex]].

[92] Khachatryan, Vardan and others, Search for neutral MSSM Higgs bosons decaying to a pair of tau leptons in pp collisions, JHEP 10, 160 (2014) [arXiv:1408.3316 [hep-ex]].

[93] CMS Collaboration, Search for dark matter in final states with an energetic jet, or a hadronically decaying W or Z boson using 12.9 fb^{-1} of data at $\sqrt{s} = 13$ TeV, CMS-PAS-EXO-16-037 (2016).

[94] Khachatryan, Vardan and others, Search for neutral MSSM Higgs bosons decaying into a pair of bottom quarks, JHEP 11, 071 (2015) [arXiv:1506.08329 [hep-ex]].

[95] ATLAS Collaboration, Search for heavy Higgs bosons A/H decaying to a top-quark pair in pp collisions at $\sqrt{s} = 8$ TeV with the ATLAS detector, (2016) ATLAS-CONF-2016-073

[96] ATLAS Collaboration, Search for new phenomena in $t\bar{t}$ final states with additional heavy-flavour jets in pp collisions at $\sqrt{s} = 13$ TeV with the ATLAS detector, (2016) ATLAS-CONF-2016-104

[97] Aaboud, Morad and others, Search for Minimal Supersymmetric Standard Model Higgs bosons H/A and for a Z' boson in the $\tau\tau$ final state produced in pp collisions at $\sqrt{s} = 13$ TeV with the ATLAS Detector, Eur. Phys. J. C76, 585 (2016) [arXiv:1608.00890[hep-ex]].

[98] CMS Collaboration, Search for a heavy scalar boson decaying into a pair of Z bosons in the $2\ell 2\nu$ final state, (2016) CMS-PAS-HIG-16-001

[99] Aaboud, Morad and others, Searches for heavy diboson resonances in pp collisions at $\sqrt{s} = 13$ TeV with the ATLAS detector, JHEP 09, 173 (2016) [arXiv:1606.04833 [hep-ex]].

[100] CMS Collaboration, Search for high mass Higgs to WW with fully leptonic decays using 2015 data, (2016) CMS-PAS-HIG-16-023

[101] Aaboud, Morad and others, Search for new resonances decaying to a W or Z boson and a Higgs boson in the $\ell^+\ell^- b\bar{b}$, $\ell\nu b\bar{b}$, and $\nu\bar{\nu}b\bar{b}$ channels with pp collisions at $\sqrt{s} = 13$ TeV with the ATLAS detector, Phys. Lett. B765, 32-52 (2017) [arXiv:1607.05621 [hep-ex]].

[102] CMS Collaboration, Search for resonant Higgs boson pair production in the $\mathrm{b\bar{b}}\tau^+\tau^-$ final state, (2016) CMS-PAS-HIG-16-013

[103] ATLAS Collaboration, Search for charged Higgs bosons in the $H^\pm \to tb$ decay channel in pp collisions at $\sqrt{s} = 13$ TeV using the ATLAS detector, (2016) ATLAS-CONF-2016-089

[104] Aaboud, Morad and others, Search for charged Higgs bosons produced in association with a top quark and decaying via $H^\pm \to \tau\nu$ using pp collision data recorded at $\sqrt{s} = 13$ TeV by the ATLAS detector, Phys. Lett. B759, 555-574 (2016) [arXiv:1603.09203 [hep-ex]].

[105] CMS Collaboration, Search for charged Higgs bosons with the $\mathrm{H}^\pm \to \tau^\pm\nu_\tau$ decay channel in the fully hadronic final state at $\sqrt{s} = 13$ TeV, (2016) CMS-PAS-HIG-16-031

[106] ATLAS Collaboration, Search for charged Higgs bosons in the $\tau+$ jets final state using 14.7 fb^{-1} of pp collision data recorded at $\sqrt{s} = 13$ TeV with the ATLAS experiment, (2016) ATLAS-CONF-2016-088

[107] CMS Collaboration, Search for charged Higgs bosons in WZ decays at 13 TeV, (2016) CMS-PAS-HIG-16-027

[108] Belanger, G., Boudjema, F., Pukhov, A. and Semenov,A., micrOMEGAs: A Tool for dark matter studies, Nuovo Cim. C033N2, 110-116 (2010) [arXiv:1005.4133 [hep-ph]].

[109] Belanger, G., Boudjema, F. and Pukhov, A., micrOMEGAs : a code for the calculation of Dark Matter properties in generic models of particle interaction, (2013) [arXiv:1402.0787 [hep-ph]].

[110] A. Alloul, N.D. Christensen, C. Degrande, C. Duhr, and B. Fuks, FeynRules 2.0 - A complete toolbox for tree-level phenomenology Comput. Phys. Commun. 185 (2014) [arXiv:1310.1921 [hep-ph]].

[111] Christensen, Neil D. and Duhr, Claude, FeynRules - Feynman rules made easy, Comput. Phys. Commun. 180, 1614-1641 (2009) [arXiv:0806.4194 [hep-ph]].

[112] C. Degrande, Automatic evaluation of UV and R2 terms for beyond the Standard Model Lagrangians: a proof-of-principle, Comput. Phys. Commun. 197 (2015) [arXiv:1406.3030 [hep-ph]].

[113] Aprile, E. and others, First Dark Matter Search Results from the XENON1T Experiment, Phys. Rev. Lett. 119, 181301 (2017) [arXiv:1705.06655 [astro-ph]].

[114] Akerib, D. S. and others, First results from the LUX dark matter experiment at the Sanford Underground Research Facility, Phys. Rev. Lett. 112, 091303 (2014) [arXiv:1310.8214 [astro-ph]].

[115] T. Hahn, Generating Feynman diagrams and amplitudes with FeynArts 3, Comput. Phys. Commun. 140 (2001) [arXiv:0012260 [hep-ph]].

[116] J. Alwall, R. Frederix, S. Frixione, V. Hirschi, F. Maltoni, O. Mattelaer, H. -S. Shao, T. Stelzer, P. Torrielli and M. Zaro, The automated computation of tree-level and next-to-leading order differential cross sections, and their matching to parton shower simulations, JHEP 07 (2014) [arXiv:1405.0301 [hep-ph]].

[117] V. Hirschi, R. Frederix, S. Frixione, M.V. Garzelli, F. Maltoni and R. Pittau, Automation of one-loop QCD corrections, JHEP 05 (2011) [arXiv:1103.0621 [hep-ph]].

[118] G. Ossola, C.G. Papadopoulos and R. Pittau, Reducing full one-loop amplitudes to scalar integrals at the integrand level, Nucl. Phys. B763 (2007) [arXiv:0609007 [hep-ph]].

[119] G. Ossola, C.G. Papadopoulos and R. Pittau, CutTools: A Program implementing the OPP reduction method to compute one-loop amplitudes, JHEP 03 (2008) [arXiv:0711.3596 [hep-ph]].

[120] T. Sjöstrand, S. Ask, J.R. Christiansen, R. Corke, N. Desai, P. Ilten, S. Mrenna, S. Prestel, C.O. Rasmussen and P.Z. Skands, An Introduction to PYTHIA 8.2, Comput. Phys. Commun. 191 (2015) [arXiv:1410.3012 [hep-ph]].

[121] J. de Favereau, C. Delaere, P. Demin, A. Giammanco, V. Lemaître, A. Mertens and M. Selvaggi, DELPHES 3, A modular framework for fast simulation of a generic collider experiment, JHEP 02 (2014) [arXiv:1307.6346 [hep-ph]].

[122] R. D. Ball et al. [NNPDF Collaboration], JHEP 1504, 040 (2015) [arXiv:1410.8849[hep-ph]].

[123] J. Alwall, S. de Visscher and F. Maltoni, QCD radiation in the production of heavy colored particles at the LHC, JHEP 02 (2009) [arXiv:0810.5350 [hep-ph]].

[124] Mattelaer, Olivier, Vryonidou, Eleni, Dark matter production through loop-induced processes at the LHC: the s-channel mediator case, Eur. Phys. J. C75, 436 (2015) [arXiv:1508.00564 [hep-ph]].

[125] E. Conte, B. Fuks and G. Serret, MadAnalysis 5, A User-Friendly Framework for Collider Phenomenology, Comput. Phys. Commun. 184 (2013) [arXiv:1206.1599 [hep-ph]].

[126] Rene Brun and Fons Rademakers, ROOT - An Object Oriented Data Analysis Framework, Proceedings AIHENP'96 Workshop, Lausanne, Sep. 1996, Nucl. Inst. & Meth. in Phys. Res. A 389, 81-86 (1997). See also http://root.cern.ch/.

[127] ATLAS collaboration, Search for dark matter and other new phenomena in events with an energetic jet and large missing transverse momentum using the ATLAS detector, ATLAS-CONF-2017-060.

[128] CMS Collaboration, Search for dark matter in Z + $E_{\mathrm{T}}^{\mathrm{miss}}$ events using 12.9 fb^{-1} of 2016 data, CMS-PAS-EXO-16-038, https://cds.cern.ch/record/2205763.

[129] A.M. Sirunyan and others, Search for dark matter produced in association with heavy-flavor quarks in proton-proton collisions at sqrt(s)=13 TeV, [arXiv:1706.02581 [hep-ph]].

[130] Abercrombie, Daniel and others, Dark Matter Benchmark Models for Early LHC Run-2 Searches: Report of the ATLAS/CMS Dark Matter Forum, (2015) [arXiv:1507.00966 [hep-ex]].

[131] T. Ahmed, M. C. Kumar, P. Mathews, N. Rana and V. Ravindran, Eur. Phys. J. C 76, no. 6, 355 (2016) [arXiv:1510.02235 [hep-ph]].

[132] L. M. Carpenter, A. Nelson, C. Shimmin, T. M. P. Tait and D. Whiteson, Phys. Rev. D 87, no. 7, 074005 (2013) [arXiv:1212.3352 [hep-ex]].

[133] T. Ahmed, M. C. Kumar, P. Mathews, N. Rana and V. Ravindran, Eur. Phys. J. C 76, no. 6, 355 (2016) [arXiv:1510.02235 [hep-ph]].

[134] R. V. Harlander and W. B. Kilgore, Phys. Rev. Lett. 88, 201801 (2002) [arXiv:0201206 [hep-ph]].

[135] F. Maltoni, E. Vryonidou and C. Zhang, JHEP 1610, 123 (2016) [arXiv:1607.05330[hep-ph]].

[136] Bernon, Jérémy, Gunion, John F.,Haber, Howard E., Jiang, Yun and Kraml, Sabine, Scrutinizing the alignment limit in two-Higgs-doublet models: $m_h = 125$ GeV, Phys. Rev. D92, 075004 (2015) [arXiv:1507.00933 [hep-ph]].

[137] J. F. Gunion, H. E. Haber, G. L. Kane and S. Dawson, Front. Phys. 80, 1 (2000).

List of Figures

Acknowledgement

First of all, I like to thank Martin Bauer for his close supervision during the past year. I want to thank Prof. Tilman Plehn for hosting me in his group and for reading this thesis. Similarly I want to thank Jörg Jäckel for being my second examiner.
I would like to thank all my office colleagues for the inspiring discussions. It has been a pleasure to stay with you while having an uncountable amount of cakes, barbecues and of course ice-cream.
A special thanks goes in particular to those of my friends reading this manuscript and providing some feedback: Alexander, Franz, Jan, Jenny, Laura, Lukas, Marleen, and Paul.
Finally, I like to thank my family for their support, all my friends and especially Iris as they all cared so amiable about my feelings and the progress of this thesis especially during the last weeks.

Declaration

I confirm that the work of the thesis was solely undertaken by myself and that no help was provided from other sources as those allowed. I confirm that all sections of the thesis that use quotes or describe an argument or concept developed by another author are referenced.

Heidelberg, December 01, 2017